BRNO UNIVERSITY OF TECHNOLOGY
VYSOKÉ UČENÍ TECHNICKÉ V BRNĚ

FACULTY OF CHEMISTRY
MATERIALS RESEARCH CENTRE

FAKULTA CHEMICKÁ
CENTRUM MATERIÁLOVÉHO VÝZKUMU

ADVANCED MATERIALS FOR ORGANIC PHOTONICS

POKROČILÉ MATERIÁLY PRO ORGANICKOU FOTONIKU

Ph. D. THESIS
DIZERTAČNÍ PRÁCE

AUTHOR: D.E.A. IMAD OUZZANE

AUTOR PRÁCE

SUPERVISOR: Prof. Ing. MARTIN WEITER Ph. D.

VEDOUCÍ PRÁCE

BRNO 2014

Abstrakt:

V oblasti nových nízkomolekulárních organických materiálů patří deriváty difenyldiketopyrrolopyrrolu (DPP), používané dříve jako barviva a pigmenty, k objektům vysokého zájmu pro jejich potencionální aplikace v moderních technologiích. Studium jejich optických vlastností ve vztahu k jejich chemické struktuře umožní využití jejich vysokého potenciálu ve vývoji pokročilých inteligentních materiálů. Přehled chemických a fyzikálních vlastností DPP derivátů a zhodnocení současného stavu řešené problematiky jsou uvedeny v teoretické části této práce. Tři hlavní procesy studované v této práci jsou: klasická absorpce a emise, dvoufotonová absorpce (TPA) a zesílená spontánní emise (ASE). Výsledky budou diskutovány a shrnuty ve dvou částech: první zahrnuje první dvě výše zmíněné oblasti a druhá problematiku zesílené spontánní emise.

Abstract:

Among low molecular organic materials, diphenyl-diketo-pyrrolopyrrole (DPP) derivatives used earlier as dyes are of high interest in modern technologies. The study of their optical properties related to their chemical structure will provide more information on the later relationship and comfort the high potential of DPP derivatives in the making of more performant smart materials. An overview of their chemical and physical properties is described in the theoretical part and followed by the state of the art in the field of interest concerning this thesis. The three main processes studied in this work are: The classic absorption and emission, the two photon absorption (TPA) and the amplified spontaneous emission (ASE). The results will be discussed and summarized in two parts: The first concerning the one and the two photon absorption and the second the amplified spontaneous emission.

Klíčová slova:

Dvoufotonová absorpce, zesílená spontánní emise, absorpce světla, prahová hodnota, průřez, deriváty difenyldiketopyrrolopyrrolu, časově rozlišená fluorescence, laser, tenké vrstvy

Keywords:

Two photon excitation fluorescence, amplified spontaneous emission, light absorption, thin films, organic photonics, diphenyl-diketo-pyrrolopyrrole derivatives, gain, laser, thin films

OUZZANE, I.: Pokročilé materiály pro organickou fotoniku. Brno: Vysoké učení technické v Brně, Fakulta chemická, 2014. 124 s. Vedoucí dizertační práce Prof. Ing. Martin Weiter, Ph.D.

PROHLÁŠENÍ

Prohlašuji, že tuto disertačni práci jsem vykonal samostatně a že všechny použite literárni zdroje jsem správně a úplně citoval. Disertačni prace je z hlediska obsahu majetkem chemické VUT v Brně a může být využita ke komerčnim účelům jen se souhlasem vedouciho disertačni práce a děkana FCH VUT.

.....

podpis studenta

DECLARATION

I hereby declare that this doctoral thesis was done by myself. All used references were correctly and completely cited. This PhD. Thesis is, from the content point of view, a property of Faculty of Chemistry, Brno University of Technology, and thereby can be used for commercial purposes only with the permission of this thesis supervisor and the dean of FCH BUT.

.....

Signature of the Ph.D. thesis author

Remerciements

Je tiens à citer en premier lieu maman, papa et ma sœur pour leur aide précieuse et constante. Merci aux amis pour leur appui et encouragements aux moments adéquats.

Je souhaite également exprimer ma gratitude envers tous mes collègues, étudiants et employés de l'Université Technologique de Brno (BUT, VUT), qui ont, chacun à sa façon, contribué au succès de ce travail.

Sans oublier mes remerciements aux Dr. Jozef Krajčovič et Dr. Martin Vala pour leur aide ainsi qu'au prof. S. Luňák pour sa collaboration, nous fournissant une majeure partie des molécules étudiées. Je cite aussi le Dr. Ivaylo Zhivkov pour les mesures de couche minces ainsi que Doc. Otta Salyk et Dr. Alexander Kovalenko pour leur aide nécessaire. Je tiens à souligner ma gratitude envers le prof. Zmeškal Oldřich dont l'aide a été cruciale durant mon examen d'état doctoral mené sous la présidence du prof. Stanislav Nešpůrek.

Grand merci au prof. Jean-Philippe Bouillon pour m'avoir appris mon métier avec passion, faisant de moi un chimiste organicien de synthèse.

En particulier, mes plus chaleureux et sincères remerciements vont vers Mr Le Professeur Martin Weiter pour son aide financière, matérielle et humaine, oh ! Combien précieuse ! M'offrant l'opportunité de soumettre la présente thèse à votre appréciation. Merci patron !

Acknowledgment

This work is dedicated to my family and close friends: Thank you mom, dad and sister for giving me an amazing youth and so much love.

Thanks to the staff of Brno VUT, my colleagues, students and professors. Thanks to those who smiled, said hello, took some coffee breaks, smoky talk in winter, those who repaired, cleaned, installed...

Thanks also to prof. S. Luňák, Dr. Ivaylo Zhivkov, Dr. Martin Vala, Dr. Otta Salyk, Dr. Alexander Kovalenko as well as Dr. Jozef Krajčovič for their collaboration and help during this study. Special thanks to prof. Oldřich Zmeškal for being an exceptional advisor for my doctoral state exam held under the direction of prof. Stanislav Nešpůrek. Many thanks to Prof. Jean-Philippe Bouillon for his collaboration help and support.

And the last but not the least, I would like to express my deep gratitude to prof. Martin Weiter for the job, the finances, the material to work with, the ideas, the research, the inspiration, and the freedom at work.

Thank you Martin

Un petit clin d'œil pour résumer pas mal de travail abattu dédié à EYE

"Quand on ne sait pas vomir, on ne boit pas." J.P. Sartre
"Une injustice faite à un seul est une menace faite à tous." Montesquieu
"L'imagination est plus importante que la connaissance" Albert Einstein.

Contents

1 Introduction

The end of the XIXth century and its historical second industrial revolution opened doors to new inventions and drastically changed our way of life. The replacement of steam engines by the internal combustion engine brought a great social impact but also developed the extraction of raw energy resources like petroleum for the purpose of petrol driven engine. The XXth century could not manage the replacement of the internal combustion engine and so for enable to preserve natural resources. On the contrary, the extraction of petroleum went growing with the increasing number of transport systems and the exponential development and needs in pharmaceutics and plastic industries. We are not yet at this point ready to find a new efficient and nondestructive source of energy but nevertheless we labor everyday on studying how to better use the ones already among us. Human kind struggles for new energy resources and low consuming devices as for, bigger efforts are to be done towards green chemistry, recyclability and the understanding of chemical and physical properties of all our surrounding materials respecting the gift that is our nature. In fact, getting to know better the specific electronic and optical characteristics of a chemical structure can only lead to a better consuming of energy and therefore lowering the waste which is still until now dissipated into unused energy like the heat.

Intelligent packaging, organic photovoltaic cells (OPV), printed radio-frequency identification (RFID), organic memories, organic sensors, flexible batteries, organic thin film transistor (OTFT) displays backplanes to look at flexible displays, electroluminescence (EL), organic light emitting diode (OLED) among other smart objects are part of actual organic and printed electronics association (OE-A) field and main interest of research in chemistry like in physics. The growing list, and it is likely that it will increase in the future, of applications reflects the complexity of the topic and the wide possible uses for organics. Used for actual design and esthetic purposes in many lighting applications, the OLED technology is meant to be sooner rather than later part of general illumination [1]. Displays based on liquid crystals are still being used; however the color purity, the lifetime, high efficiency as well as the production costs of organic materials are being improved constantly. Solar cells are usually made of crystals but they come up to be nowadays modified and replaced by organic materials for making soft and low cost layers with an increase in efficiency and a decrease in toxicity. Organic solar cells are made of an active layer, a charge transport layer for one of the charge carriers (electron or holes) type or two transport layers for both types of charges and finally of electrodes like shown in **Figure 1** representing the general scheme of an organic photovoltaic cell.

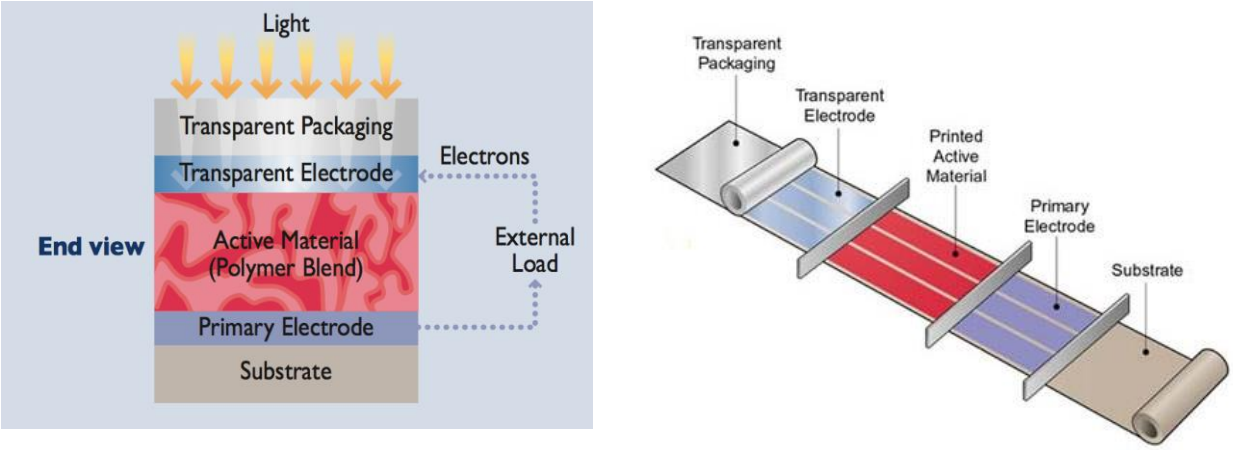

***Figure 1**: Typical structure of organic solar cells which consist of active layer for photogeneration free charge carriers. The charge carriers are selectively transported by means of transport layers according to charge (hole or electron) transported to electrodes, where one of the electrodes needs to be transparent for light. The picture on the right represents the scheme of a print solar cell [2].*

Actually there are electronics everywhere like integrated circuits, sensors, displays, memory, photovoltaic cells or batteries which can be made out of organic molecules. Applications like flexible solar cells, radio-frequency identification (RFID) tags, flexible displays, organic light-emitting diode (OLED) lighting based products, single-use diagnostic devices or simple consumer products and games are only a few examples like seen in **Figure 2** that represent a promising future. Nowadays smart materials or multi stable molecular systems attract much attention because of their potential use in optical and opto-electronical devices such as broadband optical modulators. Organic electronics stands for a revolutionary way of making electronics: thin, lightweight, flexible, produced at low cost, better recyclable, enabling single use, ubiquitous electronic devices and new applications.

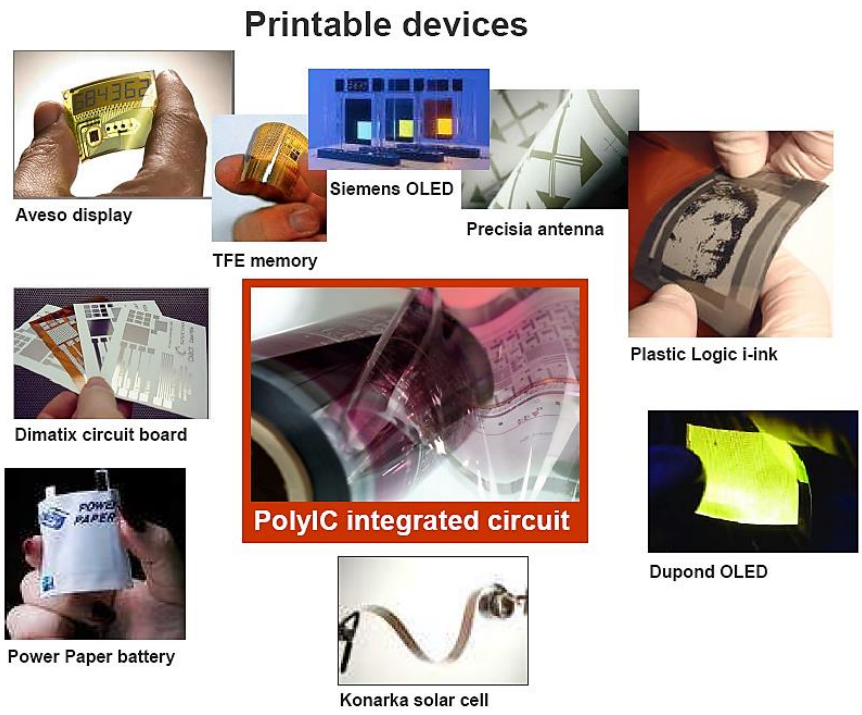

***Figure 2**: Organic light-emitting diode so called OLED and printed devices composed of organic molecules [3].*

The OLED technology possesses many benefits and one of the most important is the possibility to reduce the thickness of such systems making them spatially very flexible. Additional products, like flexible or large unbreakable displays with organic TFT backplanes, printed radio frequency tags and organic memory, have been demonstrated technically and already reached the market in 2012. The growth of interest in the use of modern technologies and understanding better physical properties of raw materials leads to new routes and processes to be used in all surrounding electronic composed materials. Worldwide needs and industrial growth seek for efficient and ecological response as the demands in energy gets higher with the increasing population, **Figure 3** represents the market growth in printed electronics and their potentials in many other applications.

Organic materials play an important role in producing electronic devices. OE-A as Organic Electronic Association is one of many international associations including worldwide competencies in this field providing expert consulting and information concerning printed electronics covering the whole range of technologies and applications: These materials like new organic polymers, chromophores derivatives and more multistable molecular systems have found great interest for actual new industrial technologies. The contribution of organic electronics to printed electronics devices, flexible solar cells, rollable displays and future energy technologies is essential and necessary for the future.

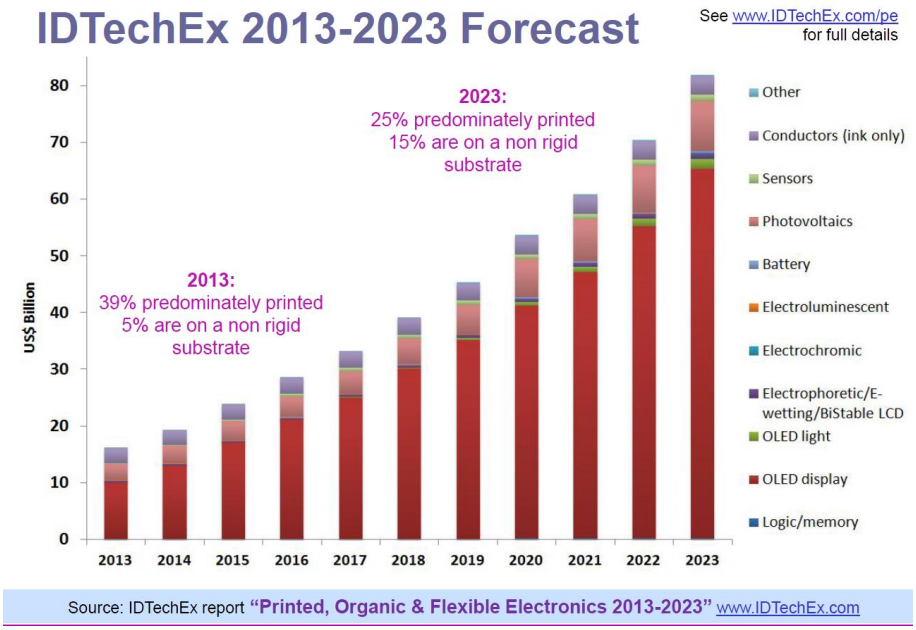

***Figure 3**: Market evolution of printed electronics worldwide [4].*

Π-conjugated materials and mostly polymers are essential for the preparation of the charge-transporting and the emissive layers of organic solar cells and OLED. Polymer light-emitting diodes (PLEDs) are perfect candidates as they enhance low operating voltage, film forming abilities via spin coating, tunable luminescence properties, potential full-color flat panel and flexible displays as well as easy fabrication at low cost [5, 6]. The contribution of polymers to electronics is a major advancement in the modern field of organic electronics. Polymer, containing chromophore subunit, prepared by polycoupling reaction recently appeared into another progressive area which is nonlinear optics (NLO), concretely two-photon absorption (TPA). TPA fields of application are numerous like: Microfabrication and lithography, 3D photopolymerization, imaging, optical power limiting, photodynamic therapy, optical data storage. Further paper on this topic appeared reporting relatively high TPA cross-sections of the simple (not polymeric) symmetrical diphenylamino diketopyrrolopyrrole (DPP) derivatives [7]. Interest in non-polymeric materials such as DPP derivatives for the use in OLED technology and NLO is increased and was already demonstrated.

Their advantageous properties such as high quantum yields, recyclability, lifetime and thermic resistance, non-toxicity, low cost fabrication and tunable emissive luminescence makes them ideal candidates for the purpose of these processes. Problems that arises this beginning of 21st century comforts the existence of our poly competent group composed of physicists, biochemist, organic, inorganic and physical chemists that struggle every day on studying new

modern advanced molecular materials. The aim of our team is to lead our research to better efficiency solar cells, better energy transport systems and the use in optics like in electronics of cheap recyclable organic materials.

This Ph.D. thesis focuses mainly on the optical study and the synthetic development of new DPP derivatives suitable for devices to be used in photonic applications. These materials were substituted with electro-withdrawing and/or electro-donating chemical groups in specific positions and their physical property changes were observed and will be discussed in later chapters.

During this work I have also studied different types of materials other than DPP derivatives. We also investigated the optical properties of phtalocyanines derivatives and the synthesis of poly[methyl(phenyl)silylene] (PMPSi) (not included in this dissertation). The optical study depending mostly of the equipment like the LASER and a photon intensified charge-coupled device (ICCD) camera to be installed; this work started therefore with the synthesis of PMPSi to be coupled with a chromophore. Once the apparatus installed, this synthesis was left beside for further investigation. Few years after the beginning of my thesis and with the development of our group I proposed the synthesis of functionalized DPP derivative in N position with phenyl containing F or NO_2 function (the latest being the most probable to synthesize as a derivative was already published [35]). DPP derivatives with functionalized N position containing other than simple alkyl or acyl were then rarely reported.

The beginning of the first chapter concerning this thesis, deals with the chemical materials description and their synthesis like their amelioration according to optical results and feedback. The second part is dedicated to their optical properties and determination mainly focused on two physical processes: The nonlinear two photon excitation study and the amplified spontaneous emission of relevant DPP derivatives. The experimental part concerns the description of the analysing apparatus specificities like the different laboratory technics and disposition used for the ASE and TPA experience.

The aim of this thesis is to compare several DPP derivatives and the effect of their distinct substituents on their optical properties to determine their relevance in modern applications for advanced devices. The results obtained should provide us with crucial information for the preparation of new type of DPP derivatives with enhanced characteristics.

2 State of the art

This thesis focuses on the optical study of suitable molecules for organic photonics playing a great role in modern applications. Organic photonics is an interdisciplinary and innovative research field with many materials systems and application areas resulting also in strong interactions between academic institutions and industry. In the **Figure 4** bellow we see a general map of photonics materials represented in green circles and their applications in blue rectangles.

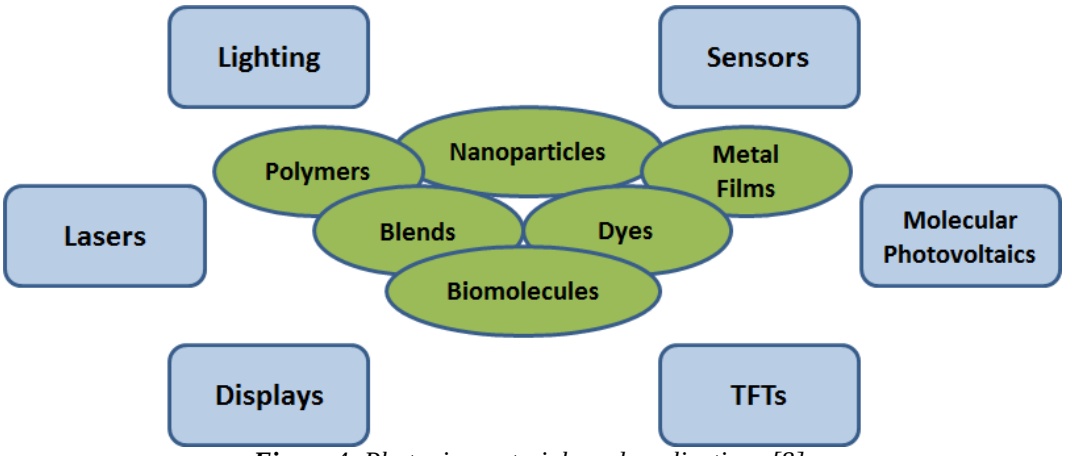

***Figure** 4: Photonics materials and applications [8].*

"Photonics" originates from the Greek word "photos" meaning light and is used in composed words designating news sciences or technologies using the light. The science of photonics includes the generation, emission, transmission, modulation, signal processing, switching, amplification and detection and sensing of light. The term photonics thereby emphasizes that photons have both particle and wave nature. This field focused earlier mostly on optical telecommunications and began with the invention of the laser in 1960 [9]. It covers all technical applications of light over the whole spectrum from ultraviolet over the visible to the near-, mid- and far-infrared. Organic photonics applications use the photon in the same way that electronic applications use the electron. It covers a huge range of science and technology applications, including laser manufacturing, biological and chemical sensing, medical diagnostics and therapy, display technology, electroluminescent diodes, optical modulators, optical amplifiers and optical computing.

The following part of this chapter is dedicated to the physical and chemical background of low molecular organic compounds, mostly DPP derivatives involved in this study.

The second part deals with the physical characterization of these materials focused on their

spectroscopic study. The luminescence of DPP derivatives will be investigated throughout modern photo-processes which will be hereby introduced and described.

2.1 Organic photonics

Organics photonics is an interdisciplinary and innovative research field involving many materials like dyes, nanoparticles, polymers, metal films and biomolecules. The increasing interest towards organic materials is mainly justified not only by actual economy and ecological threats but also for advantageous processing properties and hereby resumed in **Table 1** where MBE stands for molecular beam epitaxy and MOVPE for metal-organic vapor phase epitaxy.

***Table 1**: Comparison of inorganic and organic electronics and photonics.*

Inorganic Materials	Organic Materials
Materials	
Hard, fragile	*Soft, molecular, flexible*
Material Processing	
Vacuum deposition *Ultra high temperatures*	*Solution processing, low temperature*
Fabrication Equipment	
MBE, MOVPE	*Spin coated, printing*
Cost	
Highly specialized, expensive *Difficultly recyclable*	*Simple, inexpensive* *Recyclable*

Modern photonic devices are the main center of attention in high technology industries exploring this field with growing interest. According to different needs we could consider differently functionalized molecular structures. Polymers play an important role in the development of materials for photonics in industries because they are relatively inexpensive and can be functionalized to achieve required optical, electronic or mechanical properties. They can possess useful optical properties such as electroluminescence, photoluminescence, or nonlinear optical properties [10]. They can also be used as matrices for optically active species, e.g. for dyes and possess topographic patterns that can coherently scatter light. The Polymer based display

technology is based on the discovery of conjugated polymer electroluminescence [11]. Actually polymer and small molecule based displays are already on the market and studied modern fields of research and industries. Poly(3,4-ethylendioxythiophen) (PEDOT) which is a p-type electron acceptor is a conductive and transparent compound [12]. Poly(3-hexylthiophen) (P3HT) is also a p-type electron but donor compound actively studied in the conception of organic electroluminescent diodes [13] and photovoltaic solar cells.

Low molecular organic molecules like dyes, pigments or chromophores are as much attractive materials and actually accurately studied in the field of photonics. [6,6]-phenyl-C61-butyric acid methyl ester (PCBM) which is a n-type organic semiconductor electron acceptor [14] has been widely used as the photoactive layer in bulk- heterojunction. Systems and application areas are wide such as lighting, molecular photovoltaics, lasers, displays, sensors and TFTs.

Among many other organic materials, DPP derivatives are also highly suitable for electro-optical applications [15] as they provide many advantages and we shall present them in following chapter.

2.2 Diphenyl-diketo-pyrrolopyrrole derivatives

Nowadays, we can see a strong effort in seeking for highly performing materials for cheap organic photonics. Together with high performance of the materials, the usual second requirement is their high photo and thermal stability. Among other materials, the diketo-pyrrolo-pyrroles (DPPs) are suitable candidates due to these requirements. DPPs were widely used in inks and paints for their great color properties. Lately, interest towards DPPs has increased in the field of organic photonics because of their great fluorescent properties and good charge carrier mobility.

Several derivatives of symmetrical diphenyl-diketo-pyrrolopyrrole were already synthesized and their optical properties in solutions like in solid state lasing were already partly investigated and described in the literature [16]. **Figure 5** illustrates the basic chemical structure of these organic chromophores where the R_1 and R_2 positions can be differently substituted with whether a withdrawing or a donating group [17] knowing that in symmetrical DPPs R_1=R_2 and R_3=R_4.

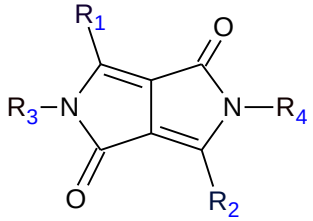

***Figure 5**: Basic structure of diketo-pyrrolopyrrole derivatives.*

Usually symmetrical diphenyl-diketo-pyrrolopyrroles are synthesized according to the fashion way described in the literature [18] and presented in **Figure 6**.

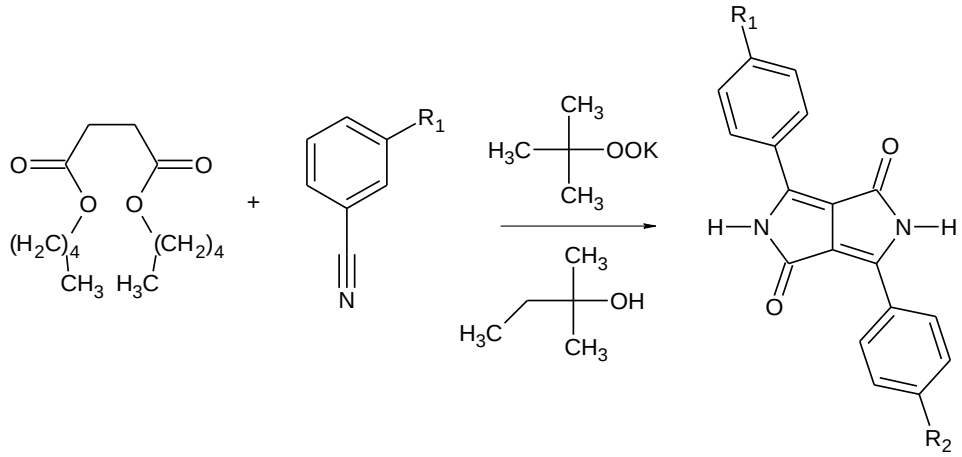

***Figure 6**: General modern synthesis symmetrical (R_1=R_2) of diphenyl-diketo-pyrrolopyrrole with non-saturated nitrogen.*

DPPs are usually insoluble in most common solvents and one of its reasons is the presence of hydrogen bonding between the N-H function and oxygen. In R_3 and R_4 position (**Figure 5**) were usually added alkyl groups to the non-saturated secondary amine making it tertiary substituted to allow an increase of their solubility. In para position of phenyls (R_1, R_2) were substituted electro withdrawing (W) or donating (D) groups to the 3,6-diphenyl-2,5-dihydro-pyrrolo[3,4-c]pyrrole-1,4 dione, commonly referred to as a DPP derivative.

Unsymmetrical DPPs are also usually common to synthetize [19] (**Figure 7**, where R= Br, Cl, and D= donor) but the difficult part is their purification. In this case, final products of the reaction are very difficult to separate, non-including also solubility problems.

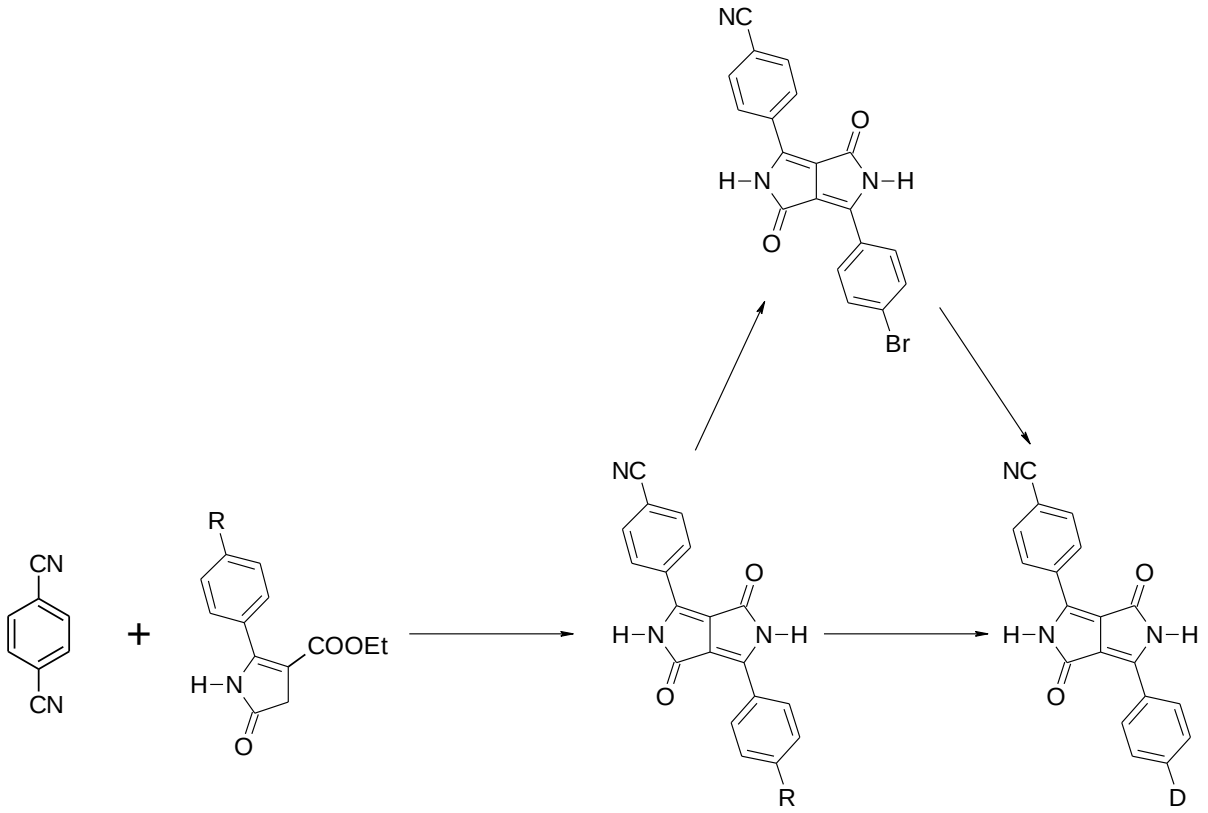

Figure 7*: General synthesis of unsymmetrical diketo-pyrrolopyrrole derivatives with non-saturated nitrogen.*

DPP derivatives present generally photostable systems and modifying them by introduction of polar substituents allows getting dipolar or quadrupolar molecules which are very promising. The push-pull (electron donating, electron withdrawing) substituted organic π-conjugated compounds are actually of a great interest for physicists as they can produce strong second-order nonlinear effects [20]. Quadrupolar chromophores are more suitable for creating a third order NLO behavior. DPPs are more and more interesting as advanced materials for modern optoelectronic technologies: Organic electroluminescent devices (OLED) to be used as full color flat panel displays and new generation of lamps, organic field-effect transistors (OFET) [39] and photovoltaic solar cells. They constitute recent industrial important class of highly efficient dyes [21] because of their outstanding chemical and physical properties such as a high melting point unusual for such a low molecular weight molecule relative to standard pigments. Studies has shown that the introduction of DPP units into polymers [22], dendrimers [23], polymer-surfactant complexes [24] and oligomers [25] resulted in wide colored, highly photoluminescent and electroluminescent [26] materials. Due to all these exceptional properties, DPP molecules fit in a wide range of applied fields like charge generating materials for laser printers, information storage systems [27, 28], solid-state dye lasing device or gas detectors [29, 30].

Lately, DPPs where investigated as laser active media [31], and results were reported on

symmetrical pigments used for doping polymers like PMMA suitable for the making of thin films. Amplified spontaneous emission was detected but this effect was not stable as the system PMMA doped DPP underwent photodegradation.

2.3 New types of DPP derivatives

Common strategy to develop materials with desired properties for organic electronics applications is to combine various building blocks and transform them into new sophisticated molecular structures with enhanced properties. The incorporation of polar groups into these organic chromophores causes a redistribution of the electronic density in the ground states like in the excited one. This can strongly affect their absorption and fluorescence properties [32]. New types of DPP derivatives were synthetized considering that in position R_3 and R_4 seen in **Figure 8** could be other subsequent substituents than only alkyl (or acyl) solubilizing groups. The blue arrows represent electron withdrawing group whereas the green arrows represent electron donating groups (attraction towards the arrow's head).

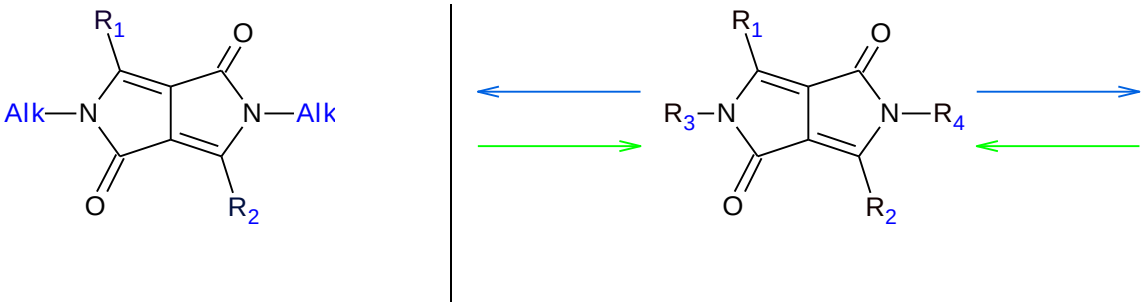

***Figure 8**: (left) Classical DPP derivatives with solubilizing alkyl groups in position R_1-R_2. (right): New types of DPP electron withdrawing or donating effects of pendent groups in amine position R_3-R_4.*

It has been proved that diketo-pyrrolopyrroles (DPP) can serve as an efficient base structure for organic solar cells materials [33]. It has drawn attention for its strong light absorption, photochemical stability and extended π-conjugated system.

The best concept design for performing new chromophores for organic solar cells (OSC) so far utilizes donor-acceptor (D-A) alternation for lowering the band-gap due to formation of intermolecular charge transfer states. One of the building blocks with acceptor character commonly used in such design is diketo-pyrrolopyrrole (DPP). However, the synthesis of DPP with donating substituents leads to the increase of both frontier molecular orbitals (FMO) and thus do not resonate with the needs mentioned above [98]. It is therefore necessary to develop strategies to move the DPP's lowest unoccupied molecular orbital (LUMO) in the optimal (low)

position and simultaneously allow precise highest occupied molecular orbital (HOMO) modulation. Generally, the lowering of the FMOs energy requires the introduction of electron deficient group. The common strategy is to use substitution on pendant phenyls or thienyls [34] present in position R_1 and R_2 of DPPs like shown in **Figure 9**. However, once these positions are occupied, it does not allow further FMOs modifications.

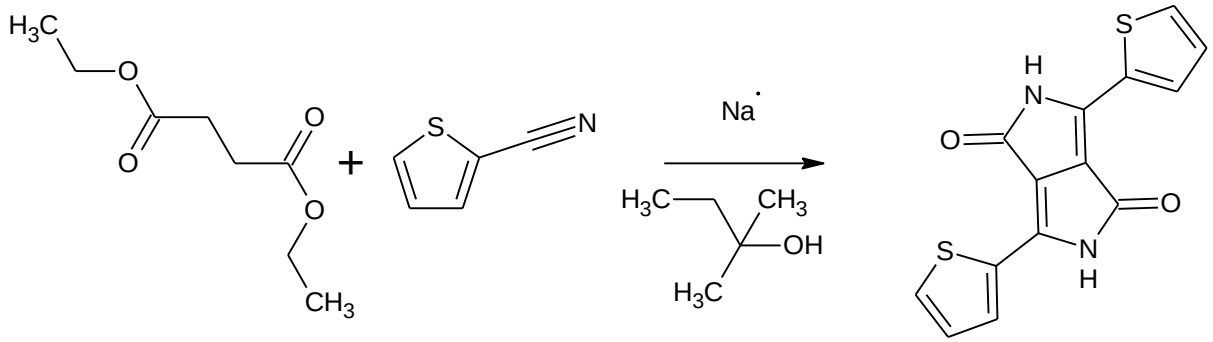

***Figure 9**: General scheme for the synthesis of DPP substituted thiophene in position R_1 and R_2.*

Up to now, the *N*-substitution was almost exclusively used to increase the solubility. Common substituents are various alkyl chains allowing good processability, both during the synthesis, and during the sample preparation. It is generally supposed, that the *N*-substitution by alkyls does not influence that much the molecular orbitals.

The *N*-substitution is not only here to increase the solubility but also to modulate the FMO and thus improve its energy balance for materials in organic solar cells. This should allow the lowering of the FMOs and simultaneously leave the phenyls or thienyls in position R_1 and R_2 for free for further substitutions. Other possible substitutions in position R_3 and R_4 is by using electron deficient substituents on DPP's lactam group.

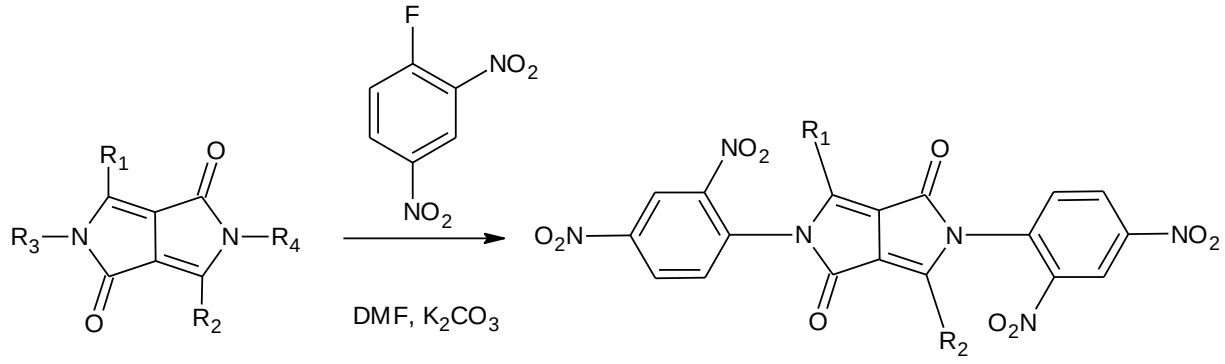

***Figure 10** : Synthesis reaction of N-substituted DPP derivative with other than alkyl in position R_3 and R_4.*

Such substituted type of DPP was already synthetized [35] and the reaction is described here

above in **Figure 10** representing the general synthesis of substituted dinitro-phenyl in N position R_3 and R_4 of DPP derivative. Originally developed as high performance organic pigments [36, 37, 38], various structural modifications make diketo-pyrrolo-pyrroles (DPPs) very interesting as advanced materials for modern optoelectronic technologies like organic light-emitting diodes (OLED) [39], organic field-effect transistors (OFET) [40] and photovoltaic solar cells [41]. DPPs for these purposes are usually *N*-alkylated and (co)polymerised by coupling reactions [42, 43] or electrochemically [44] from halogen (often bromo) substituted precursors.

2.4 Optical study of organic material

In this chapter we introduce the optical and theoretical background involved in this doctoral thesis and used further for determining particular optical properties of the molecules investigated. All of the materials presented will be subject to specific optical studies according to their properties.

2.4.1 Linear absorption and fluorescence emission

During light excitation, photons are absorbed by the atom or molecule and therefore an electron is promoted from the ground state S_0 to the upper transition allowed excited state S_1 of higher energy like seen in **Figure 11**. Following the Franck-Condon principle [45] which states that since electronic motions are much faster than nuclear motion, electronic transitions occur most favorably when the nuclear structure of the initial and final states are most similar [46].

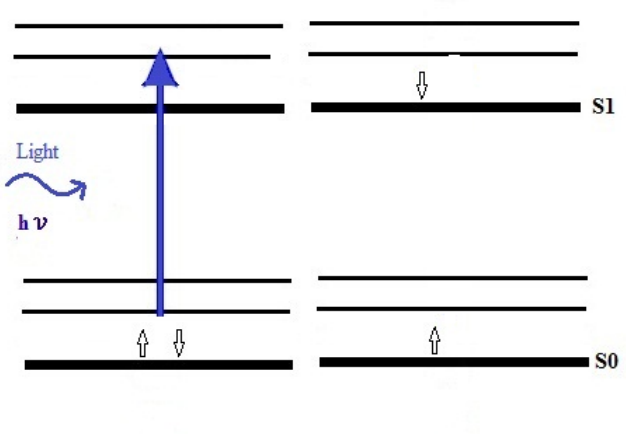

***Figure 11**: Absorption from the ground state to the excited state.*

The transition from the ground state S_0 to the excited state S_1 corresponds to the absorption of a photon (OPA) or thermal energy, promoting the molecule to higher excited state energy level. Once excited by light for instance, it can be found in various excited states undergoing various processes and transitions. When absorbing a photon of the necessary energy, the molecule makes a transition from the ground electronic state to the excited electronic state. This excitation of the molecule corresponds to the absorption represented in **Figure 12** in blue transition (arrow going upwards). In the electronic excited state molecules quickly relax to the lowest vibrational level (Kasha's rule), and from there can decay to the lowest electronic state via photon emission. Classically, the Franck–Condon principle is the approximation that an electronic transition is most likely to occur without changes in the positions of the nuclei in the molecular entity and its environment. The resulting state is called a Franck–Condon state, and the transition involved a vertical transition [47]. Electronic transitions to and from the lowest vibrational states are often referred to as 0-0 (zero zero) transitions and have the same energy in both absorption and fluorescence. The Franck–Condon principle for vibronic transitions in a molecule is illustrated in **Figure 12** in both the ground and excited electronic states. The shift in nuclear coordinates (electron configuration) between the ground and the first excited state is labeled as q_{01}.

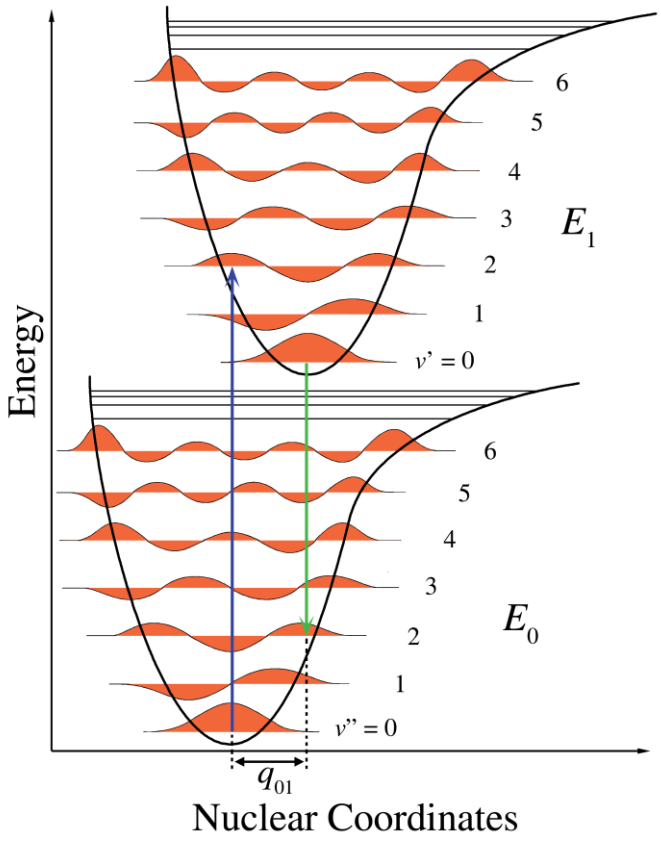

***Figure 12**: Franck–Condon principle energy diagram. Since electronic transitions are very fast compared with nuclear motions, vibrational levels are favored when they correspond to a minimal change in the nuclear coordinates [48].*

If not excited, usually an atom or molecule would adopt the energy level of its more stable state configuration which is the ground state S_0. The applicability of the Franck–Condon principle in both absorption and fluorescence, along with Kasha's rule leads to an approximate mirror symmetry shown in **Figure 13**. The now excited molecule may lose its energy by radiative process emitting a photon (spontaneous emission) by fluorescence or non-radiative loss of energy (like heat, relaxation) allowing the molecule to relax to its lower stable ground state. There are two processes that emit light from a molecule and therefore also two transitions:

-The first is fluorescence (represented above in green-arrow downwards) which corresponds to the spontaneous emission of a photon and a transition of the molecule's electron from the excited state S_1 to the ground state S_0.

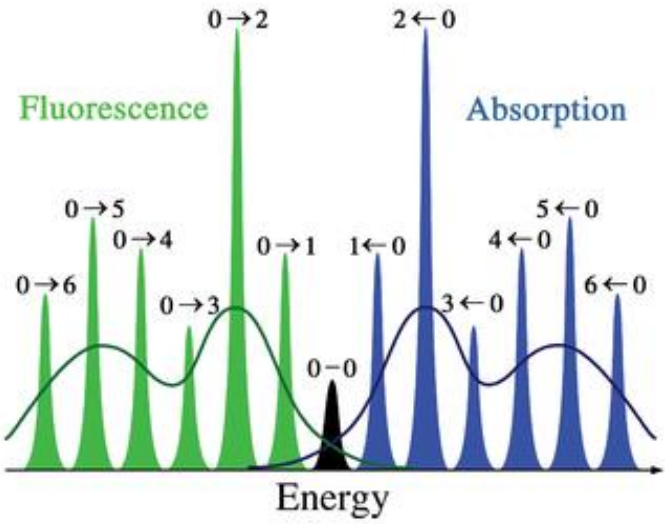

***Figure 13**: Schematic representation of the absorption and fluorescence spectra corresponding to the energy diagram in **Figure 12** [32].*

The energies playing a determining role are in a wide range of wavelength same as the domain of atomic orbital. The fluorescence is the photon released when the excited electron on S_1 falls back to the ground state according to the allowed transitions $S_0 \rightarrow S_1 \rightarrow S_0$. As it is paired with another electron of opposite spin; the total spin being zero, the ground state S_0 is Singlet.

-The second emitting process much slower is the phosphorescence corresponding to the transition from the triplet state T_1 to the electronic ground state S_0. The energy difference between the two S_1-S_0 states equals the energy carried off by the photon:

$$E = h\nu = hc/\lambda \qquad (1)$$

Where h is Planck's constant, ν the frequency and λ the wavelength of the emitted radiation. To a given wavelength corresponds a photon of certain energy. The smaller the wavelength, the bigger is the energy. Good lasing properties would require a low concentration of dye molecules and non-competing processes like phosphorescence or non-radiative transitions. The triplet state has a long lifetime and if it is at lower energy than the singlet one, it competes with the populating of the excited state S_1 and therefore lowering the quantum yield of the fluorescence.

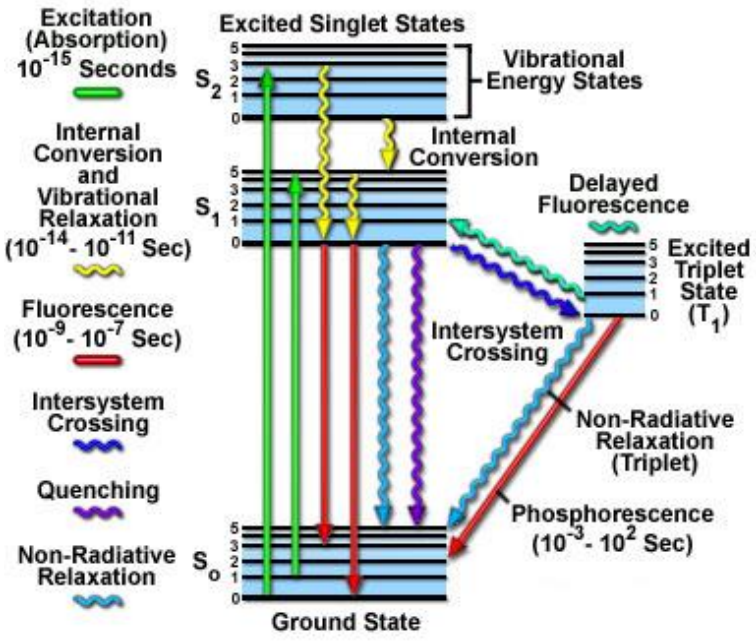

***Figure 14**: Jablonski Energy Diagram [49].*

All these processes descried earlier are resumed in **Figure 14,** representing the Alexander Jabloński energy diagram.

2.4.2 Nonlinear and two photon absorption (TPA)

The difference between one-photon absorption (OPA) and two-photon absorption (TPA) lies in that OPA depends linearly on the light intensity, whereas TPA involves the simultaneous interaction of two photons and so it increases with the square of the intensity. To accomplish two-photon absorption events, we need to generate a very high instantaneous photon density. As for the linear absorption, an electron is promoted from the ground state to an excited state; not by absorbing one but two photons at the same time given they are both within the absorption band gap of the molecule. In 1931, the theoretical basis of two photon excitation was first established

by Maria Göppert-Mayer [50], and the photophysical effect was demonstrated experimentally by Kaiser and Garret in 1961 [51]. TPA is a way of accessing a given excited state by using photons of half the energy (or twice the wavelength) of the corresponding one-photon transition. Therefore TPA is of a great interest in numerous applications [52] including microscopy, optical power limiting, 3-D fluorescence imaging [53], photodynamic therapy, localized release of bio-active species, up-converted lasing, microfabrication and three-dimensional data storage. Two-photon fluorescence microscopy offers the advantages of deeper tissue penetration and less photodamage minimizing photobleaching compared with confocal microscopy. These applications have generated a demand for new dyes with high two-photon absorption cross-sections. The designing of dye molecules (chromophores) with large two-photon cross sections will offer lower pump energies with less optical damage to the host materials.

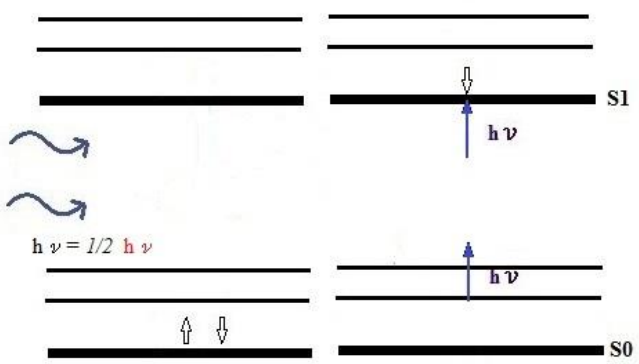

***Figure 15**: Two photon absorption promoting an electron from the ground state to the excited state.*

The discovery of two-photon fluorescence light microscopy by Denk, Webb and co-workers (Denk et al., 1990) revolutionized three-dimensional (3D) in vivo imaging of cells and tissues. Two-photon excitation is a fluorescence process in which a fluorophore is excited by the simultaneous absorption of two photons like shown in **Figure 15**. OPA process typically requires photons in the ultraviolet or blue/green spectral range. However, the same excitation process can be generated by the simultaneous absorption of two less energetic photons (typically in the infrared spectral range) under sufficiently intense laser illumination.

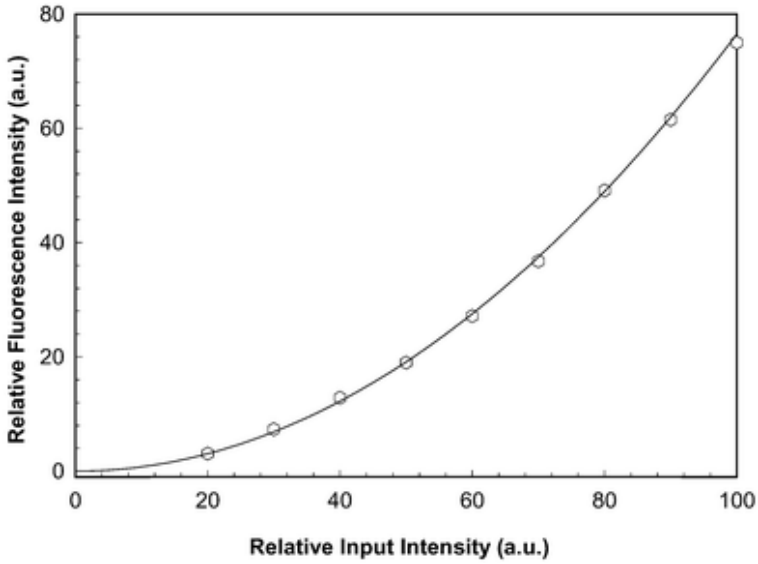

***Figure 16**: Fluorescence intensity dependency on the incoming LASER power [118].*

When we measure the out coming fluorescence intensity of TPA emission related to the growing incoming excitation light we could notice the non-linear response of the process at higher excitation energy. This nonlinear process represented with the black curve (circles) in **Figure 16** can occur if the sum of the energies of the two photons is greater than the energy gap between the molecule's ground and excited states. Since this process depends on the simultaneous absorption of two infrared photons, the probability of two-photon absorption by a fluorescent molecule is a quadratic function of the excitation radiance. Under sufficiently intense excitation, three-photon [54] and higher photon excitation is also possible (deep UV microscopy based on these processes has been developed).

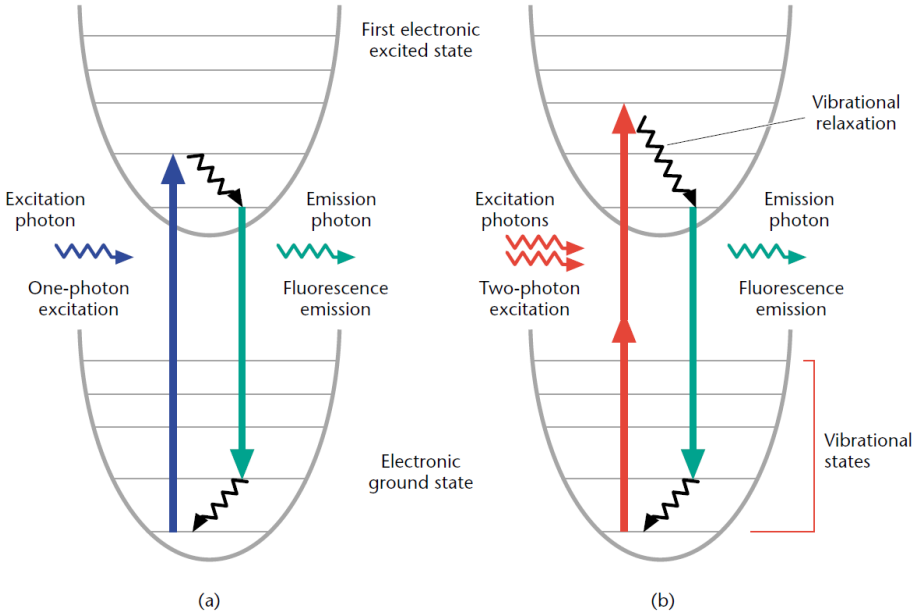

***Figure 17**: Jablonski diagram of one-photon (a) and two-photon (b) excitation, which occurs as fluorophores are excited from the ground state to the first electronic states[55].*

The general scheme for the two photon absorption compared to the single photon absorption process is represented in **Figure 17**. After either excitation process, the fluorophore relaxes to the lowest energy level of the first excited electronic states via vibrational processes. The subsequent fluorescence emission process for both relaxation modes is nearly similar.

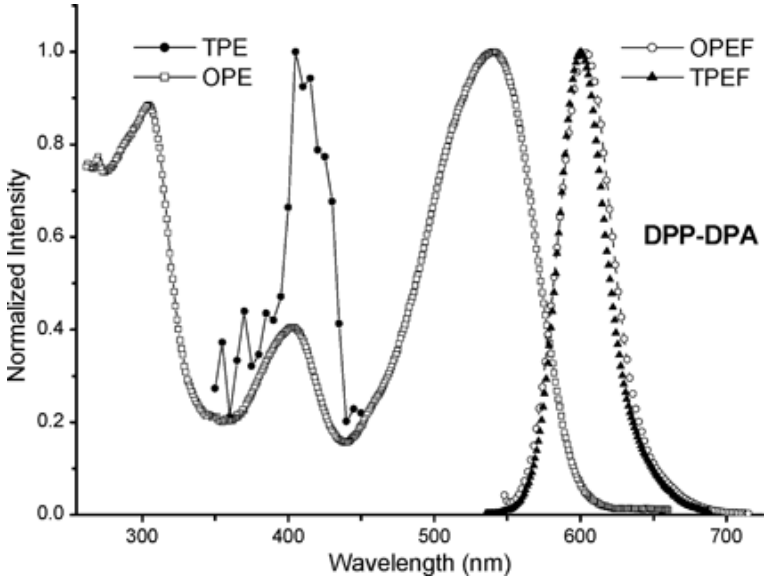

***Figure 18**: One-photon excited fluorescence (OPEF) and two-photon excited fluorescence (TPEF) spectra of DPP-DPA. Where TPE and OPE stand for respectively one- (OPE) and two-photon (TPE) excitation [56].*

Here in **Figure 18** is represented the one and two-photon fluorescence spectra for DPP-DPA Diphenylamine end-capped 1,4-diketo-3,6-diphenylpyrrolo[3,4-c]pyrrole (DPP). We can see clearly that the fluorescence emission of the one and two-photon excitations are very similar and their shape is Gaussian.

Polymer, containing N-alkylated DPP chromophore subunit, prepared by polycoupling reaction recently penetrated into another progressive area – nonlinear optics (NLO), concretely two-photon absorption (TPA) [57]. And further paper on this topic appeared reporting relatively high TPA cross-sections of the simple (not polymeric) symmetrical diphenylamino DPP derivatives [7]. TPA is a third order NLO process, in which the absorbed energy is quadratically proportional to the intensity of incident radiation [58]. With respect to the hierarchy of third order NLO processes it is a special case of degenerate four wave mixing, during which two photons of the same energy are absorbed simultaneously [59].

2.4.2.1 Two photon absorption and two photon absorption cross section

The double photon excitation has recently attracted much interest since a number of technical applications can be derived from the fact that the TPA cross section depends quadratically on the intensity of the exciting light and that fundamental excitations can be reached by applying half the wavelength, thereby considerably increasing the penetrability of materials and tissue [60]. The simplest determination of two-photon absorption cross section (σ_{2PA}) can be done by measuring the fluorescence signal generated after two-photon absorption (TPA). Such measurement yields TPEF [61] (two photon excitation fluorescence) action cross section (σ_{2PE}) which is linearly proportional to the $\sigma_{2PA:}$

$$\sigma_{2PE} = \phi_{2PE}\sigma_{2PA} \quad (1)$$

The proportionality constant Φ_{2PE} in **Equation 1** is the fluorescence quantum yield after TPA. In the case, when OPEF (One Photon Excitation Fluorescence) and TPEF spectra show close similarity. Because the fluorescence depends on the second order temporal coherence of the optical field, direct determination of the OPE cross section is not a trivial task.

Two-photon absorption cross sections (σ_{2PA}) were estimated from fluorescence signal intensity generated after TPA by a comparative method. The OPEF cross section can be expressed [62] as:

$$\sigma_{2PE(NEW)} = \sigma_{2PE(STD)} \frac{c_{STD}}{c_{NEW}} \frac{P_{STD}^2}{P_{NEW}^2} \frac{F_{NEW}}{F_{STD}} \frac{n_{STD}}{n_{NEW}} \quad (2)$$

where c is the concentration, n is refractive index and P and F are the time-averaged laser source power incident on the sample and time-averaged fluorescence emission.

To obtain more reliable results one can measure several concentrations of the fluorophores and replace the F/c ratio by the slope of the $F=f(c)$ dependence in precedent **Equation 2**. This treatment is similar to the estimation of the fluorescence quantum yields using the comparative method [63]. However it is experimentally much simpler to alter the laser power than to prepare many samples with different concentrations. Therefore we substituted the F/P^2 ratio for slope S of the $F=f(P^2)$ dependence.

In that case we get final expression in **Equation 3**:

$$\sigma_{2PE(NEW)} = \sigma_{2PE(STD)} \frac{c_{STD}}{c_{NEW}} \frac{S_{NEW}}{S_{STD}} \frac{n_{STD}}{n_{NEW}} \quad (3)$$

The slope *S* is obtained from the plot of integrated fluorescence intensity vs. the square of average laser power P^2 ($W.s^{-1}$).

On the contrary to one-photon absorption (OPA), for which the relation between molecular structure and absorption spectral characteristics, including molar absorptivity, is generally known for many years [64, 65], the corresponding relation between the structure and TPA parameters, especially TPA cross-sections, is not so clear. There is a general opinion, that the centrosymmetric quadrupolar chromophores of D-π-A-π-D or A-π-D-π-A type are more efficient TP absorbers than simple dipolar ones (D-π-A) [66, 67] and this trend continues to octupolar (branched multipolar) structures [68, 69]. From the theory, the requirement for maximizing the TPA cross-section of a chromophore includes:

- Long π-conjugated chains with enforced coplanarity that ensure large conjugation lengths
- Donor and acceptor groups at the center and ends of the molecule
- Centrosymmetric chromophores that possess a strong OPA transition close to the TPA laser wavelength.
- Chromophores with narrow one- and two-photon absorption bands.

Functional organic materials with enhanced TPA cross-sections are in the center of scientific interest now, as TPA process should be crucial for various novel technologies in photonics, spectroscopy, microfabrication or tissue engineering [70]. A lot of dyes from different structural classes like phtalocyanines [59], perylenes [71], polymethines [72] and squaraines [73] were studied from this point of view earlier.

2.4.3 Spontaneous & stimulated emission

Spontaneous and stimulated emissions are the fundamental processes that occur in lasing and stand for being the predominant physical phenomena that allows lasers to work, by favoring in the case of the stimulation the population inversion. If a laser-active atom, ion or media is in an excited state (quantum-mechanical energy level), it may after some time spontaneously decay into a lower energy level, releasing energy in the form of a photon, emitted in a random spatial

direction. This process is called the spontaneous emission and is represented in **Figure 19**, where the input energy would be the flash lamps of a laser that excites the active media.

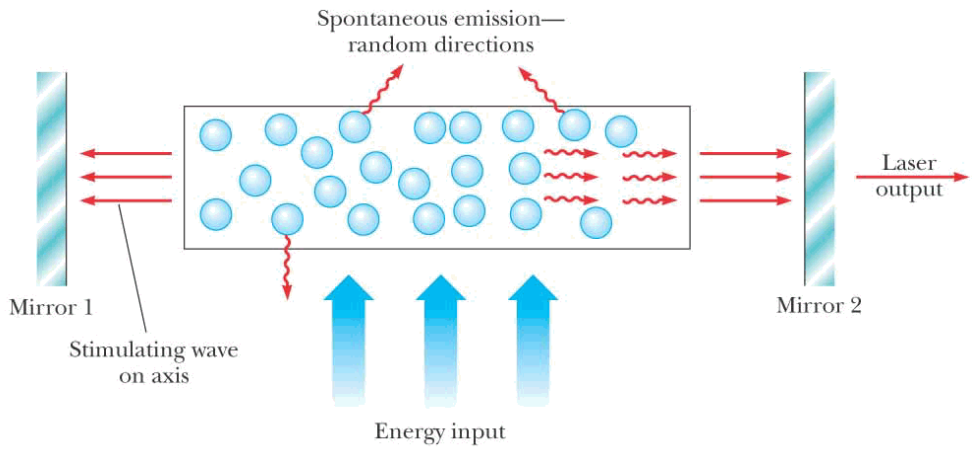

***Figure 19**: The spontaneous emission in a laser* [*74*].

The spontaneous emission is in general incoherent and is emitted randomly in all directions. However, it is also possible that the photon emission is stimulated by other incoming photons like drawn in **Figure 20**, if these have a suitable photon energy (or optical frequency) and this is called the stimulated emission.

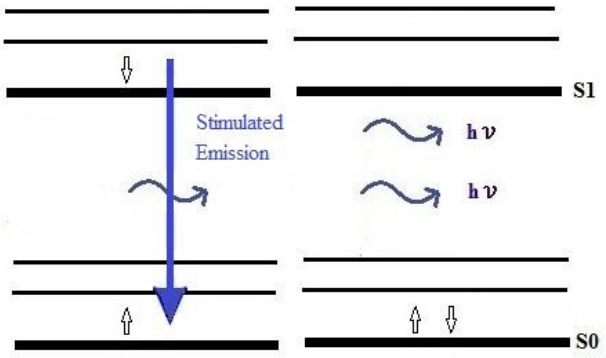

***Figure 20**: The Stimulated Emission.*

When a pump light excites a photo sensible molecule to emit two coherent photons of same phase and energy, occurs a stimulated emission. In that case, a photon is emitted into the mode of the incoming photon. In effect, the power of the incoming radiation is amplified. This is the physical basis of light amplification in laser amplifiers and laser oscillators. These same

photons can than undergo collisions with other excited molecules which results in a cascade of stimulated spontaneous emissions, or simply excite more non excited molecules and therefore favoring population inversion. Population inversion followed by pump amplification is one of the key principles of laser amplification which makes of spontaneous emission in this case an anti-productive process. Note that the amplification effect of stimulated emission can be reduced or entirely suppressed in a medium where too many laser-active atoms are in the lower state of the laser transition, because these atoms absorb photons and thus attenuate light. The spontaneous emission followed by the stimulated emission (photon bouncing back from the mirror to the already excited active media) defines generally the amplified spontaneous emission (ASE).

2.4.4 Amplified spontaneous emission

Amplified spontaneous emission (ASE) [75] arises where the emitters are non-interacting and the spontaneous emission from one emitter is amplified as it propagates through a region containing an ensemble of other emitters [76].This cascade of emission from dye molecules is stimulated by the spontaneous emission from other emitting dipole molecules or dipole-dipole interacting molecules. The emitted photons, amplified by further coherent stimulated emission, are of the same frequency centered around the wavelength of the maximum gain. The dye molecules involved did not need a buildup cavity, a square shaped intense pump pulse in a single pass waveguide was sufficient for the narrowing of the fluorescence maximum wavelength. The increase in ASE is a function of the incident intensity.

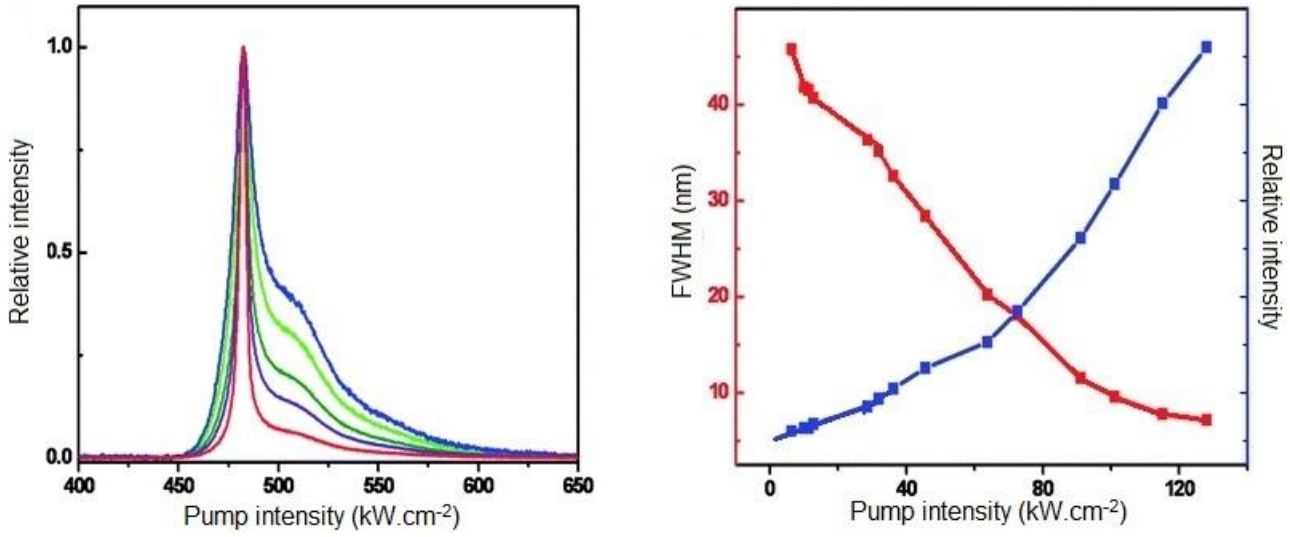

(a) (b)

***Figure 21**: a) The ASE phenomenon represented as the fluorescence emission (from blue to red) function of the increasing exciting pump power. b) The full width at half maximum (FWHM) representing the narrowing of the emission range wavelength with the increasing exciting energy [77].*

Spontaneously stimulated fluorescence emission of optically pumped thin films leads to the spectral narrowing of fluorescence spectrum of organic luminescent dyes dissolved in polymer films as a potential source of monochromatic light. The optical waveguide formed confines the emitted light within the films making possible stimulated emission (SE) processes which results in gain narrowing of the emission spectra and as for the amplified spontaneous emission [78] represented in red **Figure 21 (a)**. Different dyes doped to various classes of polymeric films demonstrated good results [79] in the line narrowing of the photoluminescence (PL) with increasing incoming pump energy and confirmed low threshold [80] values corresponding to the lasing of the material.

With the development of laser equipment and technics [81, 82], interest towards organic semiconductor materials as active materials in solid-state organic laser device and in the field of light-emitting diodes (LED), went growing since then to replace inorganic materials usually very expensive to make and difficultly recyclable. Lately several studies were conducted with organic molecules such as π-conjugated polymers like polyfluorene [83], fluorene derivatives [84], polyphenylenevinylene [85, 86], polythiophene derivatives and polyphenylen [87], for realizing light-emitting diodes. Attractive results were achieved with low threshold values (around $3\mu J/cm^2$), acceptable photostability and low cost processing as well as tunable spectral range.

Among most promising materials are diketopyrrolopyrrole (DPP) derivatives and their luminescence in solution was described in our previous work and enhance large wavelength range tunability [19], high quantum yields [88], large stokes shifts [89] and good chemical stability [90].

Moreover the *N*-substitution with alkylated groups on DPP derivatives concerned by this study affords a better solubility of these molecules which is a crucial point for the making of thin films from solutions.

The light amplification in PMMA doped DPP derivatives have been studied [91] and the photopumping of its thin films leaded to the narrowing of the full width at half maximum (FWHM) of the emission spectra while increasing the incoming pump intensity like seen in **Figure 21 (b)**. However these molecules showed photodegrading characteristic similar to that of Rhodamine B (Rh B) when PMMA was used as a hosting matrix [92].

The ASE phenomenon is observed along the thin layer waveguide excited perpendicularly by the laser pump incident beam [93] like shown in **Figure 22**.

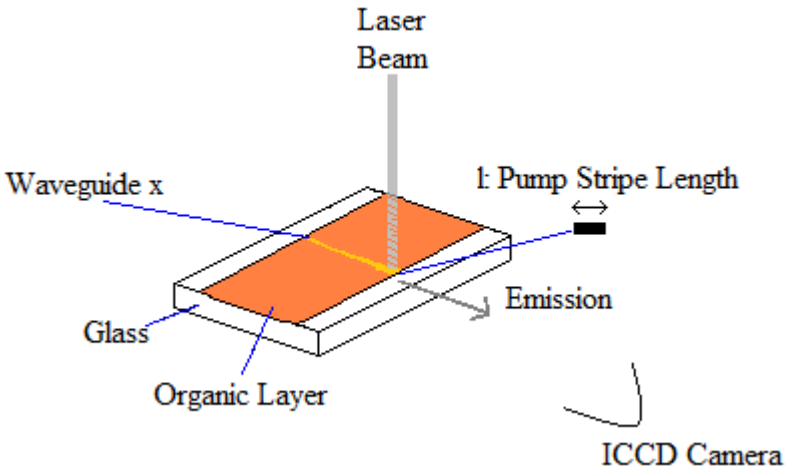

***Figure 22**: Solid state laser with newly synthesized pigment thin layer.*

ASE is a one-pass amplification that arises when there is no feedback to establish lasing and its role has also been considered as to have cooperative emission processes. Lasing occurs with feedback provided by waveguiding (along x axes) in the thin film. The line narrowing phenomenon seen in **Figure 21 (a)** is well documented but still subjected to discussions as many other processes are to be taken into account like amplified spontaneous emission (ASE), lasing, superradiance (SR) and superfluorescence (SF). Super Radiance (SR) and Super Fluorescence (SF) [94] are distinct cooperative emission processes distinguished by the way in which the cooperative state is established. Both effects arise through the dipole coupling of an ensemble of emitters. The coupling leads to the establishment of a super dipole transition moment that gives rise to an intense, spectrally narrowed and short time duration coherent emission.

ASE and SF are processes that are expected to coexist in competition with each other and they

may be considered to be extremes of a continuous range of processes.

2.4.4.1 Net gain

Laser beam is produced by excited dye molecules (pumped molecules) that undergo spontaneous emission producing photons resonating as coherent monochromatic directional light. The more we limit the loss by scattering or reabsorption effect, the better the gain is. The gain depends on both wavelength and incident beam intensity and is expressed as the logarithm of the ratio of photons emitted on the absorbed ones [95]. So when the gain exceeds the loss, gain material starts lasing by an increase in the number of emitted photons.

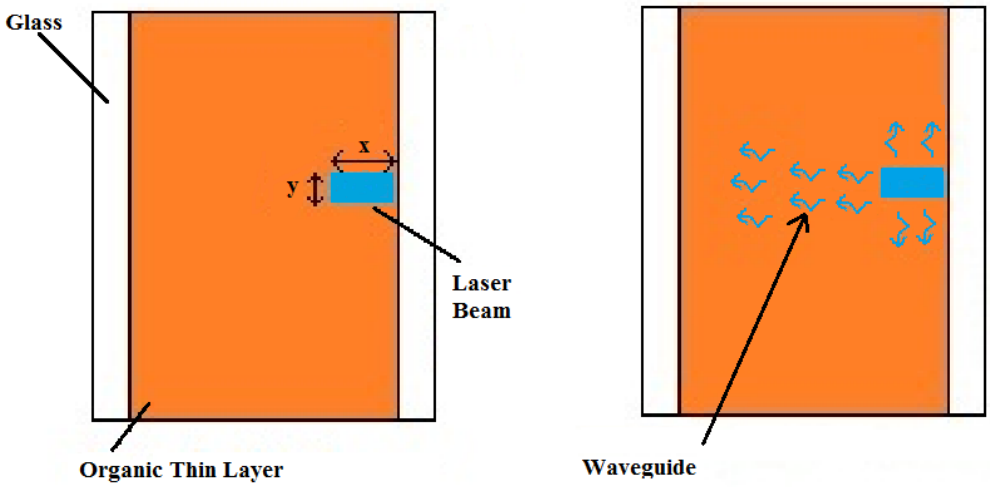

***Figure 23**: Organic thin layer pumping and wave guiding process.*

Like shown in **Figure 23** a shaped determined surface was pumped (shaped beam) along the x axes of the waveguide thin layer material. The gain was measured and obtained with **Equation 4** by keeping all settings constant changing only the shape of the beam along the x axes and measuring the ASE's intensity for different values of x.

$$I_{\mathrm{ASE}} = \frac{A_{(\lambda)} I_{(P)}}{g_{(\lambda)}} \left(\mathrm{e}^{g(\lambda) l} - 1 \right) \qquad (4)$$

Where I_{ASE} is the amplified spontaneous emission intensity at a sample edge, $A(\lambda)\ I(p)$ defines the spontaneous emission proportional to the pump energy, l is the length of the pump stripe, and g(λ) is the net gain coefficient. The output intensity from the sample edge is given by **Equation 5** [81].

$$I_{out} = I_0 \exp(-\alpha x) \quad (5)$$

where, x is the length of the unexcited region between the end of the excitation strip and the edge of the sample, I_0 is the output intensity at x=0, and α is the loss coefficient of the waveguide.

2.5 Summary

The chemical background of DPP derivatives, their synthesis as well as their field of applications were described. A particular attention was also given to the physical processes involved in this study like the single photon absorption, the two photon absorption and the amplified spontaneous emission. DPP derivatives with different chemical structure were selected accordingly to the process studied and their physical properties were determined with methods that shall be described in following chapter.

3 Experimental part

Hereby we present the DPP derivatives involved in this work and later describe the apparatus and methods used for the purpose of this study divided into three main topics concerning this thesis: Firstly we will present the molecules involved in this work followed by their two photon absorption and finally their amplified spontaneous emission study.

At first, we shall present the chemical structure of the molecules under optical investigation, their synthesis and chemical determination, followed by the optical methods, experimental settings and devices used for their optical study.

3.1 DPP materials studied

Diphenyl-Diketo-Pyrrolopyrrole derivatives commonly referred to as DPPs can be easily modified by chemical substitution in position R_1, R_2, R_3 and R_4 (**Figure 24**) modifying their electronic properties by effect of electro-donating (blue arrows) and electro-attracting (green arrows) pendent groups.

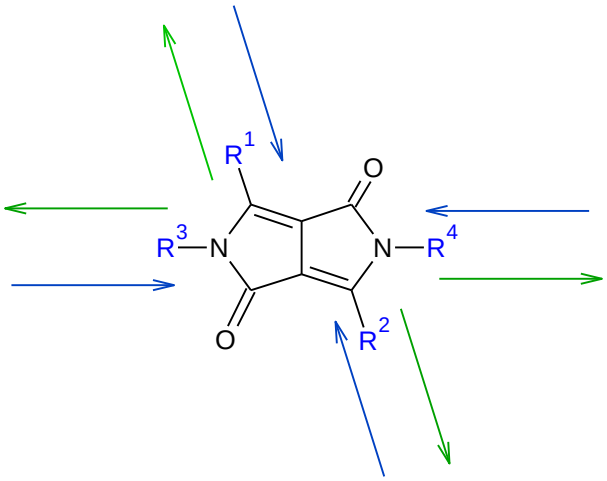

***Figure 24**: General scheme of DPP derivatives and pendent group's electronic effects.*

The main task of this work was to investigate the optical properties of organic low molecular materials like newly synthetized diphenyl-diketo-pyrrolopyrrole derivatives and to correlate these results with their chemical structure for further optimization. These molecules present potential advantages like high efficiency, versatility in their application (flexibility, transparency), low weight, cheap production and environmental friendly [96]. Except the pioneering work of

Langhals [97], there is a limited knowledge of the relation that is between the chemical structures and the optical properties of DPPs. These derivatives can be then modified to suite the best latest modern technologies with high efficient and low consuming optoelectronic devices like lasers, OLED, modern lightning or parts of solar cells with low coast fabrication, switchable, miniaturized and easily recyclable.

3.1.1 Synthesis of new DPP derivatives

New DPP derivatives were prepared by nucleophilic aromatic substitution using 1-fluoro-2,4-dinitrobenzene in presence of potassium carbonate in DMF like see in **Figure 25** bellow. The synthesis of N,N'-arylated DPP derivatives is a one-step reaction but mono N-arylated products were not isolated. The process is complicated because of extremely low solubility of starting derivatives. Reaction progress was monitored by TLC. According to TLC and 1H NMR, it is obvious that a significant amount of starting material remains in reaction mixtures even after several days.

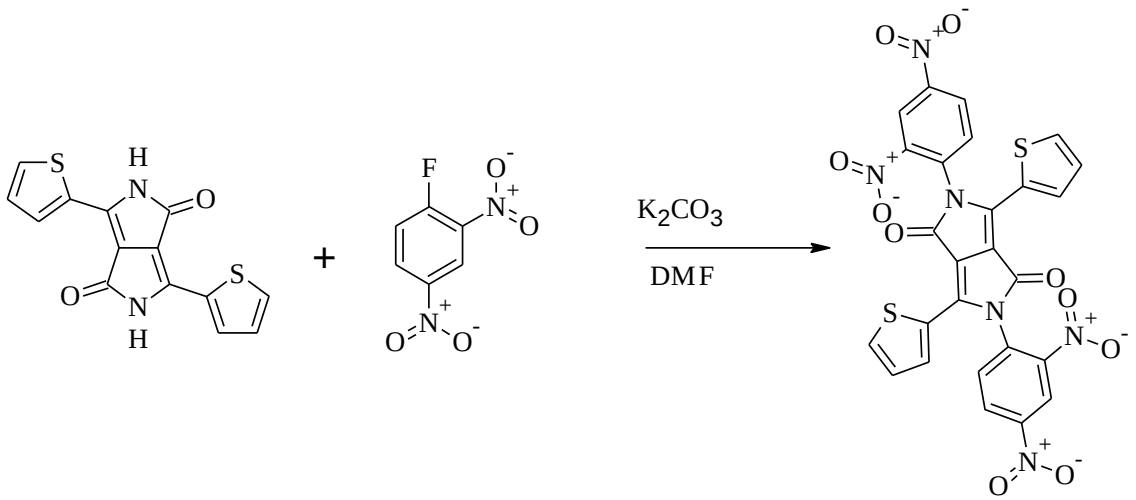

***Figure 25** : Synthesis reaction of 2,5-Bis(2,4-dinitrophenyl)-3,6-diphenylpyrrolo[3,4-c]pyrrole-1,4(2H,5H)-dione.*

The same protocol was used for the N-Arylation of other DPP derivatives represented here in **Table 2** here bellow.

***Table 2**: New DPP derivatives synthetized by N-Arylation.*

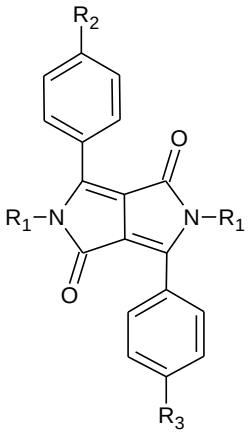	**R_1**	**R_2**	**R_3**
	Dinitrophenyl	H	H
	Dinitrophenyl		H
	Dinitrophenyl		
	Dinitrophenyl	CN	

1-Fluoro-2,4-dinitrobenzene and potassium carbonate were purchased from Sigma-Aldrich. N,N-dimethylformamide (Sigma-Aldrich) was dried by azeotropic distillation with benzene (10% v/v). Acetone, dichloromethane (DCM), petroleum ether and ethyl acetate (EA) were analytical grade purchased from Riedel-de-Haën and used without further purification. All chromatographic separations were carried out on silica gel 60 (220-440 mesh, Sigma-Aldrich).

This Erasmus project started earlier in France in the laboratory of Professor Jean-Philippe Bouillon (IRCOF, Université de Rouen, France) with whom we have initiated a collaboration work with the participation of Dr. Jozef Krajčovič (VUT- Brno University of Technology, Czech Republic). According to common recommendations we could provide suitable molecular structure [98] and we had also the privilege to supervise student's work and exchange between our universities for the purpose of their training courses. The synthesis presented in **Figure 25** and the optical properties (not presented in this work) were made in the laboratories of Professor Martin Weiter at the Brno University of Technology and synthetized by Melissa Oursel (Erasmus student).

3.2 Structural characterization

The synthesis, nuclear magnetic resonance and the mass spectrometry measurements were done in France at the University of Rouen under the direction of Professor Jean-Philippe Bouillon with the collaboration of Dr Jozef Krajčovič.

3.3 Absorption and emission spectra

The referred UV-Vis absorption spectra in solution were recorded using Varian Carry 50 UV-Vis spectrometer. Fluorescence measurements were also driven with:

- Excitation and fluorescence emission were made with a Thermo Spectronic AMINCO Bowman Series 2 luminescence spectrometer (model FA-357).
- Excitation and fluorescence emission were confirmed with a Fluorolog Spectrofluorometer via an excitation source composed with a 450 W xenon lamp and its power supply, inside a housing, a single-grating excitation monochromator, a T-format sample compartment with excitation reference detector, a single-grating emission monochromator and an emission photomultiplier tube with photon-counting detection.
- A LASER class IV was used as a strong excitation source, mainly for the amplified spontaneous emission and the two photon absorption experiments. The LASER was coupled with and Andor Shamrock SR-303i spectrograph iStar ICCD camera for the fluorescence spectra determination.

3.3.1 Lifetime fluorescence measurements

The fluorescence lifetime was measured using Andor Shamrock SR-303i spectrograph and Andor iStar ICCD camera. The samples were excited by first, second and third harmonic from EKSPLA PG400 Nd:YAG laser (1064, 532, 355 nm) with a 10Hz repetition rate. The temporal resolution of the system is approximately 25 ps. In order to avoid chromatic aberrations, the emitted light from the sample was collected by two off-axis mirrors.

The fluorescence lifetime was also measured with the Fluorocube: NanoLED wavelength from 260 nm up to 740 nm with working frequency of 1 MHz. The FluoroCube combines the latest miniaturized light source and detector technology with proven time correlated single photon counting (TCSPC) electronics.

3.3.2 Fluorescence quantum yield determination

The fluorescence quantum yields (ΦF) in solution were calculated according to the comparative method [99], where for each test sample gradient of integrated fluorescence intensity versus absorbance F=f(A) is used to calculate the ΦF using two known standards. The standards were previously cross-calibrated to verify the method. This calibration revealed accuracy about

5%. As the reference we used Rhodamine B [100] and Rhodamine 6G (Rh 6G) [101] with ΦFl 0.49 and 0.950±0.005, respectively. The excitation wavelength was chosen to be the same as for the laser excited experiments i.e. 532 nm. Since the II has very low absorption coefficient at this exciting wavelength, we used Fluorescein [102] (0.91±0.02) and Coumarin [103] (0.78) because of the better spectral overlap and excited at 460 nm.

The fluorescence quantum yields were also measured with a *Quanta*-φ integrating sphere part of the Fluorolog Spectrofluorometer from Horiba.

3.3.3 Computational procedures

The following computational measurements were done by Dr Alexander Kovalenko with whom were many discussions providing information concerning the organic point of view of the molecular aspect helping the bettering the calculations with prevised conditions. For the purpose of these measurements, the methods presented here below were used.

The quantum chemical calculations were performed by using Gaussian 09 software package (Gaussian 09 [104]). The ground state geometry was fully optimized using the Becke-style three-parameter hybrid correlation functional (B3LYP) [105], which have proven to be superior to the traditional functionals defined so far [88]. All structures were optimized with quadruple 6-311G(d,p) basis set. Same level of theory with wider basis set containing additional set of diffuse orbitals (6-311+G(d,p)) was applied in TD-DFT (time dependent density functional theory) calculations to analyze the electronic transitions in the discussed compounds.

The electronic structures of variously modified DPPs have been modeled using Gaussian 09 software package. For the ground state molecular confirmation was chosen the hybrid Hartree-Fock/Density Functional Theory method, which combines Becke's three-parameter exchange functional with the Lee-Yang-Paar correlation functional. Such method has been already successfully applied for the conformation study of various conjugated systems.

For the ground state geometry optimization and spectral calculations, quadruple 6-311G(d,p) Pople split-valence polarized basis sets for all atoms were used. The bond orders were characterized by the Wiberg bond indexes, which simply mean bond multiplicity – the number of valence electrons between atoms. The geometry optimizations and spectral calculations were carried out without any symmetry restriction.

Electronic excitations were calculated by time-dependent DFT (TD-DFT) at optimized geometries. TD-DFT is an extension of DFT determined to investigate the excited states and non-equilibrium properties of many-body systems in the presence of time-dependent potentials. This

method enables the analysis of the character and localization of individual excited states.
The UV-Vis absorption spectra of the considered DPPs were simulated using same B3LYP hybrid functional, but wider 6-311+G(d,p), Pople split-valence polarized basis sets basis set containing diffuse orbitals for all atoms except hydrogen, which is required for the excited states calculations.

3.4 Two photon absorption study

All DPP derivatives were prepared in solutions with a known concentration at approximatively 10^{-5} mole.L^{-1} to avoid reabsorption effects or low fluorescence intensity problems in case of too low concentration. As seen below in **Figure 26** the cuvette was placed on a sample handler positioned after a plano-convex and plano-concave lens placed at a specific distance so that the focal point of the incoming beam is focalized after the cuvette allowing a small conical section of the beam passing through the sample.

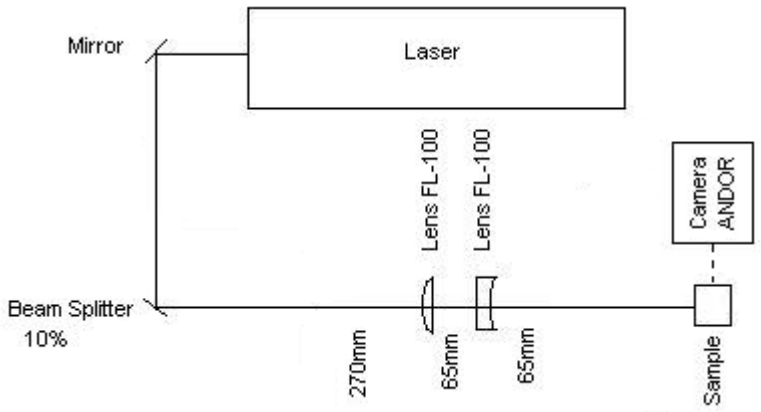

***Figure 26**: Montage scheme of optical bench for two photon absorption spectra measurments*.

The incoming energy from the laser had to be lowerd to afford accurate measurment of the non-linear absorption determination held at low energy. As for, we decreased the beam energy with beam splitters to finally concentrate that same beam just after the sample through focalizing lens into the middle of the handler allowing at that point a double photonic absorption of the excited area in the solution. The cuvette containing the sample was placed next to hyperbolic mirrors that collected the emission signal to be sent to the ICCD camera's detector.

3.5 Amplified spontaneous emission study

It is possible to make solid state lasers from doped polymers if stimulated emission plays the dominant role. In this work we used newly synthesized DPP derivatives as dopant in polymer. We mixed the DPP molecule with poly(methyl methacrylate) (PMMA) and polystyrene (PS) to form thin films by spin coating meant to be used as a laser media. We measured the ASE emission spectra from the end edges of the waveguide when the pump intensity and the pump stripe length varied. Most of the light is emitted from the ends of the strip and this is why we localized the pump stripe right up to the edge of the thin film so that we could collect the edge emission with an ICCD photon counting camera (ANDOR).

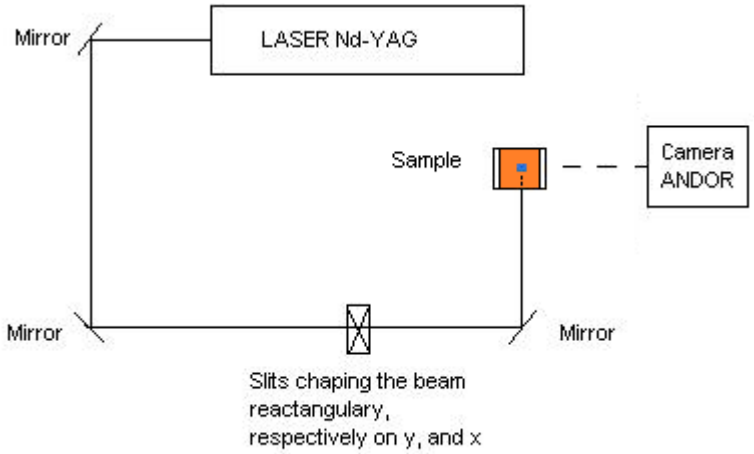

***Figure 27**: Montage scheme of optical bench for amplified spontaneous emission study.*

Figure 27 represents the optical table settings installed for the purpose of this experiment. The sample was placed before collecting hyperbolic mirrors placed before Andor ICCD camera and pumped with a laser beam emitted by a Nd-YAG LASER from EKSPLA. The ASE was obtained by shaping the incoming beam into a square of approximately 1mm high (h) and keeping its width (w) constant around 1.47 mm along the waveguide x represented in **Figure 28**.

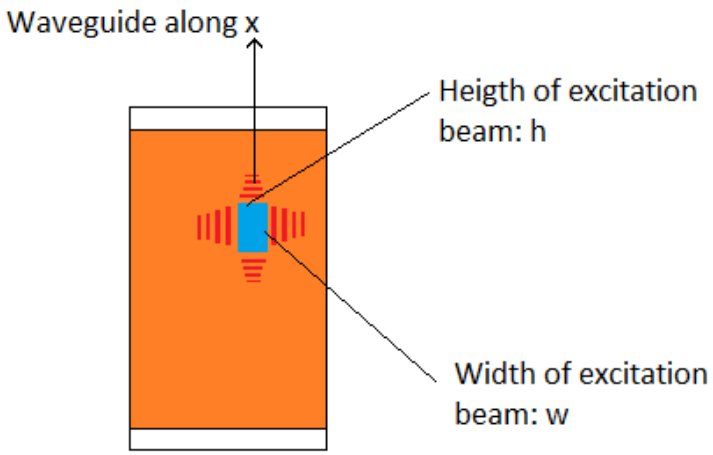

***Figure 28**: Quartz glass coated with a mixture of polymer with DPP pumped with a Nd:YAG laser at an excitation wavelength pulse of λ_{ex}=355nm.*

Most of the light is emitted from the ends of the strip; this is why we localized the pump stripe right up to the edge of the thin film so that we could collect the edge's emission with a photon counting camera placed along x. Thin layers were made by spin coating (1500tr/min, during 1min.) a mixture of 4mg of DPP mixed with 158mg of polystyrene (PS) solubilized in 1mL of chloroform. The thin layers samples were dried and placed on a sample holder at normal room temperature.

3.5.1 Thin layers thickness determination

The thickness of the thin layers was measured by CWL MicroProf® FRT optical surface measuring system. The samples for thickness measurement were prepared by scratching the film and aluminum films of about 100 nm was evaporated in vacuum to achieve similar reflection from both scratched and unscratched areas. The data were processed after film surface level correction. Every point was obtained as an average value of at least 10 measurements scanning the surface with a resolution of 1-1.5µm. This work was performed with the collaboration of Daniela Mladenova (Ph.D. student) and doc. Mgr. Ivaylo Zhivkov.

4 Results and discussion

This part of the work concerns the optical study of DPP derivatives according to classical absorption and emission spectra, which could provide suitable information concerning these materials according to their chemical properties and correlate the effect of their pendant groups on their luminescent properties. Newly synthesized DPP derivatives where investigated in liquid state like thin solid films. Spectroscopic properties were investigated throughout the following defined optical characterization: Simple absorption, two photon absorption and amplified spontaneous emission measurements.

The two photon absorption like the amplified spontaneous study of the following DPP derivatives will lead to new perspectives in modern applications. Results concerning their optical characterization previously presented will be discussed throughout following chapters.

4.1 *One photon absorption and fluorescence emission study*

DPP derivatives were developed with various structural modifications making them interesting as advanced materials for modern optical and electronic technologies. DPP derivatives **I - V** (**Table 3**) were prepared with moderate to high yields by *N*-alkylation with an excess of both alkylation agent (ethyl bromoacetate) and HBr neutralizing potassium carbonate. The substituted pyrrolinone nitrogens with alkylated or acylated substituents allowed their solubility enabling wet solution based processing. These DPP derivatives possess good solubility provided by the *N*-substitution; therefore they are estimated good candidates for the study of their one and two photon absorption process.

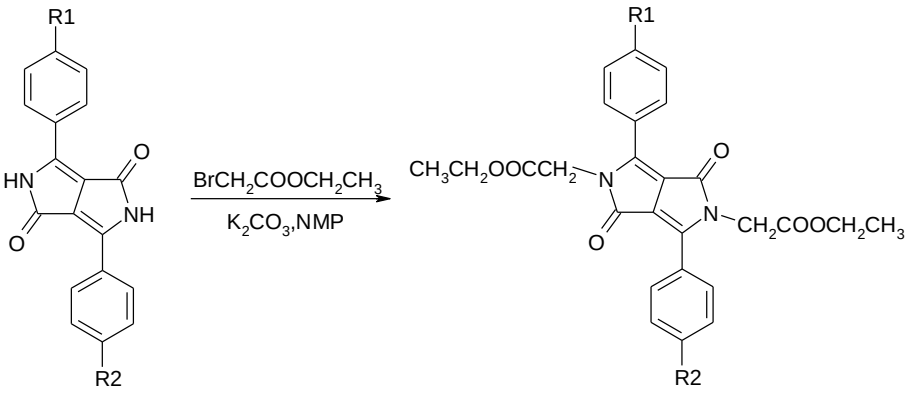

***Figure 29**: Synthesis reaction of N-alkylated DPP derivative.*

For the purpose of the one photon absorption study we have chosen symmetrically and unsymmetrically differently substituted DPP derivatives with donor or withdrawing groups on para position of pendent phenyls. In order to make these compounds better treatable they were substituted on pyrrolinone nitrogens to eliminate the intermolecular hydrogen bonding [36].

***Table 3**: DPP derivatives involved in the one and two PA study.*

Symbol	R_1	R_2	Symbol
Ip	H	H	**I**
IIp	CN	CN	**II**
IIIp	H		**III**
IVp			**IV**
Vp	CN		**V**

DPP derivatives involved in this process where *N*-substituted to afford a better solubility of these materials contrary to their non *N*-substituted precursor **Ip-Vp**. Compound **III** and **IV** were mono and bis substituted on para position of pendent phenyl with piperidine electron donating groups. Compound **II** was substituted on same position with nitrile withdrawing groups whereas compound **V** was unsymmetrically substituted with electron withdrawing nitrile and electron donating piperidine combining both effects. Compound **I** was the only one left unsubstituted on para penyl position but still taking benefit of the electron donating character of phenyl groups. The compounds are non-planar with phenyl rings rotated out of the diket-pyrrolo-pyrrole plane. The degree of this rotation is decreased by the electron-donating substituents, while increased by the electron-withdrawing groups.

Dimethyl sulfoxide (DMSO) was found to be the only common solvent able to dissolve all compound presented here above. Contrary to more usual N nucleophilic substitution on alkylhalogen [16], we applied in this case (**Figure 29**) the substitution on ethyl bromoacetate. Such substitution was reported only once resulting in compound **I** [106] giving thus a good chance to be highly soluble because of the absence of π-π stacking, another insolubility implicating phenomenon aside from CO-NH hydrogen bonding [107]. The compounds show good solubility over a wide range of solvents, so we have carried out the spectral measurements in DMSO, in

order to have direct comparison with our previous results obtained for non-alkylated DPP precursors **Ip** - **Vp** [19] or N-butylated analogues of **I** and **V** [16, 111], in polar aprotic solvents like acetonitrile and in almost non-polar toluene. One photon absorption (or one photon activation) (OPA), one photon excitation fluorescence (OPEF) spectra of **I** - **V** in DMSO (**Table 4**) and the spectral data in all three solvents are summarized together with fluorescence quantum yields (ϕ_F) and lifetimes (τ_F) in **Annex, Table 9.4.1-2**.

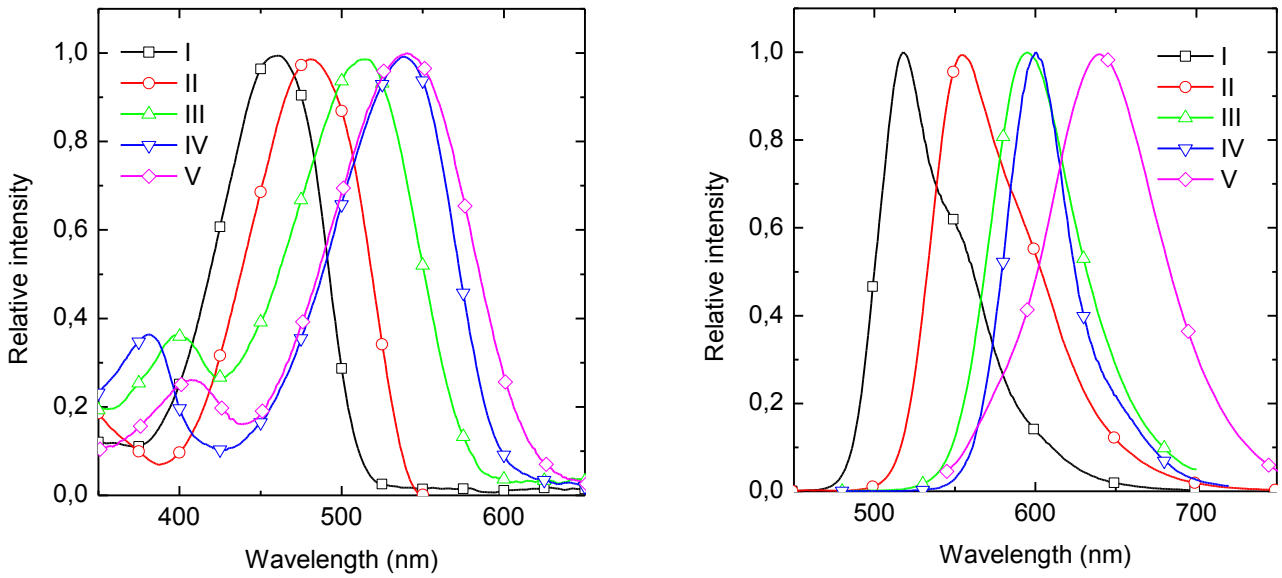

***Figure 30**: Normalized OPA (a) and OPEF (b) spectra of DPP I-V in DMSO.*

The absorption maxima of **I** - **V** in DMSO (**Figure 30)** show hypsochromic and hypochromic shifts with respect to corresponding precursors **Ip** - **Vp** [19]. It was impossible to measure the absorption and fluorescence solvatochromism of **Ip** – **Vp** because of their insolubility in other than highly polar solvents. The highest hypsochromic shift was found for bis-electron-acceptor substituted on phenyl position **II** (59 nm) and rather lower for unsubstituted on phenyl position **I** (45 nm). On the other hand the lowest hypsochromic shift was observed for bis- and mono-electron-donor substituted **IV** (20 nm) and **III** (24 nm), while the shift of unsymmetrical compound **V** (35 nm) with both types of substituents lies between the symmetrically substituted **II** and **IV**. Although solute – solvent interaction may play some role and we relate this behavior mainly to the dependence of the dihedral angle describing the phenyl-pyrrolinone rotation on a nature of para substituent of this pendant phenyl. The hypsochromic shift of **I** and **IV** are slightly higher than for N,N–dibutylated [17] implicating that -$CH_2COOCH_2CH_3$ grouping is sterically

rather more efficient than $-CH_2CH_2CH_2CH_3$ with respect to above discussed sterically induced phenyl rotation in the ground electronic state.

***Table 4**: The spectroscopic properties of I - V in DMSO.*

DPPs	λ_A (nm)	$\varepsilon(\lambda_A)$ ($dm^3\ mol^{-1}\ cm^{-1}$)	λ_F (nm)	ϕ_F	$\Delta\lambda_{Stokes}$ (nm)	τ_F (ns)
I	460	15800	519	0.56±0.18	59	7.34±0.08
II	480	13300	557	0.72±0.03	77	6.50±0.04
III	516	32200	601	0.12±0.02	85	1.17±0.02 6.7±1.2
IV	540	45100	603	0.45±0.02	63	3.45
V	541	42300	654	<0.01	113	0.217±0.002 3.72±0.10

The relation between the position of fluorescence maxima of the corresponding members of *N*-alkylated and non-alkylated sets is sharply different from absorption. The maxima of *para* unsubstituted **Ip** with respect to **I** are almost the same (+2 nm on behalf of **I**), while **II** shows hypsofluoric shift with respect to IIp (-8 nm). *N*,*N*-dialkylated electron-donor substituted derivatives **III** (+14 nm) and **IV** (+15 nm) show moderate bathofluoric shifts as compared to $\mathbf{III_p}$ and **IV**, respectively. Push-pull derivative **V** shows almost identical maximum as **V** (the difference is +1 nm), i.e. its value lies between **IIp**/**II** and **IVp**/**IV** pairs as in absorption. As a consequence the Stokes shift of compound **V** is absolutely the highest one (113 nm) but it mainly comes from push-pull substitution, i.e. compound **Vp** (77.5 nm). An increment of a Stokes shift increase connected with N,N-disubstitution is relatively similar for all compounds, i.e. 35 – 39 nm for all three pairs of piperidino substituted compounds and rather higher for both **Ip**/**I** (48 nm) and **IIp**/**II** (51 nm) pair, which is probably the most distorted in the ground state and thus the highest geometrical reorganization in the fluorescent excited state is expectable.

Polar substituents generally decrease the fluorescence quantum yields of non-alkylated precursors **Ip** – **Vp** like in DMSO, but even the lowest value of ϕ_F for compound **Vp** was higher than 0.1. The similar behaviour of *N*-alkylated derivatives **I** – **V** was observed in non-polar toluene (**Tab. 3c Annex**). In both cases the monoexponential decay is observed. When going to polar solvents there

is a dramatic change for compounds **III** and **V**. Their quantum yields of fluorescence are significantly decreased, especially for **V** (**Table 4**), and the decay is biexponential. Recent publication describes the syntheses and spectral properties of basic DPP derivative 3,6-diphenyl-2,5-dihydro-pyrrolo[3,4-*c*]pyrrole-1,4-dione (**Ip**) and its electron-donor (piperidino) and electron-acceptor (cyano) symmetrically and unsymmetrically substituted derivatives (**IIp** – **Vp**) [19].

4.2 Summary

The derivatives have shown bathochromic and hyperchromic shift of OPA and bathofluoric shift of one-photon excited fluorescence (OPEF) with respect to parent molecules **Ip** invoked above containing piperidino electron donating substituent. With results provided earlier, we have chosen proper *N*-substituted derivatives **I** – **V** as candidates for the following two photon absorption study.

4.3 Two photon absorption

Five alkylated soluble DPP derivatives **I** – **V** with polar substituents in para position of pendant phenyls were synthetized and their absorption like emissive properties were determined earlier in order to insure that they are good candidates for the two photon absorption study. These molecules according to earlier described optical properties should provide reasonably high two photon cross section values. The TPA cross section shall be determined in order to compare these DPPs derivatives according to their chemical structure.

As one of the reference molecule for the cross section calculation we measured the TPA of Rhodamine B and the integrated fluorescence spectra vs the incoming exciting light power are plotted in **Figure 31** here bellow. At low incoming power intensity we can clearly notice the non-linear emissive properties of reference molecule Rhodamine B.

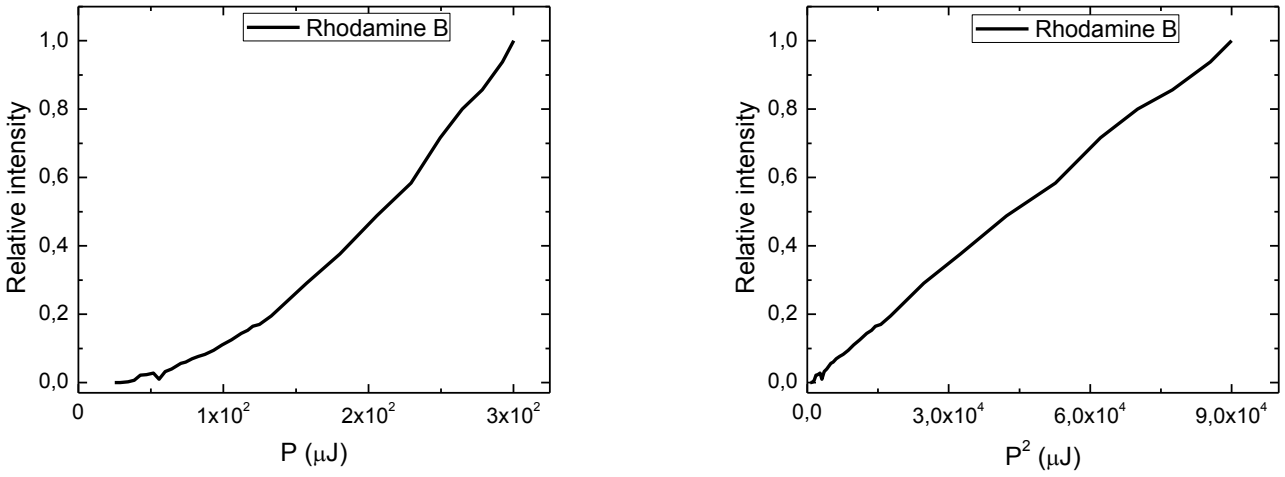

***Figure 31**: Two photon excitation fluorescence (TPEF) spectra of Rhodamine B with a) representing the integrated fluorescence intensity (F) versus the input excitation power (P) and b) representing F versus P^2.*

In our experiments, each of the fluorescence spectra used for integration consists of 500 accumulated measurements. The individual spectra were recorded a 100 ns after the laser pulse, i.e. long enough to collect every emitted photon incident on the detector.

We used two reference standards: Rhodamine B with $\sigma_{2PE} = 1.5 \times 10^{-50}$cm^{4}s [108] assuming **Equation 3** $\sigma_{2PA} = 3.1 \times 10^{-50}$cm^{4}s and Rhodamine 6G with $\sigma_{2PE} = 2.0 \times 10^{-50}$cm^{4}s [128] and consequently $\sigma_{2PA} = 2.1 \times 10^{-50}$cm^{4}s. The values of σ_{2PA} for DPP derivatives reported in **Table 5**

were calculated as the average from the results obtained using these two standards. In order to validate the power-squared dependence of the fluorescence signal we determined the logarithmic dependence of the fluorescence on the incident intensity $\log F = m \log I$ for all of the studied materials.

***Table 5**: Slope (m) in the logarithmic plot of fluorescence (F) versus the incident light intensity (I) logF = m logI.*

	Rh B	Rh 6G	I	II	III	IV	V
Slope	2,00	1,99	1,95	1,97	2,01	1,98	-

As can be seen from **Table 5** the deviation from perfect power-squared dependence did not exceeded ±2.5% indicating two-photon events in the ranges used for the analysis.

A typical fluorescence response to the laser intensity can be seen on **Figure 32** for DPP **III.**

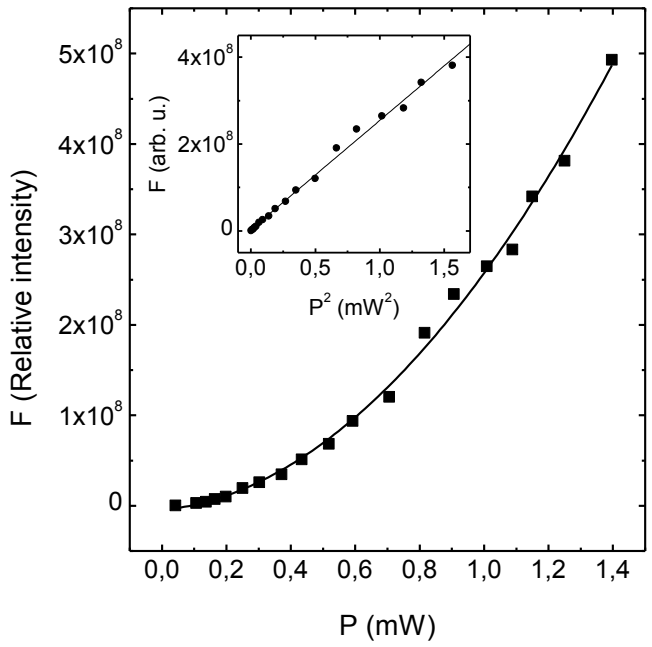

***Figure 32:** Typical response of the integrated fluorescence F on the incident light power P (here for DPP **III**). The inset shows linear fit to the F versus P^2 used for the TPEF calculations.*

Most of the compounds under study showed fluorescence caused by two-photon absorption in DMSO. The only exception is compound **V** probably due to very low ϕ_F.

Although unsubstituted N precursor **Vp** has shown significantly higher ϕ_F, its TPA was rather small in DMSO (σ_{2PA} = 0.66 ±0.13 GM). A comparison of OPEF and TPEF spectra of **II** in

DMSO at concentration of 1.10^{-5} mol l^{-1} is shown in **Figure 33**.

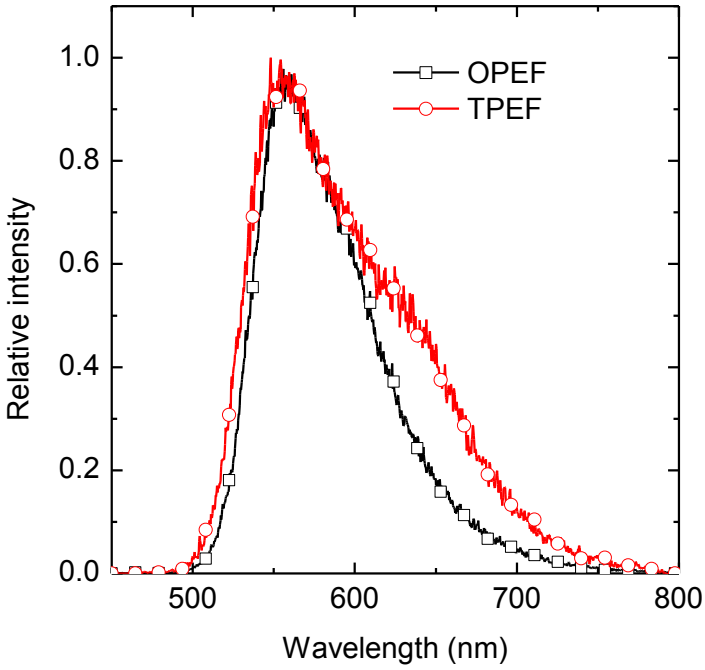

***Figure 33**: Normalized OPEF and TPEF spectra of **II**.*

The TPEF spectrum shows increased intensity at longer wavelengths near 650 nm compared to OPEF spectrum. Less pronounced, but detectable differences were also found for **III** and **IV**. However, completely different spectra for OPEF and TPEF were collected for compound **I** (**Figure 34**).

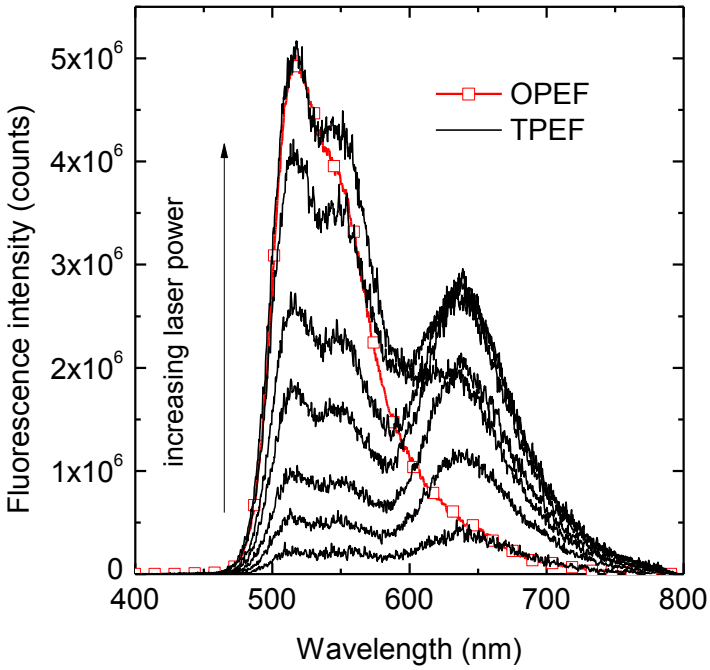

***Figure 34**: Normalized OPEF and TPEF spectra of **I**.*

We observed significant increase of the fluorescence intensity within the 600÷750 nm region with increasing intensity of excitation light. As the half of the excitation wavelength 1064 nm corresponds to the red edge of OPA spectrum of **II** and especially **I** one can only speculate, what are the entities or impurities that are excited by this strong source of light.

4.3.1 Two photon absorption cross section

The results of two photon experiments in DMSO are summarized in **Table 6**. Among the five compounds under study three ones either do not show any TPEF (**V**), or their one photon absorption does not significantly match the half of the only available excitation wavelength 1064 nm (**I**, **II**). On the other hand, compounds **III** and **IV**, which both show strong one photon absorption at 532 nm, afforded the TPA efficiency of great interest. Very high value of TPA cross section (1400±300 GM) was achieved for **III** which is hardly explainable considering piperidino group as only electron-donor and the central diketo-pyrrolo-pyrrole unit as a simple acceptor in D-π-A-π schematic pattern.

***Table 6**: Cross-section of two-photon absorption, emission and related parameters in DMSO.*

DPPs	λ_{2PF} (nm)	σ_{2PA} (GM)[a]	ε (532 nm) (dm^{-3} mol^{-1} cm^{-1})	σ_{2PE} (GM)
I	520	2,1±0,4	320	1,7±0,3
II	555	2,4±0,5	3500	1,7±0,3
III	594	1400±300	26000	170±30
IV	598	44±9	45000	20±4
V	-	-	-	-

It is rather difficult to compare the absolute values of σ_{2PA} obtained, mainly because of the dependence on a time profile of the experiment and probable contamination of TPA process by excited state absorption in transmission experiments [101]. From this point of view the values obtained by TPEF method can be generally considered as the most conservative, i.e. the lowest as compared to other methods, and they are often used in comparative reviews, if available [109]. With respect to the fact, that prior to 21st century no value higher than 100 GM was reported [101], and that the values over 1000 GM obtained by TPEF method are mostly obtained on molecules with a chain or branched conjugated system significantly extended with respect to 1,4-diphenyl-1.3-butadiene hydrocarbon backbone of DPP chromophore, the value σ_{2PA} for compound **III** can be considered here as surprisingly high.

The TPA cross-section of **IV** (44±9 GM at 1064 nm in DMSO) is more than an order of magnitude lower than for *N*-alkylated DPP derivative with both piperidine substituents replaced by diphenylamino groups (1200 GM at maximum in chloroform [7]). As a reaction to these results we have prepared its non-alkylated analogue, i.e. 3,6-bis(4-(diphenylamino)phenyl)-pyrrolo[3,4-c]pyrrole-1,4-dione, and we preliminary report its TPA cross-section to be 1100±200 GM at 1064 nm in DMSO, which means an even higher value at maximum than for its *N*,*N*-dialkylated derivative.

Thus it implies that the role of diphenylamino substitution is of primary importance in this case. All the more the high value of TPA cross-section for **III** without this efficient substituent is interesting. As we mentioned recently [110], the number of papers dealing with unsymmetrical DPPs is dramatically lower compared to the symmetrical ones, probably because of rather more complicated purification process during their synthesis. We expect, that the reported efficiency of TPA process in compound **III** will stimulate the investigation of further compounds of this type, necessary to explain these complicated phenomena and promising with respect to above mentioned future advanced technologies.

Diphenylamino monosubstituted DPP derivatives were recently finalized in our laboratory, and we expect by analogy, that joined effect of unsymmetrical substitution and diphenylamino donor group would improve the TPA cross-section. The optical properties of these diphenylamino monosubstituted DPPs (**annex 9.5**, **Table 9.5.1**) in DMSO and acetonitrile are presented in **annex** part **Table 9.5.2-3** and their nonlinear properties and ability to undergo TPA is demonstrated in **annex** part **Figure A4**.

4.3.2 Summary

These five *N*-alkylated DPP derivatives presented in this chapter were studied optically in liquid state and have demonstrated nonlinear absorption properties corresponding to their TPA and enhanced strong two-photon cross section. They have also provided precious information on possible more appropriate chemically structured DPPs.

4.4 DPP derivatives thin layers

Interest towards organic semiconductor materials as active materials in solid-state organic laser device and in the field of light-emitting diodes (LED) went growing to replace inorganic materials usually very expensive to make and difficultly recyclable. Luminescence of DiketoPyrroloPyrrole (DPP) derivatives in solution was described in previous chapter [16], [111], [17] and enhance large wavelength range tunability, high quantum yields and good chemical thermo stability [90].

4.4.1 Solid state fluorescence

All five DPP derivatives **I-V** under study show pronounced solid state fluorescence, on the contrary to any of their non-alkylated precursors $\mathbf{I_p}$ **-** $\mathbf{V_p}$. Generally, the solid state fluorescence of organic pigments is considered as a property of individual molecule conserved in crystal phase [112].

***Figure 35**: Polycrystalline photos of DPP **I** to **V** made under daylight with a Panasonic DMC-FZ7 camera.*

Figure 35 represents photos taken in the laboratory of DPP derivatives in solid state involved in the two photon absorption study just before solubilizing them for the purpose of their analysis.

All studied DPP derivatives show pronounced solid-state fluorescence, on the contrary to any of their non-alkylated precursors $\mathbf{I_p}$ to $\mathbf{VI_p}$. The fluorescence of symmetrical **I**, **II** and **IV** is strong, easily observable by naked eye under UV irradiation (**Figure 7**). The fluorescence of

unsymmetrical **VIII** and **X** is less intense, but observable. Solid-state fluorescence of push-pull derivative **XII** is almost not observable (and totally undetectable by a camera) partly because of its significantly lower intensity and also as it falls almost fully into the infrared region. Their fluorescence spectra in solid state are shown in **Figure 36** and the wide emissive wave range corresponds with the one observed in the liquid state.

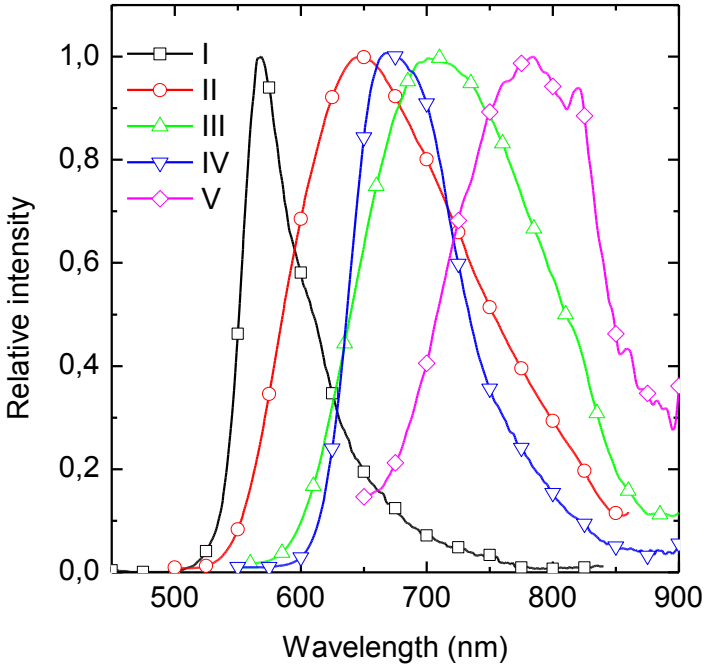

***Figure 36**: Solid state fluorescence of DPPs under study*

The fluorescence of symmetrical DPP **I**, **II**, **IV** is strong, easily observable by naked eye under UV irradiation like seen in **Figure 37**. The fluorescence of unsymmetrical DPP **III** is less intense but still observable unlike DPP **V** which is almost not observable and totally undetectable by the camera.

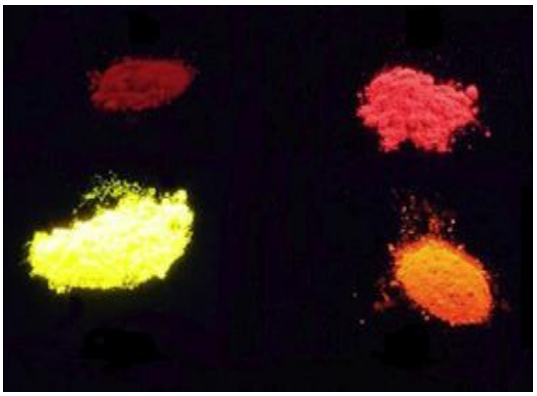

***Figure 37:** Polycrystalline samples (from top left-to bottom right) of DPP **III**, **IV**, **I** and **II** under UV irradiation (365 nm) with a Panasonic DMC-FZ7 camera.*

We can notice that molecules **II** and **IV** studied correspond respectively to molecules **IX** and **VIII** used for the following study of their optical properties in solid state in the form of thin layers. The DPP derivatives involved in the following study possess good emissive properties like high quantum yields, large stokes shift, high molecular coefficient of absorption and already reported [16, 88, 89] in articles. DPP molecules with good solubility provided by the *N*-substitution, high quantum yields and short fluorescence lifetime are estimated good candidates for the study of their amplified spontaneous emission process.

4.4.2 DPP derivatives used for the ASE study

In **Table 7** are represented the DPP derivatives which underwent amplified spontaneous emission and for which were collected data results are discussed below. Comparing DPP derivatives differently substituted could lead to a better understanding of the push and pull effects on DPP core and their planarity with phenyl rings rotated out of the diketo-pyrrolo-pyrrole plane [88].

In this work we studied the luminescence in thin layer of *N*-alkylated DPP derivatives differently substituted on para position of phenyl with electro donating functionalizing groups, demonstrated a good stabilization of the ASE phenomenon in polystyrene (PS) matrix and tried to compare the effect of their side groups on its amplified emission. The goal of this work was to obtain a stable ASE signal for our differently substituted DPP derivatives and retrieve their ASE threshold values.

***Table 7**: DPP derivatives involved in the amplified spontaneous emission study*

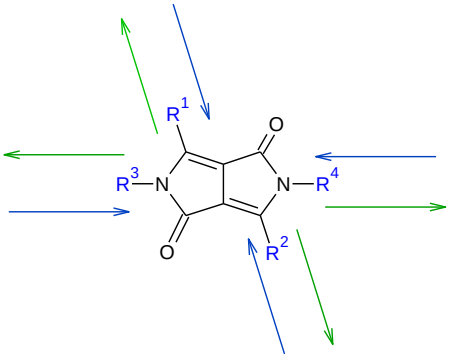

DPP	R_1	R_2	R_3	R_4
VI	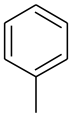	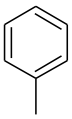	C_7H_{15}	C_7H_{15}
VII	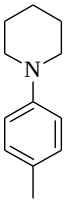	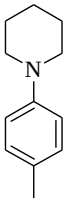	C_4H_9	C_4H_9
VIII	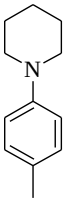	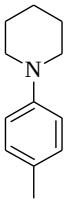		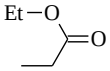
IX	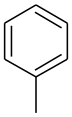	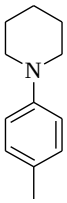		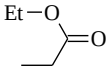
X	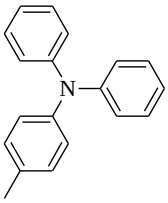	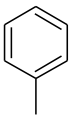		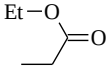

Spectral emissive and absorptive properties of DPP **VII**-PS presented in **Figure 38** were determined before the threshold determination for the amplified spontaneous emission measurements. The absorption spectra of DPP-PS was obtained by placing the glass samples at an angle of 45° according to the incoming light and out coming to detector avoiding the 90° angle mostly used for the ASE determination. The same method was used to determine the normal fluorescence emission collected by an ICCD camera using a 355 nm wavelength excitation light. Theoretical absorption of these DPP derivatives is represented in **annex 9.3** and correlate with our following results.

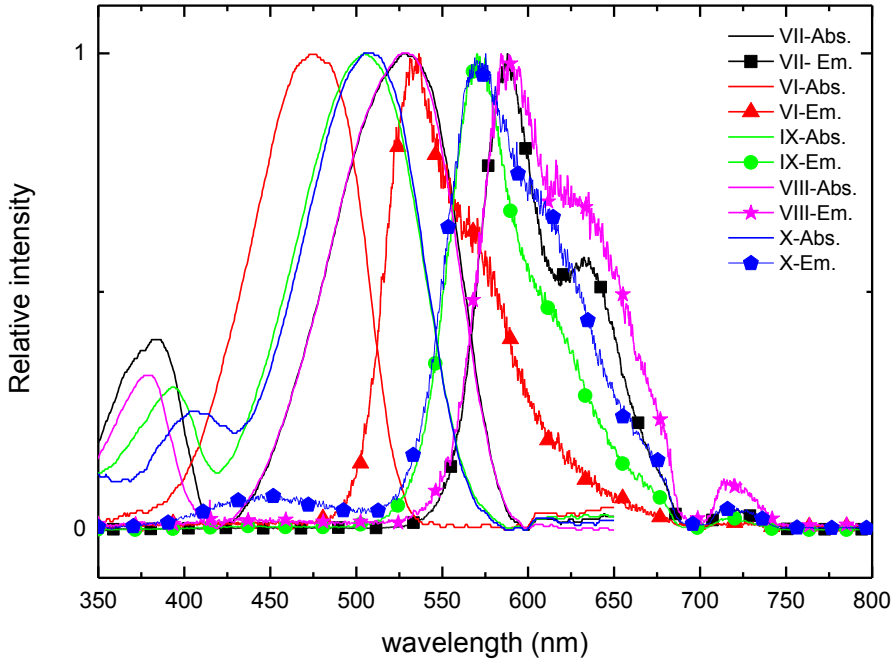

***Figure 38**: Absorption and emission spectra of thin layers of DPP derivatives mixed with PS.*

The absorption region of DPP **VII**-PS thin film is relatively broad and presents a first maxima at λ_{abs} =384 nm and a second higher at λ_{abs} =528 nm. Its emission at λ_{em} =578 nm is also wide and the luminescence band of the FWHM is around 100 nm. Compared to DPP **VI** (λ_{abs} =475 nm) the change of the peak position of the maximum absorption to higher wavelength was achieved when using piperidin substituents on phenyl groups like for DPP **VIII**, **IX and X** with absorption around respectively λ_{abs} =537nm, λ_{abs} =504 nm, λ_{abs} =508nm. PL of DPP **VI** and **VIII** are also wide with a maximum peak around respectively 533 and 590 nm. Nous constatons une différence de 30 nm (constante coïncidence) entre la seconde transition électronique et l'émission ASE.

Using electron-donating groups, hyperchromic and bathochromic shift in absorption was also observed in earlier study [16].

4.4.3 Summary

The *N*-alkylation of these DPP had minor impact on the values of the emission or the absorption spectra but helped with their solubility in polar solvent. This was accompanied by the hypsochromic shift and blurring of the vibration structure. In this study we could observe this same behavior of the shift in absorption in the solid state of DPP **VII** compared to the other non-symmetric derivative DPP **IX** and **X**. DPP **VIII**, **IX** and **X** were *N*-acylated with the same substituents but only DPP **IX**, **X** possesses the same non-symmetry of pendent groups R_1 and R_2.

4.5 Amplified spontaneous emission study

Among other materials, the light amplification in PMMA doped DPP derivatives have been studied [113] and the photopumping of its thin films leaded to the narrowing of the full width at half maximum (FWHM) of the emission spectra while increasing the incoming pump intensity. However these molecules showed photodegrading characteristic similar to that of Rhodamine B when PMMA was used as a waveguide matrix like described in the literature [114]. The main difficulty in this task was to perform from DPP mixed polymer thin layer a stable ASE signal in time without undergoing any photo degradation or alteration which would provoke the loss of the ASE signal.

The following part of the study aims on analyzing the ASE properties of some synthesized DiketoPyrroloPyrrole (DPP) derivatives. These molecules were substituted by donating groups "push" type, like piperidine (DPP **VII**, **VIII** and **IX**) or diphenyl amine (DPP **X**) attached on (para) phenyl position of the DDP core. Therefore we could afford symmetrical and unsymmetrical derivatives that were then mixed with a polymer to prepare homogenous thin layers. The DPPs were doped in hosting transparent polymers and their thin film layers were then pumped with a picosecond pulsed laser. By using known techniques developed for inorganic laser materials, we achieved amplified spontaneous emission (ASE) of these compounds to be used further on in solid state laser and we studied and compared results for differently substituted DPP derivatives. The results demonstrated that these dye molecules are potentially good candidates to be used as organic laser dyes as we have proven an accurate lasing threshold rate leading to their amplified spontaneous emission (**Figure 39** curve in green).

To provide evidence of ASE one has to establish the intrinsic relation between the incoming pump energy and emission output intensity compared with the narrowing emission of the full-width at half maximum.

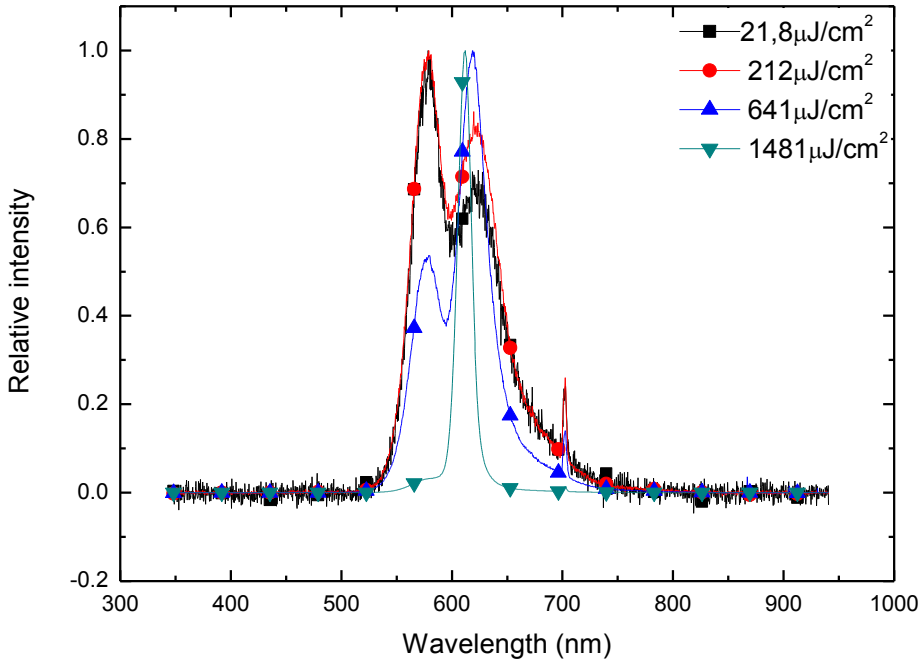

***Figure 39**: Normalized emission intensity of DPP **VII**-PS collected, at the waveguide edge with a determined excitation stripe and at increasing pump intensities.*

In this experiment the light emitted from the edge of the film at constant pump strip length but growing income energy was measured. The narrowing of the emission spectra of DPP **VII**-PS with increasing pump energy is well observed in **Figure 39**. Higher incoming intensity gets the emission maxima narrower at λASE = 612 nm and the FWHM value decreases from 100 nm to 16 nm. Same experimental mode was used to determine the maximum ASE emission value for DPP **VI**, **IX**, **VIII** and **X** and was determined respectively at λASE= 602 nm, 626 nm, 659 nm and 641 nm.

Light amplification by stimulated emission of radiation in a resonator is determined by these means [115]: 1st- the narrowing linewidth emission, 2nd- light output consist of a beam, 3rd- clear threshold in both the output power and the linewidth, 4th- light emission is characteristic of the specific gain medium and resonator.

By plotting the dependency of the full width at half maximum and the total emission intensity integrated over all wavelengths versus the growing pump intensity we could determine the threshold corresponding to the start of the lasing process. The curve with the red squares in **Figure 40**, showing the evolution of the FWHM with its values represented on the right axis, decreases at incoming energy around 0,15 μJ corresponding to lasing start.

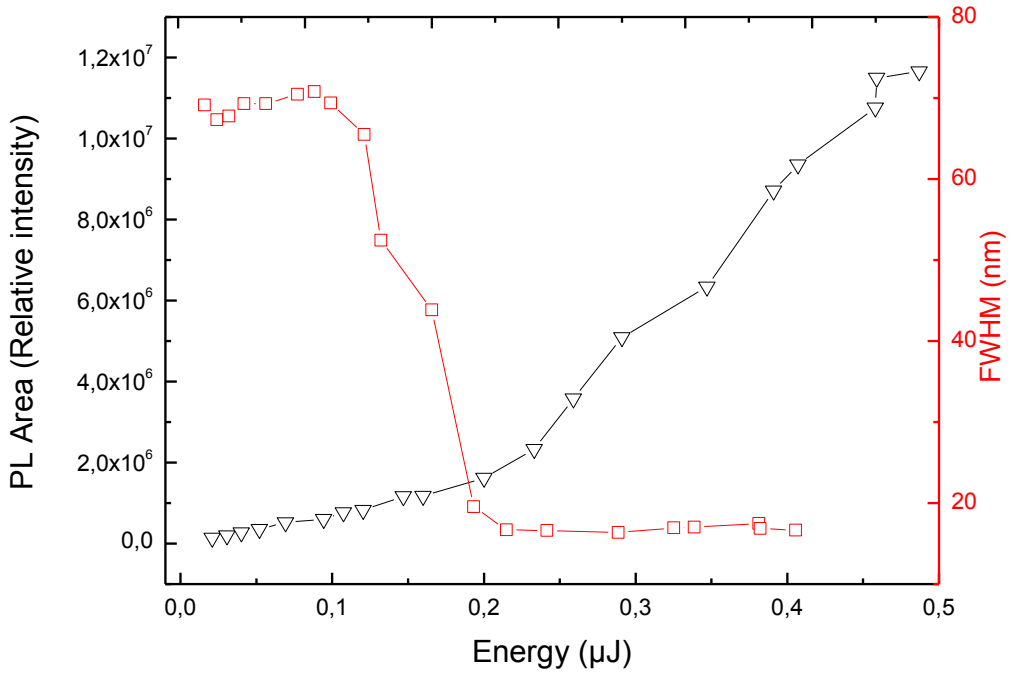

***Figure 40**: Dependency of the FWHM of the emission versus the incoming pump intensity (red squares) and total emission intensity integrated over all wavelength vs pump intensity (black triangles) for DPP29-PS.*

The curve with black triangles exhibits an exponential growth of the photoluminescence, with the incoming energy around 0,2 µJ, after the start of the lasing. From these two curves we could calculate and estimate the threshold energy for DPP **VII** with ρ_{th}= 28 µJ/cm^2. Higher values of threshold were determined for DPP **VI** and **IX** respectively ρ_{th}= 63 µJ/cm^2 and ρ_{th}= 79 µJ/cm^2.

4.5.1 Electron distribution contribution to ASE

Organic molecules concerned with ASE process are usually composed of π-conjugated systems which usually provide good electron delocalization. Moreover all DPP derivatives used for the purpose of this study were *N*-alkylated or Acylated because of their better solubility. The *N*-alkylation or acylation of DPP in solution providing a tertiary amine did not have a consequent impact on the phenyl torsion [16] at the ground state. With the *N*-alkylation the difference between the torsion angle in the ground and excited state is bigger in the point of view of the phenyl torsion angle making the molecule vibrate more. With N-ester function the torsion angle is smaller so the molecule is vibrating less favoring the conjugation in the molecule, therefore allowing electron transfer. Also a smaller rotation of the phenyl betters the conjugation as the molecule encounters planarity and favorites also the electron transfer which in our case is not so advantageous.

The piperidin donor group pushes the electron density toward the DPP core through the pi-conjugation of phenyl localizing and confining the electron cloud inside the DPP center unit.

Providing donating group concentrates the electronic density into the DPP core in the ground like in the excited state keeping it localized. The donating effect of the substituents on phenyl provides essentially a longer distribution more homogeneous in space and reduces the torsion angle. The specific localization of electron in space especially for non-symmetrical DPP **IX** constrained in the excited state as a localized particle which provokes a bigger energy loss and higher stock shift. However DPP **VI** is not substituted on phenyl by donating piperidin groups which is normally an advantage for the fluorescence processes but its electronic cloud is better contained as it is symmetrically substituted by phenyl groups unlike unsymmetrically mono substituted DPP **IX** with piperidin. Non symmetrical character of the DPP causes the reorganization of the electronic distribution like seen in **Figure 41(b)** bellow in the excited state, which in its turn results in energy losses not favorable for the fluorescence.

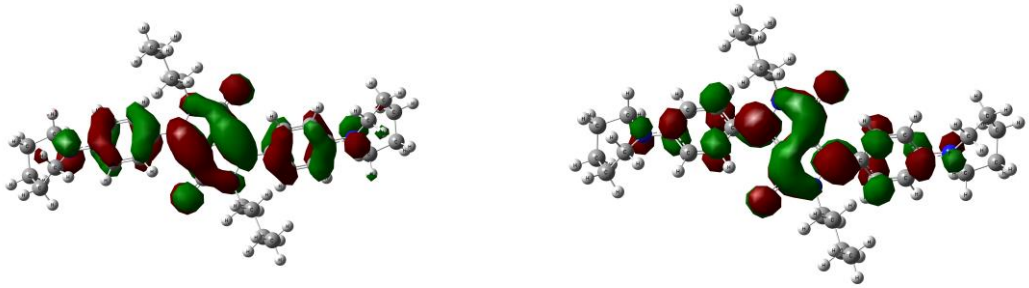

HOMO LUMO

(a)

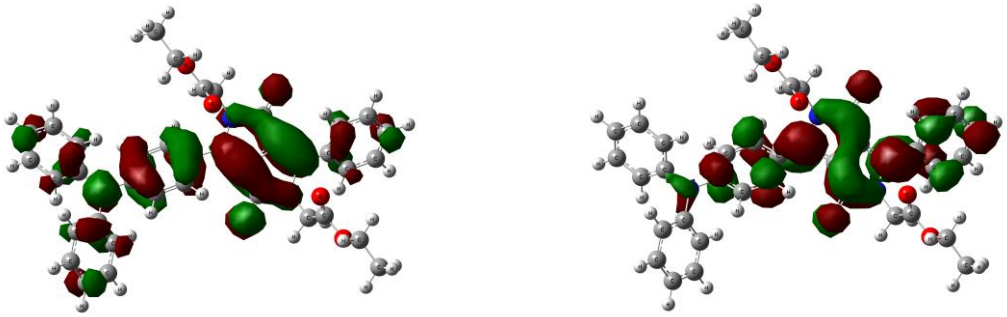

HOMO LUMO

(b)

***Figure 41**: Representation of the electronic density of HOMO and LUMO level of DPP VII (a) and X (b).*

The representation of the electronic distribution of other DPP derivatives VI VIII and IX can be found in the **annex 9.2**. As it can be seen in the **Figure 41** above, the distribution of electrons is not located on the solubilizing groups (amine function) in either case. In the case of DPP **VI** and **VII**, the molecules are symmetric and the electron during the excitation is located at its initial position causing low reorganization energy (**Table A1, annex 9.1**). However alkylation of the initial unsubstituted DPP causes significant rotation of the phenyl groups by (phenyl torsion angles α and β), for the comparison basic unsubstituted DPP molecule has α=β=0°. Phenyl group's rotation strongly affects properties of the molecules, reducing the charge transfer integral between phenyl and central DPP unit. On the one hand such conditions would be disadvantageous for the charge transfer, but on the other hand electron "stretched" all over the molecule, low reorganization energy and low conjugation caused by phenyl groups rotation's gives the proper conditions for Lasing because excited electron is not transferred and energy losses are smaller. In

case of DPP **IX** and **X** the considered molecules are asymmetric, and in spite of the fact that phenyl torsion angles are relatively big, slight electron reorganization takes place as in the excited state electron are pulled from the pyridine towards the non-substituted phenyl thus the reorganization energy is much higher (**Table A1, annex 9.1**). The rotation of phenyl groups bonded to DPP core remained the same at the ground like in the excited state for DPP **VI**, **VII** and **VIII** contrary to DPP **IX** and **X** for which the phenyl rotation changed. However for above mentioned molecules also undergoing lasing, slight delocalization of the excited electron causes lower lasing properties in comparison with considered DPP **VI**, **VII** and **VIII**.

The *N*-alkylated derivatives possess significantly rotated phenyl groups of the central DPP unit in the position adjacent to the *N*-alkyl contrary to the non-substituted DPP on phenyl and *N*-alkyl which are planar and consequently absorption like the luminescence spectra were modified. Electron distribution is more homogeneous in case of planar molecules; this causes the increase in molar coefficient of absorption which in its turn increases the possibility of fluorescence. The phenyl torsion acting on the planarity of the molecule, influences its emission but comes also in account many other factors like the molar coefficient absorption, the stock shift, the quantum yield, the ability to radiationless processes, the donating or withdrawing effect of the substituents and the thin layer morphology favoring waveguiding which also improves ASE process. The *N*-alkylation rises up slightly the level of the HOMO and LUMO because of the week donor character of alkyl. *N*-Acylated DPP's HOMO and LUMO orbitals are slightly lowered than in the case of *N*-alkylated because of the accepting character of the Carbonyl function. The electron distribution in the ground state like in the excited remained the same in both cases.

4.5.2 Net gain of the ASE

When ASE occurs in a long narrow excitation region, most of the light is emitted out of the two ends of the region because light is highly amplified if it travels across the full length of the gain region. The pre-shaped laser beam is displaced along x axis between the edges creating a waveguide along it. We measured the emission spectra from waveguide's edges as the pump intensity and the pump stripe length varied.

The net gain of DPP **VII** was calculated by changing the excitation strip length (l) of the incoming beam and preceded the measurement at different pump energy. The emitted light was collected from the edges at different input pump energies. This allowed us to plot and fit the curves in **Figure 42** with **Equation 4** to determine the gain value at different pump intensity. In previous study it was reported that amplification saturated at higher pump intensities because of sample

degradation. The other possibility states that gain saturation occurred because the light traveling in the waveguide was so strongly amplified that it depleted a substantial fraction of the excitation [116].

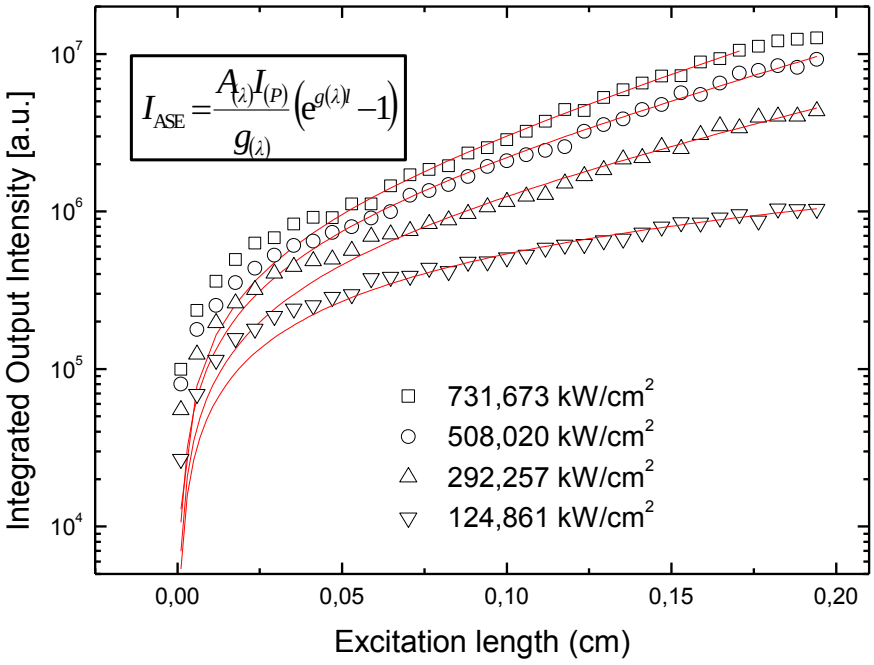

***Figure 42**: Integrated fluorescence intensity versus the excitation length measured at different pump intensities. The inner square represents equation **Equation 4** used to calculate the gain of DPP VII-PS.*

The net gain was higher at high pump intensity and the output intensity increased exponentially at excitation lengths less than 2 mm. Gain saturation occurs as the pump stripe is increased, the gain coefficient is reduced and light is not amplified furthermore.

The gain coefficient value is obtained with **Equation 4** where, I_{ASE} is the ASE intensity at the sample's edge, $A_\lambda I_p$ defines the spontaneous emission proportional to the pump energy, l is the length of the pump stripe, and g_λ is the net gain coefficient. The output intensity from the sample edge is given by **Equation 5** where, x is the length of the unexcited region between the end of the excitation strip and the edge of the sample, I_0 is the output intensity at an x of 0, and α is the loss coefficient of the waveguide. The length of the pumped stripe excitation region varied from l = 0 to l = 2 mm

All the obtained results from the amplified spontaneous emission of DPP derivatives mixed with polystyrene like the absorption, emission, ASE threshold and gain coefficient are presented in **Table 8**.

***Table 8**: Absorption λABS, emission λEm, threshold energy Eth, fluorescence emission λFl, ASE emission max λASE, Fluorescence lifetime τF, quantum yields ΦFL and calculated gain G for DPP **VII**, **VIII** and **X**.*

DPP	λ_{ABS} [nm]	λ_{Fl} [nm]	λ_{ASE} [nm]	ASE threshold ρ_{th} [μJ/cm2]	ΦFL in DSMO	Layer Thickness [μm]	τ_F [ns]	Pump Intensity [kW/cm2]	G [cm-1]
VI	301 475	533	602	63	0.77	1.51	0.5		
VII	384 528	578	612	28	0.41	1.41	2	292 508 732	10.7 13.2 15.2
VIII	380 537	590	659	30	0.45	1.45	0.2	297 393 857	4,7 5,7 5,7
IX	398 504	571	626	79	0.12	1.40	0.4		
X	404 508	572	641	74	-	1.45	0.3	857 1163 1636	23,7 26,6 28,3

From the table above we could notice that DPP **VII** for which we get the lowest threshold, enhances the highest value for the fluorescence lifetime and a relatively high quantum yield value. The second lowest threshold value corresponds to DPP **VIII** with nearly the same results for the ΦFL but a lower fluorescence lifetime.

4.5.3 Photodegradation

Polymers like PMMA and PS were doped with our derivatives and spin coated onto a 1mm thick quartz glass to form thin films. Because of the low stability of the ASE signal when PMMA is the hosting polymer [117], the major work of this study was done using PS.

In **Figure 43** bellow we compared the stability of the emitted light (ASE) depending on the doped polymer and we clearly notice a decrease of the photoluminescence intensity after few incoming laser beam shots when PMMA is used as a matrix.

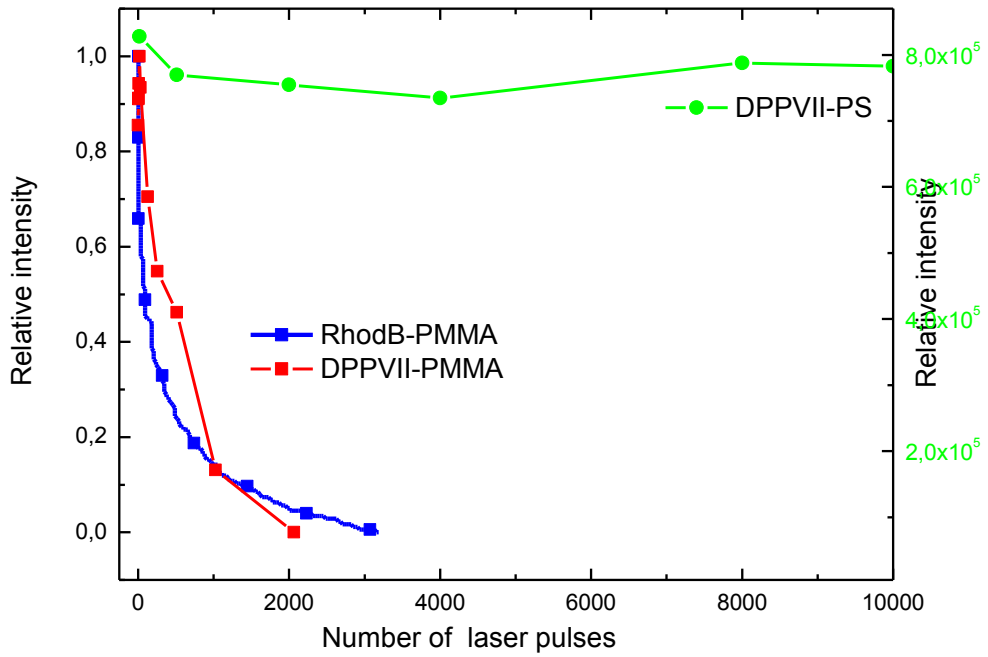

***Figure 43**: Evolution of the fluorescence intensity depending on the number of pulses of differently doped DPP VII and RhodamineB mixed with PMMA.*

The main problematic was to keep the ASE signal stable in time undergoing slower photo degradation, like described in the literature [113] when PMMA doped DPP or Rhodamine B was used as a hosting polymer. These DPP molecules were already mentioned in this field and used as a dopant mixed with PMMA (poly methyl methacrylate) polymer processed into thin film and demonstrated a short but clear ASE process. On the contrary, photoluminescence intensity above the threshold stays more stable in time when the hosting polymer used is PS. For PMMA doped DPP thin layers, the ASE signal in our experiment was observable only few seconds and tended to disappear completely (red curve in **Figure 43**) to give place to normal fluorescence emission spectra with no possibility to repeat this process at the same excited area. As this operation was not reproducible neither stable, we concluded that PMMA doped DPP thin layer underwent quick photo degradation. In **Figure 44** is shown one of the possible photo degradation of PMMA but the ASE lasing can be also altered by the formation of excimer complex. Exposure to deep UV radiation (DUV) induces chain scission, which makes the polymer more soluble. However PMMA is not very sensitive requiring a high dose around 250 mJ/cm2.

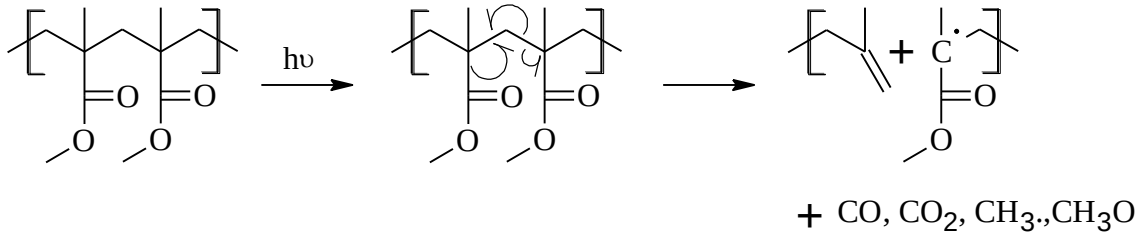

***Figure 44**: Mechanism of radiation-induced chain scission in PMMA.*

We performed this experiment respecting inert atmosphere conditions and again we could neither afford measuring the exact threshold nor the gain concerning the ASE using PMMA. The same phenomenon was observed with Rhodamine B used as a standard (blue curve in **Figure 43**) for the photodegrading experiment. Mixing DPP derivatives with PS polymer leaded to the photo-stability of the ASE signal by maintaining steadied the narrowing of the emission spectra at input pump energy higher than the threshold (green curve in **Figure 43**).

4.5.4 Summary

When comparing these five DPPs, the best photo stability was obtained by making films of mixture of DPP derivatives and polystyrene (PS), to exhibit light amplification by stimulated emission. The lowest threshold found was for the symmetrical push-push system DPP **VII** around 30 uJ/cm^{-1}. With one order magnitude above the lowest threshold found, these materials are very promising and enhance high perspectives in lasing and organic light emitting diode (OLED) technology.

5 Conclusion

This thesis is dedicated on their optical study related with their chemical structure to provide key information on DPP derivatives confirming their potential in the making of more performant modern smart materials. The main task was to provide conclusive results for their possible attractiveness in modern applied organic electronics and photonics by analysing their optical properties in the following three main fields: The one photon absorption, the two photon absorption and the amplified spontaneous emission.

5.1 One photon and two photon absorption

N-alkylated soluble DPP derivatives with polar substituents in para positions of pendant phenyls were synthesized, in order to make original non-alkylated precursors better treatable. The compounds are non-planar with phenyl rings rotated out of diketo-pyrrolo-pyrrole plane. The degree of this rotation is decreased by the electron-donating substituents, while increased by the electron-withdrawing substituents, contrary to the density functional theory (DFT) predictions. The compounds show small solvatochromism of absorption and a moderate positive solvatochromism of fluorescence, if substituted by strong electron-donating substituent. The significant decrease of fluorescence quantum yields and its biexponential decay for dipolar derivatives in polar solvents was tentatively ascribed to the formation of non-fluorescent twisted intramolecular charge transfer excited state (TICT). All compounds show fluorescence in polycrystalline solid-state with the maxima covering a range over 200 nm in visible and near infrared region, where the solid-state fluorescence is quite rare.

These *N*-alkylated DPP derivatives were studied optically and have demonstrated nonlinear absorption properties corresponding to their TPA and enhanced strong two-photon cross section.

To afford these results we had to determine earlier the most suitable DPP derivatives and the appropriate concentration range of the solutions involved in the measurement as well as the appropriate excitation (laser) and detection (Andor camera) settings.

The two photon excitation fluorescence (TPEF) was used to obtain two photon absorption (TPA) cross sections. A considerably high value of σ_{2PA} was obtained for mono piperidino substituted derivative **III** (1400 GM at excitation wavelength 1064 nm), making DPP derivatives promising materials for the applications based on the two-photon excitation.

5.2 Amplified spontaneous emission

Organic thin films of DPP derivatives mixed with polymer were made and their amplified spontaneous emission was studied. For this purpose, the best stoichiometry, thickness of the mixture and the most suitable polymer were determined before their optical study and lasing properties was made in evidence. With polymethylmethacrylate (PMMA) we managed to observe the spectral narrowing of the emitted light but the observation was restricted by the pronounced degradation of the film which limits the repetition of the experiment. We had to perform and obtain a stable amplified spontaneous emission (ASE) signal and therefore, one of the important tasks was to find some stable system with the proper polymer to achieve low degradation. The best photo stability was obtained by making films with a mixture of DPP derivatives and polystyrene (PS), to exhibit light amplification by stimulated emission. The second important question was to find the proper geometry of the system so that the layers obtained were thick enough to afford a reliably strong and stable ASE signal.

The main goal was to characterize these derivatives made into thin layers to obtain their threshold intensity, which is the main parameter for lasing materials. Results obtained for the threshold measurement were higher in energy compared to other published results. The lowest threshold found was around 30 uJ/cm^{-1} for DPP **VII** (the symmetrical push-push system**)**, which is only one order of magnitude higher than the state of the art. Therefore, these materials are very promising and enhance high perspectives in lasing and organic light emitting diode (OLED) technology. Using a more appropriate excitation wavelength would certainly give better threshold values as we conducted all our analysis at a lower absorption band of the DPPs studied.

The thesis brings new insight into the relation between the molecular structure of DPP and their related properties. Based on these results, new organic synthesis should provide more suitable DPP derivatives with appropriate substituents, strictly organized π-conjugated and symmetrical systems leading to improved ASE properties.

6 Literature

[1] LUPO, D., CLEMENS, W., BREITUNG, S., HECKER, K.: Applications of organic and printed electronics; Integrated Circuits and Systems (2013), 1-26. DOI: 10.1007/978-1-4614-3160-2_1.

[2] GAUDIANA, R., BRABEC, C.: Organic materials: Fantastic plastic; *Industry Perspective Nature Photonics 2* (2008), 287 - 289. doi:10.1038/nphoton.2008.69.

[3] Images from source: www.eclairages-led.net.

[4] DAS, R., HARROP, P.: Market data; market and technology appraisal; case studies: the complete picture for printed, flexible and organic electronics; *Printed, Organic & Flexible Electronics: Forecasts, Players & Opportunities* (2013-2023). Source IDTechEx:http://www.idtechex.com/research/reports/printed-organic-and-flexible-electronics-forecasts-players-and-opportunities-2013-2023-000350.asp.

[5] WILLIAM, A. M.: Engineered films for display technologies; *J. Mater. Chem.* (2004), 14, 4-10. DOI: 10.1039/B310846P.

[6] KRAFT, A., GRIMSDALE, A. C., HOLMES, A. B.: Electroluminescent conjugated polymers-Seeing polymers in a new light; *Angewandte Chemie International Edition* (1998), 37, 4, 402–428. DOI: 10.1002/(SICI)1521-3773(19980302)37:4<402::AID-ANIE402>3.0.CO;2-9.

[7] WANG, B., HE, N., LI, B., JIANG, S., QU, Y., QU, S., HUA, J.: Aggregation-Induced Emission and Large Two-Photon Absorption Cross-Sections of Diketopyrrolopyrrole (DPP) Derivatives; *Australian Journal of Chemistry* (2012), 65(4), 387-394.DOI:10.1071/CH11410.

[8] D. D. C. BRADLEY, IC talk 2004.

[9] GOULD, G.: "The LASER, Light Amplification by Stimulated Emission of Radiation" in Franken, P. A., Sands, R. H. (Eds.): The Ann Arbor conference on optical pumping, the *University of Michigan* (1959), 128. OCLC 02460155.

[10] PAQUETA, C., KUMACHEVAB, E.: Nanostructured polymers for photonics; *Materials Today* (2008), 11, 4, 48–56. DOI: 10.1016/S1369-7021(08)70056-7.

[11] FRIEND, R., BURROUGHES, J., BRADLEY, D.D.C.: Nature paper (1990), Patent (1989).

[12] ZHANG, X., MACDIARMIDA, A. G., MANOHAR, S. K.: Chemical synthesis of PEDOT nanofibers; *Chem. Commun*. (2005), Issue 42, 5328-5330.DOI: 10.1039/B511290G.

[13] VALADARESA, M., SILVESTREA, I., CALADOB, H.D.R., NEVESA, B.R.A., GUIMARÃESA, P.S.S., CURYA, L.A.: BEHP-PPV and P3HT blends for light emitting devices; *Materials Science and Engineering: C* (2009), 29, 2, 571–574. DOI: 10.1016/j.msec.2008.10.006.

[14] VANLAEKE, P., SWINNEN, A., HAELDERMANS, I., VANHOYLAND, G., AERNOUTS, T., CHEYNS, D., DEIBEL, C., D'HAEN, J., HEREMANS, P., POORTMANS, J., MANCAA, J. V.: P3HT/PCBM bulk heterojunction solar cells: Relation between morphology and electro-optical characteristics; *Solar Energy Materials and Solar Cells* (2006), 90, 14, 2150–2158. DOI: 10.1016/j.solmat.2006.02.010.

[15] BEYERLEIN, T., TIEKE, B., FORERO-LENGERB, S., BRÜTTING, W.: Red electroluminescence from a 1,4-diketopyrrolo[3,4-c]pyrrole (DPP)-based conjugated polymer; *Synthetic Metals* (2002), 130, (2), 115–119. DOI: 10.1016/S0379-6779(02)00058-9.

[16] VALA, M., WEITER, M., VYŇUCHAL, J., TOMAN, P., LUŇÁK, Jr. S.: Comparative Studies of Diphenyl-Diketo- Pyrrolopyrrole derivatives for electroluminescence applications; *Journal of Fluorescence* (2008), 18, 1181-1186. DOI: 10.1007/s10895-008-0370-x.

[17] VALA, M., VYŇUCHAL, J., TOMAN, P., WEITER, M., LUŇÁK, Jr. S.: Novel, soluble diphenyl-diketo-pyrrolopyrroles: Experimental and theoretical study; *Dyes and Pigments* (2010), 84, 176-182. DOI: 10.1016/j.dyepig.2009.07.014.

[18] FAKUDA, M., KODAMA, K., YAMAMOTO, H., MITO, K.: Evaluation of new organic pigments as laser-active media for a solid-state dye laser; *Dyes and Pigments* (2004), 63, 115-125. DOI: 10.1016/j.dyepig.2004.02.002.

[19] LUŇÁK, S.; VYŇUCHAL, J.; VALA, M.; HAVEL, L.; HRDINA, R.: The synthesis, absorption and fluorescence of polar diketo-pyrrolo- pyrroles; *Dyes and Pigments (*2009), 89, 102-108. DOI: 10.1016/j.dyepig.2008.12.001.

[20] MARDER, SR.: Organic nonlinear optical materials: where we have been and where we are going; *Chemical Communications* (2006), 2, 131-4. DOI: 10.1039/b512646k.

[21] HERBST, M., HUNGER, K., *Industrial organic pigments*. (1993) VCH, Weinheim. Third Edition (2004) ISBN 3-527-30576-9.

[22] CAO, D., LIU, Q., ZENG, W., HANG, S., PENG, J., LIU, S.: Synthesis and characterization of novel red-emitting alternating copolymers based on fluorene and diketopyrrolopyrrole derivatives; *Journal of Polymer Science Part A: Polymer Chemistry* (2006), 44, 8, 2395–2405. DOI: 10.1002/pola.21354.

[23] HOFKENS, J., VERHEIJEN, W., SHUKLA, R., DEHAEN, W., DE SCHRYVER, F. C.: Detection of a single dendrimer macromolecule with a fluorescent dihydropyrrolopyrroledione (DPP) core embedded in a thin polystyrene polymer film; *Macromolecules* (1998), 4493–4497. DOI: 10.1021/ma980346i.

[24] BEHNKE, M., TIEKE, B.: Photoluminescent amphiphilic 1,4-diketo-3,6-diphenylpyrrolo-[3,4-c]-pyrrole derivative and its complexes with polyelectrolytes; *Langmuir* (2002), 18 (10), 3815–3821. DOI: 10.1021/la011773j.

[25] SMET, M., METTEN, B., DEHAEN, W.: Construction of rod-like diketopyrrolopyrrole oligomers with well-defined length; *Tetrahedron Letters* (2001), 42, 37, 6527–6530. DOI:10.1016/S0040-4039(01)01305-3.

[26] BEYERLEIN, T., TIEKE, B., FORERO-LENGER, S., BRUTTING, W.: Red electroluminescence from a 1,4-diketopyrrolo[3,4-c]pyrrole (DPP)-based conjugated polymer; *Synthetic Metals* (2002), 130, 2, 115-119 (5). DOI: 10.1016/S0379-6779(02)00058-9.

[27] ROCHAT, A.C., WALLQUIST, O., IQBAL, A., MIZUGUCHI J. Eur. Patent, (1990), 353184A.

[28] MIZUGUCHI, J.: Phasenumwandlung von 3,6-Diphenyl pyrrolo[3,4-c]pyrrole-1,4-dithione für optische Speicherungsanwendungen, *Swiss Chemical Society*, *CHIMIA International Journal for Chemistry*, (1994), 48, 9, pp. 439-442(4).

[29] MIZUGUCHI, J., IMODA, T., TAKAHASHI, H., YAMAKAMI, H.: Polymorph of 1,4-diketo-3,6-bis-(4′-dipyridyl)-pyrrolo-[3,4-c]pyrrole and their hydrogen bond network: A material for H2 gas sensor; *Dyes and Pigments* (2006), 68, 1, 47-52. DOI: 10.1016/j.dyepig.2005.01.001.

[30] HOKI, T., TAKAHASHI, H., SUZUKI, S., MIZUGUCHI, J.: Hydrogen gas sensor based upon proton acceptors integrated in copper-tetra-2,3-pyridinoporphyradine; *Sensors Journal, IEEE* (2007), 7, 5, 808-813. DOI: 10.1109/JSEN.2007.894155.

[31] FUKUDA, M., KODAMA, K., YAMAMOTO, H., MITO, K.: Solid-state laser with newly synthesized pigment Dyes and Pigments, (2002), 53, 1, pp. 67–72. DOI: 10.1016/S0143-7208(02)00002-5.

[32] GRIFFITHS, J.: Colour and constitution of organic molecules; *Academic Press London* (1976), 281. DOI: 10.1002/col.5080030213.

[33] SANYIN, Q., WENJUN, W., JIANLI, H., CONG, K., YITAO, L., HE, T.: New Diketopyrrolopyrrole (DPP) Dyes for Efficient Dye-Sensitized Solar Cells. J. Phys. Chem. C, (2010), 114 (2), 1343–1349. DOI: 10.1021/jp909786k.

[34] JIANHUA, L., Nguyen, T.-Q.: Optoelectronic devices based on diketopyrrolopyrrole (DPP)-containing conjugated small molecules; *Material Matters*, 7.1, 10. ISSN: 1933–9631.

[35] RIGGS, R. L., MORTON, C. J. H., SLAWIN, A. M. Z.,SMITH, D. M., WESTWOOD, N. J., AUSTEN, W. S. D., STUART, K. E.: Synthetic studies related to diketopyrrolopyrrole (DPP) pigments. Part 3: Syntheses of tri- and tetra-aryl DPPs; *Tetrahedron* (2005), 61, 47, pp. 11230–1243. DOI: 10.1016/j.tet.2005.09.005.

[36] IQBAL, A., JOST, M., KIRCHMAYER, R., PFENNINGER, J., ROCHAT, A. C., WALLQUIST, O.: Synthesis and properties of 1,4-diketopyrrolo[3,4-c]pyrroles, *Bulletin des Societes Chimiques Belges* (1988), 97, (8-9), 615-643.

[37] WALLQUIST O. Diketopyrrolopyrrole (DPP) Pigments. In: Smith HM, editor. High performance pigments, Weinheim, Wiley-VCH, 2002. p. 159-184.

[38] HERBST, M., HUNGER, K.: Industrial organic pigments; *Weinheim: Wiley-VCH* (2004). 487-494. ISBN: 3-527-30576-9.

[39] BEYERLEIN, T., TIEKE, B., FORERO-LENGER, S., BRÜTTING, W.: Red electroluminescence from 1,4-diketopyrrolo[3,4-c]pyrrole (DPP)–based conjugated polymer; *Synt. Met.* (2002), 130, (2), 115-119. DOI:10.1016/S0379-6779(02)00058-9.

[40] BÜRGI, L., TURBIEZ, M., PFEIFFER, R., BIENEWALD, F., KIRNER, H. J , WINNEWISSER, C.: High-mobility ambipolar near-infrared light-emitting polymer field-effect transistors; *Adv. Mater.* (2008), 20, (11), 2217-2224. DOI: 10.1002/adma.200702775.

[41] WIENK, M. M., TURBIEZ, M., GILOT, J., JANSSEN, R. A. J.: Narrow-bandgap diketo-pyrrolo-pyrrole polymer solar sells: The effect of processing on the performance; *Adv. Mater.* (2008), 20, (13), 2556-2560. DOI: 10.1002/adma.200800456.

[42] ZHU, Y., HEIM, I., TIEKE, B.: Red emitting diphenylpyrrolopyrrole (DPP)-based polymers prepared by Stille and Heck coupling; *Macromol. Chem. Phys.* (2006), 207, (23), 2206-2214. DOI: 10.1002/macp.200600363.

[43] LIU, K., Li, Y., YANG, M.: Novel 1,4-Diketo-3,6-diphenyl pyrrolo[3,4-c]pyrrole (DPP) – based Copolymers with Large Stokes Shift; *J. Appl. Polym. Sci.* (2009), 111, (4), 1976-1984. DOI: 10.1002/app.29250.

[44] ZHU, Y., ZHANG, K., TIEKE, B.: Electrochemical polymerization of bis(3,4-etkylenedioxythiophene)-substituted 1,4-diketo-3,6-diphenyl pyrrolo[3,4-c]pyrrole (DPP) derivative; *Macromolecular Chemistry and Physics* (2009); 210, (6), 431-439. DOI: 10.1002/macp.200800507.

[45] FRANCK-CONDON Principle. 1996, 68, 2243. IUPAC Compendium of Chemical Terminology 2nd Edition (1997).

[46] Modern Molecular Photochemistry N.J. Turro.

[47] IUPAC Compendium of Chemical Terminology 2nd Edition (1997).

[48] This file is licensed under the Creative Commons Attribution-Share Alike 3.0 Unported license.

[49] http://www.olympusmicro.com/copyright/index.html.

[50] GÖPPERT-MAYER, M.: Über elementarakte mit zwei quantensprüngen; *Ann. Phys.* (1931), 401, 273–294. DOI: 10.1002/andp.19314010303.

[51] KAISER, W., GARRETT, C. G. B.: Two-photon excitation in CaF_2: Eu^{2+}; *Phys. Rev. Lett.* (1961), 7, 229–231. DOI:10.1103/PhysRevLett.7.229.

[52] PAWLICKI, M., COLLINS, H. A., DENNING, R. G., ANDERSON, H. L.: Two-photon absorption and the design of two-photon dyes; *Angewandte Chemie International Edition*. 48 (2009), 18, 3244–3266. DOI: 10.1002/anie.200805257.

[53] BELFIELD, K. D., BONDAR, M. V., PRZHONSKA, O. V., SCHAFER, K. J.: One- and two-photon photostability of 9,9-didecyl-2,7-bis(N,N-diphenylamino)fluorine; *Photochemical & Photobiological Sciences* (2004), 3, 138-141. DOI: 10.1039/B307426A.

[54] JHA, P. C., LUO, Y., POLYZOS, I., PERSEPHONIS, P., ÅGREN, H.: Two- and three-photon absorption of organic ionic pyrylium based materials; *J. Chem. Phys.* (2009), 130, 174312. DOI: 10.1063/1.3123742.

[55] ENCYCLOPEDIA OF LIFE SCIENCES / & 2002 Macmillan Publishers Ltd, Nature Publishing Group / www.els.net.

[56] GUO, E. Q., REN, P. H., ZHANG, Y. L., ZHANG, H. C., YANG, W. J.: Diphenylamine end-capped 1,4-diketo-3,6-diphenylpyrrolo[3,4-c]pyrrole (DPP) derivatives with large two-photon absorption cross-sections and strong two-photon excitation red fluorescence; *Chem. Commun.* (2009), 39, 5859-5861. DOI: 10.1039/B911808J.

[57] JIANG, Y., WANG, Y., HUA, J., QU, S., QIAN, S., TIAN, H.: Synthesis and two-photon absorption properties of hyperbranched diketo-pyrrolo-pyrrole polymer with triphenylamine as the core; *J. Polym. Sci. A: Polym. Chem.* (2009); 47 (17), 4400-4408. DOI: 10.1002/pola.23493.

[58] TERENZIANI, F., KATAN, C., BADAEVA, E., TRETIAK, S., BLANCHARD-DESCE, M. Enhanced Two-Photon Absorption of Organic Chromophores: Theoretical and Experimental Assessment; *Adv. Mater.* (2008), 20(24):4641-4678. DOI: 10.1002/adma.200800402.

[59] DE LA TORRE, G., VÁZQUEZ, P., AGULLÓ-LÓPEZ, F., TORRES, T.: Role of Structural Factors in the Nonlinear Optical Properties of Phtalocyanines and Related; Compounds; *Chem. Rev.* (2004); 104(9):3723-3750. DOI: 10.1021/cr030206t.

[60] SAŁEKA, P., VAHTRASA, O., GUOA, J., LUOA, Y., HELGAKERB, T., ÅGRENA, H.: Calculations of two-photon absorption cross sections by means of density-functional theory; *Chemical Physics Letters* (2003), 374, 5–6, 446–452. DOI: 10.1016/S0009-2614(03)00681-X.

[61] WANG, X., YANG, P., JIANG, W., XU, G., GUO, X.: Strong two-photon absorption and two-photon excited fluorescence emission of heterofluorene derivatives; *Optical Materials* (2005), 27, 1163-1170. DOI: 10.1016/j.optmat.2004.08.081.

[62] ALBOTA, M. A., XU, C.: WEBB, W. W.: Two-photon fluorescence excitation cross sections of biomolecular probes from 690 to 960 nm; *Applied Optics* (1998), 37, 31, 7352-7356. DOI: 10.1364/AO.37.007352.

[63] IMODA, T., MIZUGUCHI, J.: Strikingly different luminescent properties arising from single crystals grown from solution or from the vapor phase in a diketo-pyrrolo-pyrrole analog; *Journal of Applied Physics* (2007), 102, 073529. DOI:10.1063/1.2784996.

[64] GRIFFITHS, J.: Colour and constitution of organic molecules; *Journal für Praktische Chemie* (1978), 320, 5, 878–879. DOI: 10.1002/prac.19783200524.

[65] FABIAN, J., HARTMANN, H.: Light absorption of organic colorants; *Journal für Praktische Chemie* (1982), 324, 2, 350–351. DOI: 10.1002/prac.19823240223.

[66] STREHMEL, B., SARKER, A. M., DETERT, H.: The influence of and acceptors on two-photon absorption and solvatochromism of dipolar and quadrupolar unsaturated organic compounds; *ChemPhysChem*. (2003); 4(3):249-259. DOI: 10.1002/cphc.200390041.

[67] TERENZIANI, F., PAINELLI, A., KATAN, C., CHARLOT, M., BLANCHARD-DESCE, M.: Charge Instability in Quadrupolar Chromophores: Symmetry Breaking and Solvatochromism; *J. Am. Chem. Soc.* (2006);128(49):15742-15755. DOI: 10.1021/ja064521j.

[68] TERENZIANI, F., SISSA, C., PAINELLI, A.: Symmetry breaking in octupolar chromophores: solvatochromism and electroabsorption; *J. Phys. Chem. B.* (2008);112(16):5079-5087. DOI: 10.1021/jp710241g.

[69] TERENZIANI, F., D´AVINO, G., PAINELLI, A.: Multichromophores for nonlinear optics: designing the daterial properties by electrostatic interactions; *ChemPhysChem.* (2007); 8(17):2433-2444. DOI: 10.1002/cphc.200700368.

[70] MARDER, S. R.: Organic nonlinear optical materials: where we have been and where we are going; *Chem. Commun.* (2006); (2): 131-134. DOI: 10.1039/B512646K.

[71] De BONI, L., CONSTANTINO, C. J. L., MISOGUTI, L., AROCA, R. F., ZILIO, S. C., MENDONÇA, C. R.: Two-photon absorption in perylene derivatives; *Chem. Phys. Lett.* (2003); 371(5-6): 744-749. DOI: 10.1016/S0009-2614(03)00359-2.

[72] FU, J., PADILHA, L. A., HAGAN, D. J., VAN STRYLAND, E. W., PRZHONSKA, O.V., BONDAR, M. V., SLOMINSKY, Y. L., KACHKOWSKI, A.D.: Molecular structure—two-photon absorption property relations in polymethine dyes; *J. Opt. Soc. Am. B.* (2007); 24(1): 56-66. DOI: 10.1364/JOSAB.24.000056.

[73] CHUNG S. J., ZHENG, S., ODANI, T., BEVERINA, L., FU, J., PADILHA, L. A., BIESSO, A., HALES, J. M., ZHAN, X., SCHMIDT, K., YE, A., ZOJER, E., BARLOW, S., HAGAN, D. J., VAN STRYLAND, E. W., YI, Y., SHUAI, Z., PAGANI, G. A., BRÉDAS, J. L., PERRY, J. W., MARDER, S. R.: Extended Squaraine dyes with Large Two-Photon Absorption Cross-Sections; *J. Am. Chem. Soc.* (2006), 128(45): 14444-14445. DOI: 10.1021/ja065556m.

[74] Thomson - Brooks/Cole (2004)

[75] GELINCK, G., H., WARMAN J., M., REMMERS M., NEHER D.: Narrow-band emissions from conjugated-polymer films; *Chemical Physics Letters* (1997), 265, 3, 320-326 (7).

DOI: 10.1016/S0009-2614(96)01447-9.

[76] MCGEHEE, M., GUPTA, R., VEENSTRA, S., MILLER, E. K., DIAZ-GARCIA, M. A., HEEGER, A. J.: Amplified spontaneous emission from photopumped films of a conjugated polymer; *Physical Review B* (1998), 58, 11, pp. 7035-7039. DOI: 10.1103/PhysRevB.58.7035.

[77] YUANXIANG, X., HOUYU Z., FENG, L., FANGZHONG, S., HUAN, W., XIANJIE, L., YANG, Y., YUGUANG, M.: Supramolecular interaction-induced self-assembly of organic molecules into ultra-long tubular crystals with wave guiding and amplified spontaneous emission; Journal of Materials (2012), 4, 22, 1592-1597. DOI: 10.1039/C1JM14815J.

[78] SALBECK, J., SCHÖRNER, M., FUHRMANN, T.: Optical amplification in spiro-type molecular glasses; *Thin Solid Films* (2002), 417, 1–2, 20–25. DOI: 10.1016/S0040-6090(02)00650-8.

[79] LI, J.Y., LAQUAI, F., WEGNER, G.: Amplified spontaneous emission in optically pumped neat films of a polyfluorene derivative; *Chemical Physics Letters* (2009), 478, 1–3, pp. 37–41. DOI: 10.1016/j.cplett.2009.07.028.

[80] ADACHI, C., NAKANOTANI, H.: *Material Matters* (2009), 4.3, 74.

[81] SHAKLEE, K. L., LEHENY, R. F.: Direct determination of optical gain in semiconductor crystals; *Applied Physics Letters* (1971), 18, 475, 11. DOI: 10.1063/1.1754804.

[82] SOFFER, B. H., MCFARLAND, B. B.: Continuously tunable, narrow-band organic dye lasers; *Applied Physics Letters* (1967), 10, 266. DOI: 10.1063/1.1754804.

[83] KARNUTSH, C., GYTNER, C., HAUG, V., LEMMER, U., FARRELL, T., NEHLS, B. S., SCHERF, U., WANG, J., WEIMANN, T., HELIOTIS, G., PFLUMM, C., DEMELLO, J. C., BRADLEY, D. D. C.: Low threshold blue conjugated polymer lasers with first- and second-order distributed feedback; *Applied Physics Letters* (2006), 89, 20, 201108. DOI: 10.1063/1.2390644.

[84] NAKANOTANI, H., MATSUMOTO, N., UCHIUZOU, H., NISHIYAMA, M., YAHIRO, M. ADACHI, C.: Very low amplified spontaneous emission threshold and electroluminescence characteristics of 1,1′-diphenyl substituted fluorene derivatives; *Optical Materials* (2007), 30, 4, 630–636. DOI: 10.1016/j.optmat.2007.02.045.

[85] TESSLER, N., DENTON, G.. J., FRIEND, R.H.: Lasing from conjugated-polymer microcavities; *Letters to Nature* (1996), 382, 695 - 697. DOI: 10.1038/382695a0.

[86] HIDE, F., DIAZ-GARCIA, M. A., SCHWARTZ, B. J., ANDERSSON, M.R., PEI, Q., HEEGER, A. J.: Semiconducting Polymers: A New Class of Solid-State Laser Materials; *Science* (1996), 273, 5283, 1833-1836. DOI: *10.1126/science.273.5283.1833.*

[87] DIAZ-GARCIA, M. A., HEEGER, A. J.: Semiconducting polymers as materials for photonic devices; *Current Opinion in Solid State and Materials Science* (1998), 3, 1, 16–22. DOI: 10.1016/S1359-0286(98)80060-0.

[88] VALA, M., WEITER, M., VYŇUCHAL, J., TOMAN, P., LUŇÁK, S. Jr.: Comparative Studies of Diphenyl-Diketo-Pyrrolopyrrole Derivatives for Electroluminescence Applications; *Journal of Fluorescence* (2008) 18:1181-1186. DOI: 10.1007/s10895-008-0370-x.

[89] LUNÁK, S. Jr., VALA, M., VYNUCHAL, J., OUZZANE, I., HORÁKOVÁ, P., MOZÍSKOVÁ, P., ELIÁS, Z., WEITER, M.: Absorption and fluorescence of soluble polar diketo-pyrrolo-pyrroles; *Dyes and Pigments* (2011), 91, 3, 269–278. DOI: 10.1016/j.dyepig.2011.05.004.

[90] KUČERÍK, J., DAVID, J., WEITER, M., VALA, M., VYŇUCHAL, J., OUZZANE, I., SALYK, O.: Stability and physical structure tests of piperidyl and morpholinyl derivatives of diphenyl-diketo-pyrrolopyrroles (DPP); *Journal of Thermal Analysis and Calorimetry* (2012), 108, 2, 467-473. DOI: 10.1007/s10973-011-1896-8.

[91] FUKUDA, M., KODAMA, K., YAMAMOTO, H., MITO, K.: Solid-state laser with newly synthesized pigment; *Dyes and Pigments* (2002), 53, 1, pp. 67–72. DOI: 10.1016/S0143-7208(02)00002-5.

[92] FUKUDA, M., KODAMA, K., YAMAMOTO, H., MITO, K.: Evaluation of new organic pigments as laser-active media for a solid-state dye laser; *Dyes and Pigments* (2004), 63, 2, pp. 115–125. DOI: 10.1016/S0143-7208(04)00013-0.

[93] KOZLOV, V. G., PARTHASARATHY, G., BURROWS, P. E., FORREST, S. R., YOUNG, Y., THOMPSON, M. E.: Optically pumped blue organic semiconductor lasers; *Applied Physics Letters* (1998), 72 (2), 144. DOI: 10.1063/1.120669.

[94] LONG, X., MALINOWSKI, A., BRADLEY, D.D.C., INBASEKARAN, M., WOO E.P.: Emission processes in conjugated polymer solutions and thin films; *Chemical Physics Letters* (1997), 272, 1-2, pp. 6-12(7). DOI: 10.1016/S0009-2614(97)00474-0.

[95] NAKANOTANI, H., MATSUMOTO, N., UCHIUZOU, H., NISHIYAMA, M. , YAHIRO, M., ADACHI, C.: Very low amplified spontaneous emission threshold and electroluminescence characteristics of 1,1′-diphenyl substituted fluorene derivatives; *Optical Materials* (2007), 30, 4, pp. 630-636. DOI: 10.1016/j.optmat.2007.02.045.

[96] Safe Handling of Color Pigments (1993), Color Pigments Manufacturers Association Inc., Virginie, USA.

[97] LANGHALS, H., POTRAWA, T., NÖTH, H., LINTI, G.: The Influence of Packing Effects on the Solid-State Fluorescence of Diketopyrrolopyrroles; *Angewandte Chemie International Edition in English* (1989); 28(4):478-480. DOI: 10.1002/anie.198903971.

[98] VALA, M.; KRAJČOVIČ, J.; LUŇÁK Jr., S.; OUZZANE, I.; BOUILLON, J.P.; WEITER, M.: HOMO and LUMO energy levels of N,N′-dinitrophenyl-substituted polar diketopyrrolopyrroles (DPPs); *Dyes and Pigments* (2014), 106, 136–142. DOI: 10.1016/j.dyepig.2014.03.005.

[99] WILLIAMS, A. T. R., WINFIELD, S. A., MILLER, J. N.: Relative fluorescence quantum yields using a computer-controlled luminescence spectrometer; *Analyst* (1983), 108, 1067-1071. DOI: 10.1039/AN9830801067.

[100] CASEY, K.G., QUITEVIS, E.L.: Effect of solvent polarity on nonradiative processes in xanthene dyes: Rhodamine B in normal alcohols; *The Journal of Physical Chemistry* (1988), 92 (23), pp. 6590–6594. DOI: 10.1021/j100334a023.

[101] HE, G. S., TAN, L. S., ZHENG, Q., PRASAD, P. N.: Multiphoton absorbing materials: molecular designs, characterizations, and applications; *Chemical Reviews* (2008), 108(4):1245-1330. DOI: 10.1021/cr050054x.

[102] MAGDE, D., WONG, R., SEYBOLD, P. G.: Fluorescence quantum yields and their relation to lifetimes of rhodamine 6G and fluorescein in nine solvents: improved absolute standards for quantum yields; *Photochemistry and Photobiology* (2002), 75(4), 327-334. DOI: 10.1562/0031-8655(2002)0750327FQYATR2.0.CO2.

[103] REYNOLDS, G. A., DREXHAGE, K. H.: New coumarin dyes with rigidized structure for flashlamp-pumped dye lasers; *Optics Communications* (1975), 13, 3, 222-225. DOI: 10.1016/0030-4018(75)90085-1.

[104] Revision A.1, FRISCH, M. J., TRUCKS, G. W., SCHLEGEL, H. B., SCUSERIA, G. E., M. A. ROBB, J. R. CHEESEMAN, G. SCALMANI, V. BARONE, B. MENNUCCI, G. A. PETERSSON, H. NAKATSUJI, M. CARICATO, X. LI, H. P. HRATCHIAN, A. F. IZMAYLOV, J. BLOINO, G. ZHENG, J. L. SONNENBERG, M. HADA, M. EHARA, K. TOYOTA, R. FUKUDA, J. HASEGAWA, M. ISHIDA, T. NAKAJIMA, Y. HONDA, O. KITAO, H. NAKAI, T. VREVEN, J. A. MONTGOMERY, JR., J. E. PERALTA, F. OGLIARO, M. BEARPARK, J. J. HEYD, E. BROTHERS, K. N. KUDIN, V. N. STAROVEROV, R. KOBAYASHI, J. NORMAND, K. RAGHAVACHARI, A. RENDELL, J. C. BURANT, S. S. IYENGAR, J. TOMASI, M. COSSI, N. REGA, J. M. MILLAM, M. KLENE, J. E. KNOX, J. B. CROSS, V. BAKKEN, C. ADAMO, J. JARAMILLO, R. GOMPERTS, R. E. STRATMANN, O. YAZYEV, A. J. AUSTIN, R. CAMMI, C. POMELLI, J. W. OCHTERSKI, R. L. MARTIN, K. MOROKUMA, V. G. ZAKRZEWSKI, G. A. VOTH, P. SALVADOR, DANNENBERG, J. J., DAPPRICH, S., DANIELS, A. D., FARKAS, Ö., FORESMAN, J. B., ORTIZ, J. V., CIOSLOWSKI, J. and FOX, D. J., Gaussian, Inc., *Wallingford* CT, 2009.

[105] BECKE, A.D.: A new mixing of Hartree–Fock and local density functional theories; *J. Chem. Phys.*, 98, 1372 (1993). DOI: 10.1063/1.464304.

[106] COLONNA G, PILATI T, RUSCONI F, ZECCHI G.: Synthesis and properties of some new N,N′-disubstituted 2,5-dihydro-1,4-dioxo-3,6-diphenylpyrrolo[3,4-c]pyrroles; *Dyes and Pigments* (2007), 75(1):125-129. DOI: 10.1016/j.dyepig.2006.05.024.

[107] THETFORD, D., CHERRYMAN, J, CHORLTON, AP, DOCHERTY R. Theoretical molecular modelling calculations on the solid state structure of some organic pigments; *Dyes and Pigments* (2004), 63(3):259-276. DOI: 10.1016/j.dyepig.2004.03.009.

[108] KAATZ, P., SHLETON, D. P.: Two-photon fluorescence cross-section measurements calibrated with hyper-Rayleigh scattering; *J. Opt.Soc.Am.* B (1999), 16(9):998-1006. DOI: 10.1364/JOSAB.16.000998.

[109] KIM, H. M., CHO, B. R.: Two-photon materials with large two-photon cross sections; *Chemical Communications* (2009), (2): 153-164. DOI: 10.1039/B813280A.

[110] LUŇÁK, S. Jr., HAVEL, L., VYŇUCHAL, J., HORÁKOVÁ, P., KUČERÍK, J., WEITER, M., HRDINA, R.: Geometry and Absorption of Diketo-Pyrrolo-Pyrroles Substituted with Various Aryls; *Dyes and Pigments* (2010). DOI:10.1016/j.dyepig.2009.09.014.

[111] VALA, M., WEITER M., VYŇUCHAL, J., TOMAN, P., LUŇÁK Jr. S.: Comparative Studies of Diphenyl-Diketo- Pyrrolopyrrole Derivatives for Electroluminescence Applications; *Journal of Fluorescence* (2008), 18:1181-1186. ISSN: 1053-0509. DOI: 10.1007/s10895-008-0370-x.

[112] PLÖTNER, J., DREUW, A.: Solid state fluorescence of Pigment Yellow 101 and derivatives: a conserved property of the individual molecules; *Phys. Chem. Chem. Phys.* (2006), 8(10):1197-1204. DOI: 10.1039/B514815D.

[113] FUKUDA, M., KODAMA, K., YAMAMOTO, H., MITO, K.: Solid-state laser with newly synthesized pigment; *Dyes and Pigments* (2002), 53, 1, pp. 67–72. DOI: 10.1016/S0143-7208(02)00002-5.

[114] FUKUDA, M., KODAMA, K., YAMAMOTO, H., MITO, K.: Evaluation of new organic pigments as laser-active media for a solid-state dye laser; *Dyes and Pigments* (2004), 63, 2, pp. 115–125. DOI: 10.1016/j.dyepig.2004.02.002.

[115] SAMUEL, D. W., NAMDAS, E. B., TURNBULL, G.: : How to recognize lasing; *Nature Photonics* (2009), Vol 3. DOI: 10.1038/nphoton.2009.173.

[116] MCGEHEE, M. D., GUPTA, R., VEENSTRA, S., MILLER, E. K., DIAZ-GARCIA, M.A., HEEGER, A. J. : Amplified spontaneous emission from photopumped films of a conjugated polymer; *Physical Review B* (1998), 58, 7035–7039. DOI: 10.1103/PhysRevB.58.7035.

[117] SZNITKO, L., MYSLIWIEC, J., PARAFINIUK, K., SZUKALSKI, A., PALEWSKA, K., BARTKIEWICZ, S., MINIEWICZ, A.: Amplified spontaneous emission in polymethyl methacrylate doped with 3-(1,1-dicyanoethenyl)-1-phenyl-4,5-dihydro-1H-pyrazole (DCNP); *Chemical Physics Letters* (2011), 512, 4–6, pp. 247–250. DOI:10.1016/j.cplett.2011.07.046.

[118] LIN, T.C., HE, G.S., PRASAD, P.N., TANB, L.S.: Degenerate nonlinear absorption and optical power limiting properties of asymmetrically substituted stilbenoid chromophores. *Journal of Materials Chemistry* (2004), 14, 982-991. DOI: 10.1039/B313185H.

7 List of symbols and abbreviations

ASE	amplified spontaneous emission
BHJ	bulk heterojunction
D	electron donating group
DFT	density functional theory
DMSO	dimethylsulfoxide
DPP	diphenyl-diketo-pyrrolopyrrole
F	time averaged fluorescence emission
LC	liquid crystal
NLO	nonlinear optic
OPA	one photon absorption
OPEF	one photon excitation fluorescence
OFET	organic field effect transistor
P	time averaged laser source power incident on the sample
PA	photon absorption
PL	Photoluminescence
PMMA	polymethylmethacrylate
PMPSi	poly(methyl-phenylsilane)
PS	polystyrene
SR	super radiance
SF	super fluorescence
TFT	thin film transistor
TICT	twisted intramolecular charge transfer excited state
TPA	two photon absorption
TPEF	two photon excitation fluorescence
W	electron withdrawing group

A	absorbance
α	absorption coefficient
c	celerity
C	concentration
E	energy
ε	molar absorptivity
$\boldsymbol{\Phi}$	fluorescence quantum yield
$\boldsymbol{h}$	Planck constant
λ	wavelength
l	optical length
ν	frequency
η	refractive index
N	number of density
$\mathbf{P_t}$	transmitted energy (from the sample)
$\mathbf{P_0}$	incoming or applied energy
σ	cross section
$\boldsymbol{\sigma_{2PA}}$	two-photon absorption cross section
$\boldsymbol{\sigma_{2PE}}$	two photon emission fluorescence
T	transmittance
α[°]	torsion angle
β[°]	torsion angle
$\mathbf{E}_{S0 \rightarrow S1}$	singlet-singlet absorption transition (lowest excited state)
$\mathbf{E}_{lum}$	luminescence (absorption)
$\mathbf{\Delta E}_{Stockes}$	stock shift
$\mathbf{E}_{def}$	deformation energy (relaxation)

8 List of publications and activities

Article expected in 2015 on ASE results (1st author).

8.1 Publications

2014

VALA, M.; KRAJČOVIČ, J.; LUŇÁK Jr., S.; OUZZANE, I.; BOUILLON, J.P.; WEITER, M.: HOMO and LUMO energy levels of N,N′-dinitrophenyl-substituted polar diketopyrrolopyrroles (DPPs); *Dyes and Pigments* (2014), 106, 136–142. DOI: 10.1016/j.dyepig.2014.03.005.

2012

MLADENOVA, D.; ZHIVKOV, I.; OUZZANE, I.; VALA, M.; HEINRICHOVÁ, P.; BUDUROVA, D.; WEITER, M.: Thin polyphenylene vinylene electrophoretically and spin-coated films - photoelectrical properties; *Journal of Physics*: Conference Series (2012), 398, 1, 1-6. ISSN: 1742- 6596. DOI: 10.1088/1742-6596/398/1/012056.

MLADENOVA, D.; WEITER, M.; STEPANEK, P.; OUZZANE, I.; VALA, M.; SINIGERSKY, V.; ZHIVKOV, I.: Characterization of electrophoretic suspension for thin polymer film deposition; *Journal of Physics*: Conference Series (2012), 356, 1, 1-4. 1742- 6596. DOI: 10.1088/1742-6596/356/1/012040.

KUČERÍK, J.; DAVID, J.; WEITER, M.; VALA, M.; VYŇUCHAL, J.; OUZZANE, I.; SALYK, O.: Stability and physical structure tests of piperidyl and morpholinyl derivatives of diphenyl-diketo-pyrrolopyrroles (DPP); *Journal of Thermal Analysis and Calorimetry* (2012), 108, 2, 467-473. ISSN: 1388- 6150. DOI: 10.1007/s10973-011-1896-8.

2011

LUŇÁK, S.; VALA, M.; VYŇUCHAL, J.; OUZZANE, I.; HORÁKOVÁ, P.; MOŽÍŠKOVÁ, P.; WEITER, M.: Absorption and fluorescence of soluble polar diketo-pyrrolo- pyrroles; *Dyes and Pigments* (2011), 91, 1, 269-278. ISSN: 0143- 7208. DOI: 10.1016/j.dyepig.2011.05.004.

2010

VALA, M.; WEITER, M.; HEINRICHOVÁ, P.; ŠEDINA, M.; OUZZANE, I.; MOŽÍŠKOVÁ, P.: Tayloring of molecular materials for organic electronics; *Journal of Biochemical Technology,* (2010), 2, 5, S44 (S45 s.). ISSN: 0974- 2328.

8.2 Conferencies and other contributions

2013

WEITER, M.; VALA, M.; OUZZANE, I.; HONOVÁ, J.; KRAJČOVIČ, J.; DAVID, J.; VYŇUCHAL, J.; LUŇÁK, S.: Soluble Diketo-pyrrolo- pyrroles for Organic Electronics and Photonics; *The 11th International Symposium on Functional pi- electron systems* (2013), s. 1 (1 s.).

SCHMIEDOVÁ, V.; OUZZANE, I.; DZIK, P.; VESELÝ, M.; ZMEŠKAL, O.; MOROZOVÁ, M.; KLUSOŇ, P.: Optical properties of titania coatings prepared by inkjet direct patterning of the reverse micelles sol- gel composition; *Kyoto, Japan: Kyoto Research Park,* (2013), s. 77-77.

VALA, M.; KRAJČOVIČ, J.; OUZZANE, I.; WEITER, M.: Novel Diketo-pyrrolo- pyrroles for Organic Electronics; *11th International Symposium on Functional pi- Electron Systems* (2013). s. 1 (1 s.).

2011

ZHIVKOV, I.; VALA, M.; WEITER, M.; OUZZANE, I.; HEINRICHOVÁ, P.; MLADENOVA, D.: Electrophoretic deposition of thin organic films for solar energy conversion purpose; *Chemické listy; Česká společnost chemická,* (2011), s. 884-884. ISSN: 0009- 2770.

VALA, M.; WEITER, M.; OUZZANE, I.: Diketo-pyrrolo- pyrroles for organic electronics. 10th International symposium on functional pi- electron systems; *Beijing, China:* (2011), s. 238-238.

VALA, M.; WEITER, M.; HEINRICHOVÁ, P.; OUZZANE, I.: Optical properties of diketo-pyrrolo- pyrroles for organic electronic applications; *Chemické listy Brno:* (2011), s. s886 (s887 s.). ISSN: 0009- 2770.

OUZZANE, I.; WEITER, M.; VALA, M.: Novel diketo-pyrrolo- pyrroles organic derivatives for optical applications. *Chemické listy; CHL Brno:* (2011). s. 802-802. ISSN: 0009- 2770.

OUZZANE, I.; HEINRICHOVÁ, P.; ŠEDINA, M.; WEITER, M.; VALA, M.: Optical characterisation studies of novel diketo-pyrrolo- pyrroles. 44th Heyrovský Discussion Nanostructures on Electrodes; *Castle Třešť Czech Republic* (2011), s. 57-58. ISBN: 97880873518.

WEITER, M.; VALA, M.; ŠEDINA, M.; OUZZANE, I.: Tailoring of properties of molcular semiconductors for organic electronics and photonics. 10th |international symposium on functional pi- electron systems; *Beijing, China* (2011), s. 253-253.

OUZZANE, I.; WEITER, M.; VALA, M.: Optical characterisation of organic diketo-pyrrolo-pyrroles derivatives and their photo processes study *Beijing, China* (2011).

OUZZANE, I.; VALA, M.; WEITER, M.: Novel diketo-pyrrolo- pyrroles organic derivatives for optical applications. XI pracovní setkání fyzikálních chemiků a elektrochemiků. Brno XI. *Pracovní Setkání Fyzikálních Chemiků a Elektrochemiků* (2011*),* s. 200-202. ISBN: 9788073755140.

ŠEDINA, M.; OUZZANE, I.; VALA, M.; WEITER, M.: Characterization of Phthalocyanine Derivates for Application in Organic Photovoltaics; *Abstract Book.* (2011), s. 902-903.

MLADENOVA, D.; ZHIVKOV, I.; OUZZANE, I.; VALA, M.; WEITER, M.: Characterization of poly[2-methoxy-5-(3',7'-dimethyloctyloxy)-1,4-phenylenevinylene] electrophoretic suspensions used for thin film deposition; *Chemické listy.* (2011), s. 949-949. ISSN: 0009- 2770.

ŠEDINA, M.; OUZZANE, I.; FLIMEL, K.; VALA, M.; WEITER, M.: Characterization of phthalocyanine derivates for application in organic photovoltaic; *Chemické listy.* (2011), s. 902-903. ISSN: 0009- 2770.

2010

VALA, M.; OUZZANE, I.; LUŇÁK, S.; VYŇUCHAL, J.; WEITER, M. Two photon excited fluorescence of novel diphenyl-diketo- pyrrolopyrroles. *Atlanta, USA:* (2010).

2009

OUZZANE, I. Airbus Fly Your Ideas Challenge. Team member of SMART Materials.

2008

OUZZANE, I.; HERMANOVÁ, S.; VALA, M.; WEITER, M.; NEŠPUREK, S. Synthesis of substituted polysilylenes used as semiconductive polymers. *Chemické listy, (*2008), roč. 102, č. 15, s. s1259 (s1260 s.). ISSN: 1213- 7103.

2007

VALA, M.; WEITER, M.; ZMEŠKAL, O.; NAVRÁTIL, J.; OUZZANE, I.; NEŠPŮREK, S.; TOMAN, P. Photoswitchable Charge Traps in Organic Semiconducting Matrix. *International Conference on Organic Electronics. Eindhoven, Netherland:* (2007). s. 100-101.

Given speeches:

OUZZANE I. Masarkova univerzita a Mendelova univerzita. Diplom za 3. Misto va rámci sekce mladých. Commentary from the jury: "Special prize". Konference : XI. Pracovní setkání fyzikálních chemiků a elektochemiků.

Reprints of publications

VALA, M.; KRAJČOVIČ, J.; LUŇÁK Jr., S.; OUZZANE, I.; BOUILLON, J.P.; WEITER, M.: HOMO and LUMO energy levels of N,N′-dinitrophenyl-substituted polar diketopyrrolopyrroles (DPPs); *Dyes and Pigments* (2014), 106, 136–142. DOI: 10.1016/j.dyepig.2014.03.005.

MLADENOVA, D.; WEITER, M.; STEPANEK, P.; OUZZANE, I.; VALA, M.; SINIGERSKY, V.; ZHIVKOV, I.: Characterization of electrophoretic suspension for thin polymer film deposition; *Journal of Physics*: Conference Series (2012), 356, 1, 1-4. 1742- 6596. DOI: 10.1088/1742-6596/356/1/012040.

KUČERÍK, J.; DAVID, J.; WEITER, M.; VALA, M.; VYŇUCHAL, J.; OUZZANE, I.; SALYK, O.: Stability and physical structure tests of piperidyl and morpholinyl derivatives of diphenyl-diketo-pyrrolopyrroles (DPP); *Journal of Thermal Analysis and Calorimetry* (2012), 108, 2, 467-473. ISSN: 1388- 6150. DOI: 10.1007/s10973-011-1896-8.

LUŇÁK, S.; VALA, M.; VYŇUCHAL, J.; OUZZANE, I.; HORÁKOVÁ, P.; MOŽÍŠKOVÁ, P.; WEITER, M.: Absorption and fluorescence of soluble polar diketo-pyrrolo- pyrroles; *Dyes and Pigments* (2011), 91, 1, 269-278. ISSN: 0143- 7208. DOI: 10.1016/j.dyepig.2011.05.004.

VALA, M.; WEITER, M.; HEINRICHOVÁ, P.; ŠEDINA, M.; OUZZANE, I.; MOŽÍŠKOVÁ, P.: Tayloring of molecular materials for organic electronics; *Journal of Biochemical Technology,* (2010), 2, 5, S44 (S45 s.). ISSN: 0974- 2328.

Dyes and Pigments 106 (2014) 136–142

Contents lists available at ScienceDirect

Dyes and Pigments

journal homepage: www.elsevier.com/locate/dyepig

HOMO and LUMO energy levels of *N,N′*-dinitrophenyl-substituted polar diketopyrrolopyrroles (DPPs)

Martin Vala [a,*], Jozef Krajčovič [a,**], Stanislav Luňák Jr. [a], Imad Ouzzane [a], Jean-Philippe Bouillon [b], Martin Weiter [a]

[a] *Materials Research Centre, Faculty of Chemistry, Brno University of Technology, Purkyňova 118, 612 00 Brno, Czech Republic*
[b] *Université et INSA de Rouen, Laboratoire Chimie Organique Bioorganique Réactivité et Analyses (COBRA), UMR CNRS 6014, IRCOF, F-76821 Mont Saint Aignan Cedex, France*

ARTICLE INFO

Article history:
Received 19 December 2013
Received in revised form
3 March 2014
Accepted 4 March 2014
Available online 14 March 2014

Keywords:
Diketopyrrolopyrrole
Arylation
Cyclic voltammetry
Absorption
DFT
Organic photovoltaics

ABSTRACT

A series of four [*3,4*-c]pyrrole-*1,4*-diones (diketopyrrolopyrroles, DPPs) with (substituted) phenyl rings in *3,6*-positions was prepared by direct *N,N′*-arylation of corresponding diketopyrrolopyrrole pigments with *1*-fluoro-*2,4*-dinitro-benzene. While the energies of the HOMO levels depend strongly on the nature of the *p*-substituents on the *3,6*-phenyl rings, the LUMO levels obtained by cyclic and rotating disc voltammetry were found to be almost independent of the substituent. The absorption spectra show either a hypsochromic or bathochromic shift with respect to parent pigments, depending on the electron-donating and -accepting character of the *p*-substituents. This behaviour was rationalized by density functional theory calculations, showing that highest occupied molecular orbital is delocalized over the whole *3,6*-diphenyl-diketopyrrolopyrrole conjugated system as in the parent pigments, while low-lying LUMO is completely different from the precursors, as it is localized exclusively on the *2,4*-dinitrophenyl substituents, i.e. its shape and energy are not affected by a substitution on the *3,6*-phenyl rings.

1. Introduction

Diketopyrrolopyrroles (DPPs) were found as efficient materials both in organic dye-sensitized (DS) [1–4] and bulk heterojunction (BHJ) [5–8] solar cells (SC). In the latter architecture, they act as light absorbing and electron-donating materials, where the fullerene derivative (PCBM) usually serves as an electron acceptor. In order to maximize BHJ SC performance, the energy of the frontier molecular orbitals (FMO) – the HOMO and LUMO of the electron-donating material – has to be optimized. The optimal LUMO energy of the electron-donating material should be about −3.7 eV (considering the −4.0 eV for PCBM LUMO) [8,9]. This leads to minimal energy losses and still ensures sufficient energy excess to drive charge transfer and separation [9]. In order to balance the requirement of a small bandgap (to effectively harvest the solar radiation) with the simultaneous need for a high open voltage circuit (Voc), given by the difference between donor HOMO and PCBM LUMO, the bandgap (Eg) should be about 1.4–1.5 eV [8,9]. It is believed that such energy optimization of the DPP donor can lead to devices with a power conversion efficiency of over 9% [8].

Tuning the HOMO and LUMO energies and consequently the bandgap of DPPs is based mainly on the modification of *3,6*-(hetero)aryls by electron donating/accepting substitution [10], conjugation extension [11,12], or a combination of both building principles [13,14]. Formal heterosubstitutions of the central DPP core, forming either furopyrrolinones [15] and furofuranones (DFFs) [16,17] or pyrrolo-pyrrole-dionothiones and -dithiones [18], can also change the energy levels considerably. A common feature of all these structural modifications is that both frontier molecular orbital (FMO) energy levels are generally changed, either in the same or opposite direction and to a different extent. On the other hand, the substitution of DPP nitrogens is generally considered as a way of improving solubility and processability, but not as an energy tuning tool. Solubility is usually realized by *N,N′*-dialkylation with alkylhalogens [19] or *N,N′*-diacylation [20], the latter derivatives (so called latent pigments) being problematic in BHJ SC, because of their thermal instability during annealing [21]. *N,N′*-diarylated DPPs were synthesized directly by the arylation of DPP pigments only in the case of highly reactive arylhalogen (*1*-fluoro-*2,4*-dinitro-benzene [22]), because of the low reactivity of the usual arylhalogens. *N,N′*-diarylated DPPs without strong acceptor groups

* Corresponding author. Tel.: +420 541149411.
** Corresponding author.
E-mail addresses: vala@fch.vutbr.cz (M. Vala), krajcovic@fch.vutbr.cz (J. Krajčovič).

http://dx.doi.org/10.1016/j.dyepig.2014.03.005
0143-7208/

on the aryl rings were obtained by the reaction of DFFs with aromatic amines [17,22,23].

The aims of the presented paper were, first, to prepare a representative set of *N,N′*-diarylated DPPs using direct arylation by *1*-fluoro-*2,4*-dinitro-benzene acting as a highly electron-deficient aryl electrophile as in Ref. [22], and, second, to measure how efficiently such a strong electron-accepting group on both nitrogens can stabilize the FMO energy levels in the final derivatives, especially the energy of LUMO by analogy with the effect of formal hetero-substitution (*N* to more electronegative *O*), when going from DPPs to DFFs [24]. Similarly to a previously reported arylation reaction [10], variously substituted DPP derivatives were chosen as the substrates (Scheme 1). The properties of the synthesized arylated compounds were compared with previously reported absorption [25] and electrochemical [26] measurements of their analogues, alkylated on nitrogen with an ethyl ester group (Scheme 2).

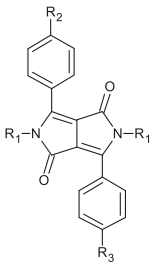

R_1	R_2	R_3	Notation	
H	H	H	BPPB	**I**
CH_2COOEt	H	H	N,N-bis(ethylester)-BPPB	**Et-I**
2,4-Dinitrophenyl	H	H	N,N-bis(dinitrophenyl)-BPPB	**Ar-I**
H	N◯	H	4-Pip-BPPB	**IV**
CH_2COOEt	N◯	H	N,N-bis(ethylester)-4-Pip-BPPB	**Et-IV**
2,4-Dinitrophenyl	N◯	H	N,N-bis(dinitrophenyl)-4-Pip-BPPB	**Ar-IV**
H	N◯	N◯	4-Pip-BPPB-4-Pip	**V**
CH_2COOEt	N◯	N◯	N,N-bis(ethylester)-4-Pip-BPPB-4-Pip	**Et-V**
2,4-Dinitrophenyl	N◯	N◯	N,N-bis(dinitrophenyl)-4-Pip-BPPB-4-Pip	**Ar-V**
H	CN	N◯	4-CN-BPPB-4-Pip	**VI**
CH_2COOEt	CN	N◯	N,N-bis(ethylester)-4-CN-BPPB-4-Pip	**Et-VI**
2,4-Dinitrophenyl	CN	N◯	N,N-bis(dinitrophenyl)-4-CN-BPPB-4-Pip	**Ar-VI**

Scheme 2. Compounds under study (Pip = piperidino).

2. Experimental and theoretical procedures

2.1. Materials and instruments

1-Fluoro-*2,4*-dinitrobenzene and potassium carbonate were purchased from Sigma–Aldrich. *N,N*-dimethylformamide (DMF, Sigma–Aldrich) was dried by azeotropic distillation with benzene (10% v/v). Acetone, dichloromethane (DCM), petroleum ether and ethyl acetate (EA) were of analytical grade purchased from Riedel-de-Haën and used without further purification. All chromatographic separations were carried out on silica gel 60 (220–440 mesh, Sigma–Aldrich). The starting DPP pigments **I**, **IV**, **V** and **VI** were the same as used in Ref. [10].

The UV–VIS absorption spectra were recorded in dimethylsulfoxide (DMSO) by a Varian Carry 50 spectrometer. Cyclic voltammetry (CV) and rotating disc voltammetry (RDV) measurements were performed in acetonitrile with 0.1 M Bu_4NPF_6 as electrolyte. A three electrode cell with a Pt disk (2 mm diameter) as the working electrode and saturated calomel electrode as the reference and Pt wire as the auxiliary electrode were used. These latter two electrodes were separated by a bridge filled with supporting electrolyte. A PGSTAT 128N potentiostat (Metrohm Autolab B.V., Utrecht, The Netherlands) operated via GPEs 4.9 software was used.

2.2. Syntheses

2.2.1. General procedure for the synthesis of N,N′-arylated derivatives of DPPs

Dry DMF (30 mL), corresponding compounds **I**, **IV**, **V** and **VI** (1 mmol), anhydrous potassium carbonate (4 mmol), and *1*-fluoro-*2,4*-dinitrobenzene (4 mmol) were charged to a dry three-necked flask flushed with argon. The reaction mixture was stirred at ambient temperature for 6 days in all cases. Reaction progress was monitored by TLC. After completion, the reaction mixture was poured into ice-water (60 mL). The crude product was filtered off and washed with water (5 × 40 mL), dried and purified by silica gel column chromatography.

2.2.2. 2,5-Bis(2,4-dinitrophenyl)-3,6-diphenylpyrrolo[3,4-c] pyrrole-1,4(2H,5H)-dione (**Ar-I**)

Product **Ar-I** was obtained as an orange solid by silica gel column chromatography with acetone as the eluent. Yield: 54%, m.p. 375–377 °C (373–376 °C [15]). IR (cm^{-1}): 1387, 1550, 1715. ^1H NMR (DMSO-d_6, 300 MHz), δ (ppm): 8.92 (1H, d, J = 2.2 Hz), 8.85 (1H, d, J = 2.2 Hz), 8.62 (1H, dd, J = 8.7, 2.2 Hz), 8.55 (1H, dd, J = 8.7, 2.2 Hz), 7.86 (1H, dm, J = 8.7 Hz), 7.6–7.4 (11H, m). $C_{30}H_{17}N_6O_{10}$: EI HRMS: Calculated *m/z* 621.4805 (M + H); Found 621.4811, Calculated: C (58.06), H (2.60), N (13.54); Found C (57.71), H (2.54), N (13.47).

2.2.3. 2,5-Bis(2,4-dinitrophenyl)-3-phenyl-6-(4-(piperidin-1-yl) phenyl)pyrrolo[3,4-c]pyrrole-1,4(2H,5H)-dione (**Ar-IV**)

Product **Ar-IV** was obtained as a deep violet solid by silica gel column chromatography with DCM/petroleum ether 7/3 (v/v) as the eluent. Yield: 69%. IR (cm^{-1}): 1203, 1250, 1345, 1520, 1686. ^1H NMR (DMSO-d_6, 300 MHz), δ (ppm): 8.88 (1H, m), 8.83 (1H, m), 8.5–8.2 (2H, m), 7.6–7.1 (9H, m), 6.67 (2H, m), 1.6–1.5 (10H, m). $C_{35}H_{26}N_7O_{10}$: EI HRMS: Calculated *m/z* 704.1741 (M + H); Found

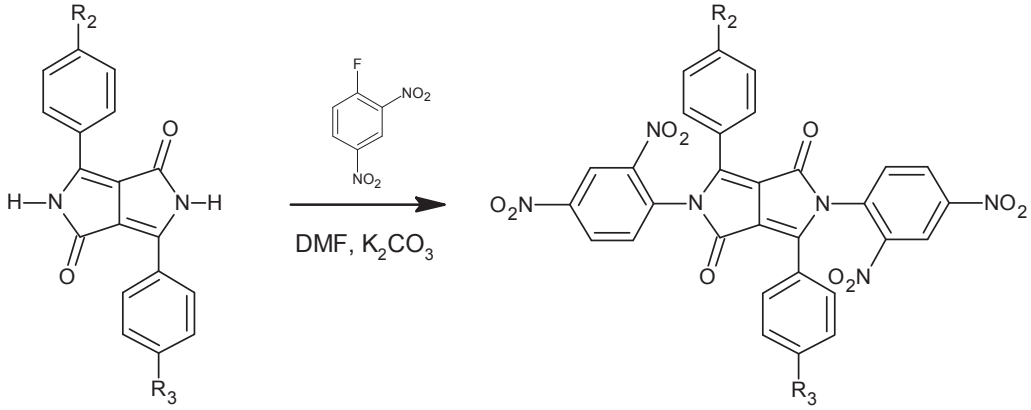

Scheme 1. General synthetic procedure of the DPP derivatives Ar-I, Ar-IV, Ar-V and Ar-VI.

704.1744, Calculated: C (64.28), H (4.20), N (12.49); Found: C (63.83), H (4.21), N (12.38).

2.2.4. 2,5-Bis(2,4-dinitrophenyl)-3,6-bis(4-(piperidin-1-yl)phenyl) pyrrolo[3,4-c]pyrrole-1,4(2H,5H)-dione (**Ar-V**)

Product **Ar-V** was obtained as a deep violet solid by silica gel column chromatography with acetone as the eluent. Yield: 14%. IR (cm^{-1}): 1215, 1243, 1347, 1510, 1530, 1682. ^1H NMR (DMSO-d_6, 300 MHz), δ (ppm): 8.86–8.82 (2H, m), 8.61–8.56 (2H, m), 7.78–7.70 (2H, m), 7.66–7.60 (2H, m), 7.56–7.48 (3H, m), 7.38–7.34 (1H, m), 7.02–6.92 (1H, m), 6.56 (1H, d, $J = 8.3$ Hz), 2.8–2.6 (8H, m), 1.2–1.1 (12H, m). $C_{40}H_{35}N_8O_{10}$: EI HRMS: Calculated *m/z* 787.7413 (M + H); Found 787.7419, Calculated: C (65.16), H (4.93), N (12.97); Found: C (64.83), H (4.99), N (12.90).

2.2.5. 4-(2,5-Bis(2,4-dinitrophenyl)-3,6-dioxo-4-(4-(piperidin-1-yl) phenyl)-2,3,5,6-tetrahydropyrrolo[3,4-c]pyrrol-1-yl)benzonitrile (**Ar-VI**)

Product **Ar-VI** was obtained as a deep violet solid by silica gel column chromatography with DCM/EA 8/2 (v/v) as the eluent. Yield: 25%. IR (cm^{-1}): 1230, 1345, 1500, 1520, 1690, 2350. ^1H NMR (DMSO-d_6, 300 MHz), δ (ppm): 9.00 (1H, m), 8.94 (1H, m), 8.6–8.3 (2H, m), 7.7–7.1 (8H, m), 6.8–6.7 (2H, m), 3.5–3.4 (4H, m), 1.8–1.6 (6H, m). $C_{36}H_{25}N_8O_{10}$: EI HRMS: Calculated *m/z* 729.1694 (M + H); Found 729.1705, Calculated: C (63.70), H (3.90), N (14.05); Found: C (63.19), H (3.86), N (13.95).

2.3. Quantum chemical calculations

The calculations of closed-shell (neutral molecules and dications) and open-shell (radical cations) species of four *N*,*N*′-bis(dinitrophenyl)-DPP derivatives were carried out on restricted and unrestricted levels. The B3LYP xc functional was always used in combination with the 6-311G(d,p) basis set for geometrical optimization in a vacuum, and with the 6-311++G(d,p) basis set for ground state energies, including the solvent effect of acetonitrile introduced by the polarized continuum model (PCM). Solvation energies were computed as the difference between the energies calculated with the 6-311++G(d,p) basis in acetonitrile and in vacuo on the same optimized geometry of a given species. This means, that the calculation accurately predicts the theoretical level used for *N*,*N*′-bis(ethylester) derivatives reported previously [26]. All methods were from the Gaussian software package [27]. The geometries of neutral and all ionized species of compounds **Ar-I** and **Ar-V** in vacuo were calculated under C_i symmetry constraints. No imaginary frequencies were detected.

3. Results and discussion

3.1. Synthesis and analytics

The synthesis of *N*,*N*′-diarylated derivatives of DPPs is a one-step process and mono *N*-arylated products were not isolated. A new family of DPP derivatives was prepared by nucleophilic aromatic substitution using *1*-fluoro-*2*,*4*-dinitrobenzene. All four synthesized derivatives (Scheme 2) were obtained in moderate yields and with sufficient purity, as confirmed by TLC, elemental analysis, ^1H NMR spectroscopy and HRMS. The reaction conditions were partially similar to those used for alkylation with ethyl bromoacetate (DMF as a solvent, potassium carbonate as base), except for the use of an argon atmosphere. The process is complicated by the extremely low solubility of the starting derivatives, which continue to remain in the reaction mixtures even after several days (partial conversion). *N*,*N*′-diarylated DPPs **Ar-I**, **Ar-IV**, **Ar-V** and **Ar-VI** possess reasonable solubility in common organic solvents such as, for example, chloroform, dichloromethane, acetone, THF, ethyl acetate, and acetonitrile compared to the starting materials. In contrast to *N*,*N*′-dialkylation, the reported arylation cannot be considered as a universal procedure, as attempts to prepare *N*,*N*′-bis(dinitrophenyl) derivatives of DPPs with only cyano group on the *p*-position of the *3*,*6*-phenyl rings (analogues of *N*,*N*′-bis(ethylester) derivatives **VIII** and **IX** from Refs. [25], starting from compounds **II** and **III** from Ref. [10], see Scheme S1 in SI) were not successful due to the low reactivity at ambient temperature.

3.2. Cyclic and rotating disc voltammetry

Although the optimal energies of HOMO and LUMO levels in BHJ SC, mentioned in the Introduction, relate to the values in solid state, it is suitable first to study the effect of a new structural modification to these energies in solution, where the same or a similar effect of an environment unaffected by different crystal packing can be supposed. Thus, the cyclic voltammetry (CV) and rotating disc voltammetry (RDV) experiments were carried out under standard conditions, exactly the same as for the *N*,*N*′-bis(ethoxycarbonylmethyl)series of compounds (Et-I – Et-VI) reported previously [26]. The measured voltammograms are in Figs. S1–S4, see SI, and the results are summarized in Table 1. The difference in HOMO and LUMO energies between *N*,*N*′-bis(dinitrophenyl) and *N*,*N*′-bis(ethylester) sets is visualized in Fig. 1.

There are several differences between the data recorded for the *N*,*N*′-bis(dinitrophenyl) and *N*,*N*′-bis(ethylester) sets. First, the LUMO energy of the former is almost independent of *p*-substituents on the *3*,*6*-phenyl rings. Consequently, the LUMO energies of all four Ar-*X* derivatives (3.65–3.69 eV) are quite close to desired values for BHJ SC application; on the other hand, the fine tuning of the HOMO energy by substitution in the *3*,*6*-positions appears to be almost impossible. Second, HOMO energies depend qualitatively on these *p*-substituents in a similar manner in both sets; however, quantitatively, this dependence is considerably different, changing the HOMO energy difference between the corresponding members of both sets from about 0.25 eV for the **Ar-I** and **Et-I** pair over 0.11–0.12 eV for asymmetrical pairs, to 0.03 eV for the **Ar-V** and **Et-V** di-piperidino substituted pair. Nevertheless, considering the latter smaller value, one must take into account that a HOMO energy of −5.00 eV for **Et-V** comes from two-electron oxidation [26], while for **Ar-V** this process is split into two one-electron oxidations relating to HOMO energies −5.029 and −5.304 eV. An average value of −5.17 eV from two one-electron processes for **Ar-V** thus differs from the two-electron one for **Et-I** by about 0.17 eV, i.e a value not far from those found for both mono-piperidino substituted pairs. To explain these slightly surprising trends, detailed quantum chemical calculations were performed as described in the following section.

3.3. DFT calculations

The geometry of four *N*,*N*′bis(dinitrophenyl) derivatives in the neutral ground singlet state was optimized by DFT calculations. Conformation with the *o*-nitro group oriented towards the DPP carbonyl was always more stable than the opposite (rotated) one,

Table 1
The energies of HOMO and LUMO measured by cyclic voltammetry in acetonitrile and recalculated by the $E_{HOMO/LUMO} = E_{ox1/red1} + 4.429$ formula [28].

	E_{LUMO} [eV]	E_{HOMO} [eV]	E_{GAP} [eV]
Ar-I	−3.670	−5.900	2.230
Ar-IV	−3.650	−5.290	1.640
Ar-V	−3.660	−5.029	1.369
Ar-VI	−3.690	−5.340	1.650

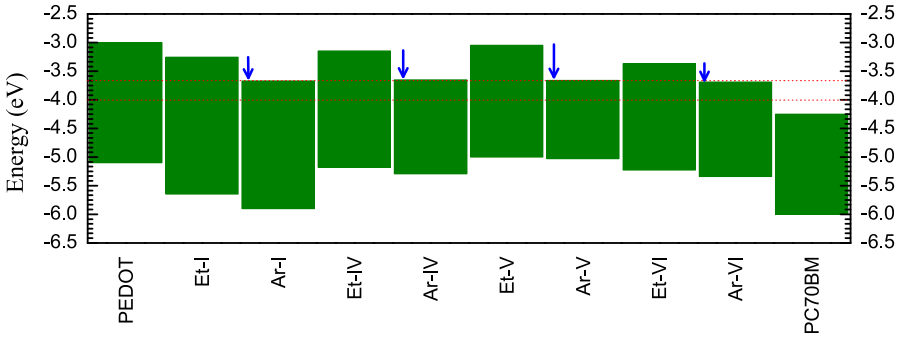

Fig. 1. HOMO and LUMO energy levels of the studied compounds. The data for Ar-*X* set come from Table 1, data for Et-*X* set from Ref. [26]; the value −4.3 eV of $PC_{70}BM$ LUMO was taken from Refs. [8,9]. The arrows show the stabilization of LUMO due to the *N*,*N*′-bis(dinitrophenyl) substitution with respect to *N*,*N*′-bis(ethylester) derivatives. The area between the lines represents the optimal LUMO energy for combination with $PC_{70}BM$ as electron acceptor in BHJ SC [8].

exactly as in the crystal [22]. The distribution of electron density in frontier molecular orbitals is drawn in Fig. 2. It is clear that the shape of the HOMO of these derivatives is qualitatively the same as for pigment precursor [10] or *N*,*N*′-bis(ethylester) analogues [25,26], i.e. delocalized over the whole *3*,*6*-di(substituted)phenyl-DPP conjugated system. On the other hand, the LUMO is formed by totally different MO than for corresponding pigments, mainly (**Ar-I**) or fully (**Ar-IV** − **Ar-VI**) localized on both *2*,*4*-dinitrophenyl substituents with minimal (**Ar-I**) or zero (**Ar-IV** − **Ar-VI**) density on *3*,*6*-(substituted)phenyl rings. Such a picture fully explains the independence of the first reduction potentials, i.e. adiabatic LUMO levels, on *p*-substitution of *3*,*6*-phenyl rings, as this potential corresponds to the addition of an electron to the LUMO orbital, forming thus a radical anion.

In order to explain the shift in HOMO energy levels in the Ar-*X* and Et-*X* series (Fig. 1), considerably more detailed computations had to be performed. In order to achieve directly comparable results for both sets, exactly the same computational methodology as in Ref. [26] was used. The results are summarized in Table 2.

The agreement between the *ab initio* computed (IP_{ad} in Table 2) and experimental (E_{HOMO} in Table 1) values is impressive: the differences are −0.028 eV, −0.005 eV, −0.078 eV and +0.026 eV, for **Ar-I**, **Ar-IV**, **Ar-V** and **Ar-VI**, respectively, advocating thus the used methodology as a relevant tool to study the gentle effects connected with the electrochemical formation of radical cations. The HOMO and LUMO energies, derived from electrochemical electron transfers, are affected by intermolecular and intramolecular reorganization energies. The former come mainly from the reorganization of solvent shells with the eventual additional effect of ion-pairing [29,30], while the source of the latter is the changes of molecular geometry upon ionization.

Comparing the solvation energies, modelling the dominant portion of external reorganization, for Ar-*X* (Table 2) and Et-*X* [26] sets the following picture is obtained: the absolute values of $E_{solv}(x)$ ($x = 0$, $+$ and $++$) are generally higher for the Ar-*X* set, probably because of a larger volume of solvent surrounding these bigger derivatives. Consequently, their changes, representing reorganization, $\Delta E_{solv}(0,+) = E_{solv}(+) - E_{solv}(0)$ are also higher for the Ar-*X* set, but the difference in $\Delta E_{solv}(0,+)$ for the corresponding members of both sets is almost constant (0.409 eV, 0.409 eV and 0.364 eV for the Ar-*X* and Et-*X* pairs, X = I, IV, and V, respectively), i.e. it is not dependent on piperidino substitution and thus does not explain the experimentally observed piperidino-dependent trend in the differences in the HOMO levels of both sets (Fig. 1).

The total intramolecular reorganization energy $\lambda(+)$ (see a legend of Table 2) is a crucial parameter in the description of self-exchange hole transfer by the hopping mechanism in the solid-state [31]. In the case of electrochemical ionization, only one of its parts ($\lambda_1(+)$ or $\lambda_2(+)$, which should be very similar in the case when the model of translated harmonic oscillators is valid) takes place, or, more specifically, one part modifies the potential of the oxidation of a neutral compound and the second acts in the back reduction of radical cation for reversible processes. The intramolecular reorganization energies of the Et-*X* series were not reported [26], thus we present them here: $\lambda_1(+) = 0.243$ eV, 0.195 eV and 0.237 eV and $\lambda(+) = 0.473$ eV, 0.529 eV and 0.488 eV for **Et-I**, **Et-IV** and **Et-V**, respectively. The total intramolecular reorganization energies $\lambda(+)$ of the Ar-*X* set (Table 2) are slightly higher than those for the Et-X set, i.e. slightly lower hole transfer rates (mobilities) in solid-state can be expected, as they decrease exponentially with rising reorganization energy [31]. However, the absolute differences in $\lambda_1(+)$ between both sets are relatively low and similar (0.04–0.06 eV for X = I, IV and V), i.e. they also do not explain the dependence of the difference in HOMO energies between both sets on piperidino substitution.

There were two significant discrepancies between the theoretical predictions and experimental results for the Et-*X* set reported [26]: a large difference between the computed and measured HOMO energies for piperidino derivatives and two-electron transfer for **Et-V**. An explanation was tentatively ascribed to the role of ion-pairing of piperidino derivatives with PF_6^- from the supporting electrolyte, bringing an additional stabilization of radical cation energy estimated to be about 0.08 eV per each piperidino group [26]. Neither of these two effects are observed for the Ar-*X* series, i.e. the theoretical/experimental agreement is excellent (Table 2) and, furthermore, **Ar-V** undergoes two one-electron oxidations. Thus, we consider that ion-pairing does not affect the HOMO energies of *N*,*N*′-bis(dinitrophenyl) derivatives derived from electrochemical experiments, maybe because of the combined sterical/electrostatic influence of dinitrophenyl substituents. Going back, if we recalculate the energies of the piperidino derivative **Et-IV**, **Et-V** and **Et-VI** radical cations by adding the contribution of ion-pairing energy (0.08 eV per each piperidine), the energies of the HOMO are thus destabilized and the differences in HOMO energies between both sets are 0.25 eV for the **Ar-I** and **Et-I** pair, about 0.19–0.20 eV for asymmetrical pairs, and 0.19 eV for the **Ar-V** and **Et-V** pair, i.e. relatively close, because there is no reason why the stabilization of HOMO by a change in *N*,*N*′-substituents of the DPP core should significantly depend on *p*-substituents on *3*,*6*-phenyl rings.

3.4. Absorption spectra

The absorption spectra of *N*,*N*′-bis(dinitrophenyl) derivatives in DMSO together with the spectra of their pigment precursors [10] and *N*,*N*′-bis(ethylester) analogues [25] are shown in Fig. 3. The effect of *N*,*N*′-alkylation on the absorption spectra of 3,6-di-(substituted)phenyl DPPs is well known. The absorption maxima of

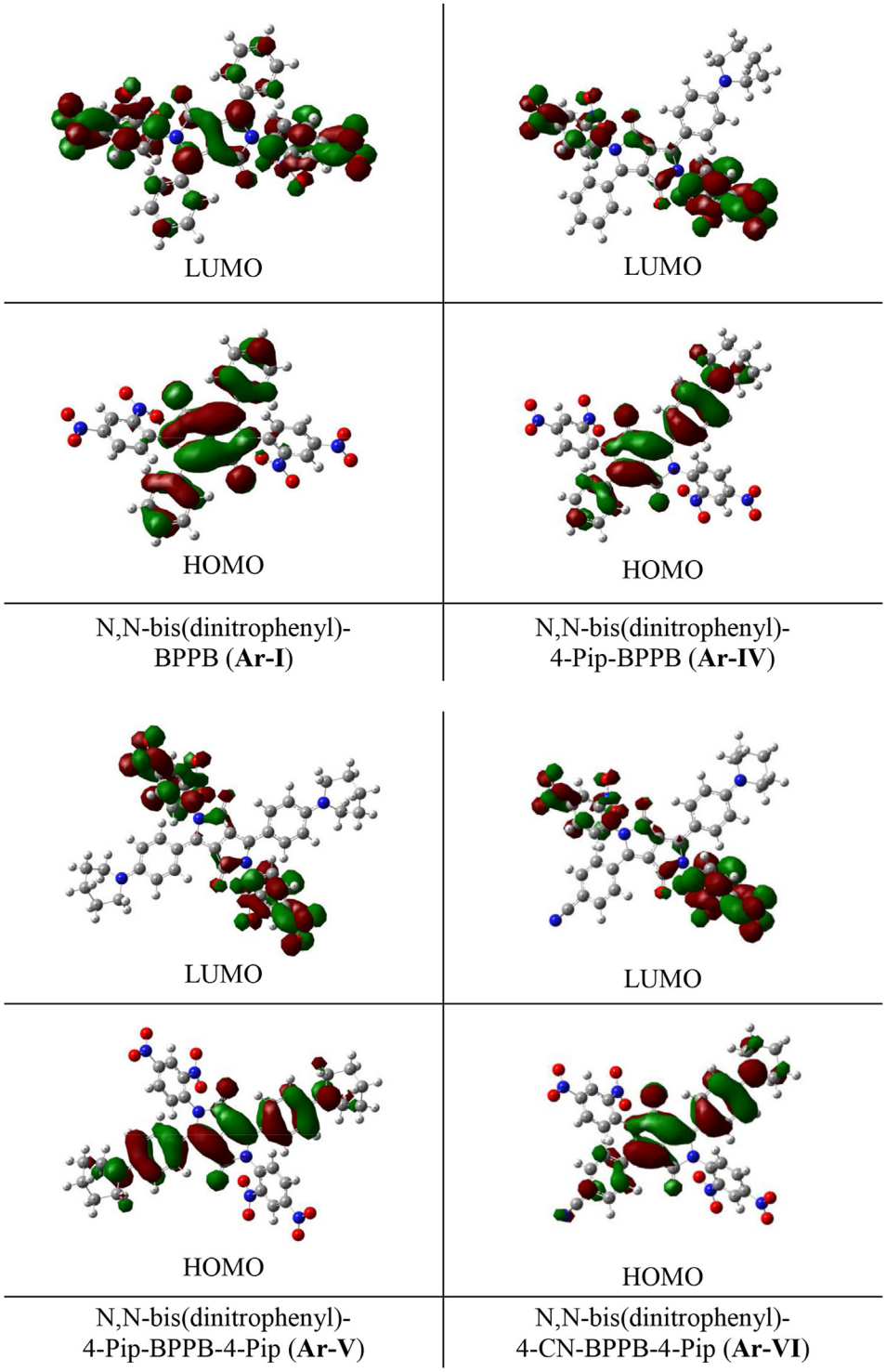

Fig. 2. Kohn–Sham molecular orbitals of *N,N′*-bis(dinitrophenyl) derivatives under study.

planar pigments correspond to the 0–0 vibronic transition, while the loss of planarity by alkylation [25,32,33] leads to 0–1 absolute maxima and an unresolved vibronic structure. Altogether, a hypsochromic shift always accompanies an alkylation. The trends in the *N,N′*-bis(dinitrophenyl) set are more complicated (Fig. 3). The vibronic structure of the longest wavelength absorption band is blurred as in the *N,N′*bis(ethylester) set, reflecting thus non-planarity and (very probably) the 0–1 vibronic band as the absolute maximum. However, the absorption maxima with respect to parent pigments are shifted either hypsochromically (**Ar-I** 462 nm) or bathochromically (**Ar-IV** 548 nm and **Ar-V** 569 nm) or are almost the same (**Ar-VI** 576 nm). In other words, the bathochromic shifts of the absorption maxima (all corresponding to the 0–1 vibronic transition) of the corresponding member of the Ar-*X* set with respect to the Et-X set are 90 cm^{-1}, 1130 cm^{-1}, 940 cm^{-1} and 1120 cm^{-1} for X = I, IV, V and VI, respectively.

Table 2
Theoretical values of the firstionization potentials $IP_{ad} = E_+(+) - E_0(0)$ in acetonitrile, where $E_x(Y)$ is the total energies of species x on the optimized geometry of species Y. $E_{solv}(0)$, $E_{solv}(+)$ and $E_{solv}(++)$ are the solvation energies of the neutral molecule, radical cation and dication. $\lambda(+) = \lambda_1(+) + \lambda_2(+) = (E_0(+) - E_0(0)) + (E_+(0) - E_+(+))$ is the total reorganization energy in vacuo accompanying the hole transfer.

	IP_{ad} [eV]	$E_{solv}(0)$ [eV]	$E_{solv}(+)$ [eV]	$E_{solv}(++)$ [eV]	$\lambda_1(+)$ [eV]	$\lambda(+)$ [eV]
Ar-I	−5.872	0.832	2.298	6.316	0.279	0.557
Ar-IV	−5.285	0.883	2.253	5.870	0.253	0.524
Ar-V	−4.951	0.918	2.144	5.504	0.296	0.635
Ar-VI	−5.366	1.030	2.531	6.209	0.222	0.480

An explanation of this behaviour of the longest wavelength HOMO–LUMO transition is based on the independence of the low-lying LUMO energy of *N*,*N*′-bis(dinitrophenyl) derivatives on *p*-substituents. In the case of parent pigments or *N*,*N*′-bis(ethylester) derivatives, the effect of piperidino substitution is clear – it destabilizes both HOMO and LUMO and a bathochromic shift is caused by the lower effect of the electron-donating piperidino group on the LUMO compared to HOMO [10,25]. The influence of the electron-accepting cyano group is opposite and smaller in absolute scale [26]. In the case of localized LUMO in the Ar-*X* set, *p*-substituents only destabilize the HOMO. Thus, the missing destabilization of LUMO leads to the lower gap and therefore the observed bathochromic shift of Ar-*X* with respect to the corresponding Et-*X* piperidino substituted derivatives, or even with respect to the parent pigments **IV** and **V** in the case of **Ar-IV** and **Ar-V**, with the most destabilized HOMO due to the presence of one or two piperidino substituents and the absence of the stabilizing cyano group.

4. Conclusion

The spectral and electrochemical study of *N*,*N*′-bis(dinitrophenyl) diketopyrrolopyrrole derivatives, together with theoretical calculations, show the significant effect of this substitution on the character and energies of the HOMO and LUMO levels. The LUMO level was found to be independent of the rest of the molecule, as it is localized on *N*,*N*′-dinitrophenyl substituents. Its energy is close to the optimal range for electron donors combined with PCBM in BHJ SC. The HOMO energy of these derivatives is stabilized at about 0.2 eV with respect to *N*,*N*′-bis(ethylester) derivatives, giving thus a good chance to increase the open circuit voltage and thus power conversion efficiency in BHJ SC. On the other hand, the higher intramolecular reorganization energy, induced by this substitution, can negatively affect hole transport in these materials. Finally, this substitution causes a bathochromic shift for DPP derivatives with electron-donors in *3*,*6*-positions, increasing thus the harvesting ability with respect to the spectral profile of sunlight.

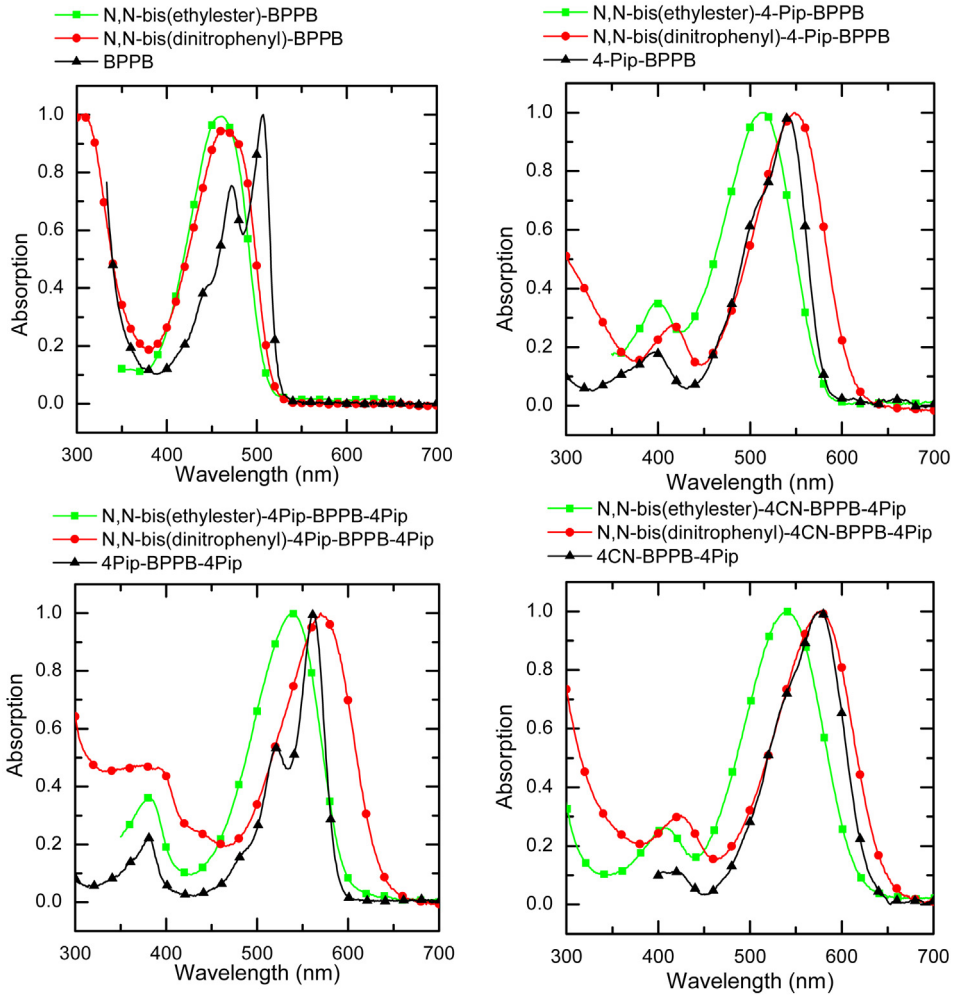

Fig. 3. Normalized absorption spectra of parent pigments and their *N*,*N*′-bis(ethylester) and *N*,*N*′-bis(dinitrophenyl) derivatives in DMSO.

Acknowledgement

The work was supported by the Grant Agency of the Czech Republic (13-29358S) (project No. P205/10/2280) and by the Ministry of Education Youth and Sports of the Czech republic (project No. LO1211). S.L. is particularly grateful for access to computing and storage facilities owned by parties and projects contributing to the National Grid Infrastructure MetaCentrum, provided under the programme "Projects of Large Infrastructure for Research, Development, and Innovations" (LM2010005). The authors would like to acknowledge Dr. Jan Vynuchal (VUOS) for providing us with the starting materials, Dr. Tomáš Mikysek (University of Pardubice) for the measurements of the cyclic voltammograms and Jana Honová (BUT) for the UV–Vis measurement.

Appendix A. Supplementary data

Supplementary data related to this article can be found at http://dx.doi.org/10.1016/j.dyepig.2014.03.005.

References

[1] Qu S, Tian H. Diketopyrrolopyrrole (DPP)-based materials for organic photovoltaics. Chem Commun 2012;48(25):3039–51.
[2] Qu S, Ch Qin, Islam A, Wu Y, Zhu W, Hua J, et al. A novel D–A-p-A organic sensitizer containing a diketopyrrolopyrrole unit with a branched alkyl chain for highly efficient and stable dye-sensitized solar cells. Chem Commun 2012;48(55):6972–4.
[3] Yum JH, Holcombe TW, Kim Y, Yoon J, Raktys K, Nazeeruddin MK, et al. Towards high-performance DPP-based sensitizers for DSC applications. Chem Commun 2012;48(87):10727–9.
[4] Holcombe TW, Kim Y, Yum JH, Yoon J, Gao P, Marszalek M, et al. A structural study of DPP-based sensitizers for DSC applications. Chem Commun 2012;48(87):10724–6.
[5] Walker B, Tamayo AB, Dang XD, Zalar P, Seo JH, Garcia A, et al. Nanoscale phase separation and high photovoltaic efficiency in solution-processed, small-molecule bulk heterojunction solar cells. Adv Funct Mater 2009;19(19):3063–9.
[6] Walker B, Kim Ch, Nguyen TQ. Small molecule solution-processed bulk heterojunction solar cells. Chem Mater 2011;23(3):470–82.
[7] Liu J, Walker B, Tamayo A, Zhang Y, Nguyen TQ. Effects of heteroatom substitutions on the crystal structure, film formation, and optoelectronic properties of diketopyrrolopyrrole-based materials. Adv Funct Mater 2013;23(1):47–56.
[8] Walker B, Liu J, Ch Kim, Welch GC, Park JK, Lin J, et al. Optimization of energy levels by molecular design: evaluation of bis-diketopyrrolopyrrole molecular donor materials for bulk heterojunction solar cells. Energ Environ Sci 2013;6(3):952–62.
[9] Janssen RAJ, Nelson J. Factors limiting device efficiency in organic photovoltaics. Adv Mater 2013;25(13):1847–58.
[10] Luňák Jr S, Vyňuchal J, Vala M, Havel L, Hrdina R. The synthesis, absorption and fluorescence of polar diketo-pyrrolo-pyroles. Dyes Pigment 2009;82(2):102–8.
[11] Luňák Jr S, Havel L, Vyňuchal J, Horáková P, Kučerík J, Weiter M, et al. The geometry and absorption of diketo-pyrrolo-pyrroles substituted with various aryls. Dyes Pigment 2010;85(1–2):27–36.
[12] Tamayo AB, Tantiwiwat M, Walker B, Nguyen TQ. Design, synthesis, and self-assembly of oligothiophene derivatives with a diketopyrrolopyrrole core. J Phys Chem C 2008;112(39):15543–52.
[13] Beninatto R, Borsato G, De Lucchi O, Fabris F, Lucchini V, Zendri E. New 3,6-bis(biphenyl)diketopyrrolopyrrole dyes and pigments *via* Suzuki-Miyaura coupling. Dyes Pigment 2013;96(3):679–85.
[14] Bürckstümmer H, Weissenstein A, Bialas D, Würthner F. Synthesis and characterization of optical and redox properties of bithiophene-functionalized diketopyrrolopyrrole chromophores. J Org Chem 2011;76(8):2426–32.
[15] Morton CJH, Riggs RL, Smith DM, Westwood NJ, Lightfoot P, Slawin AMZ. Synthetic studies related to diketopyrrolopyrrole (DPP) pigments. Part 2: the use of esters in place of nitriles in standard DPP syntheses: Claisen-type acylations and furopyrrole intermediates. Tetrahedron 2005;61(3):727–38.
[16] Rubin MB, Bargurie M, Kosti S, Kaftory M. Synthesis and reactions of 1,6-diaryl-2,5-bis(diazo)-1,3,4,6-tetraoxohexanes. J Chem Soc Perkin Trans 1980;1:2670–7.
[17] Langhals H, Grundei T, Potrawa T, Polborn K. Highly photostable organic fluorescent pigments – a simple synthesis of N-arylpyrrolopyrrolediones (DPP). Liebigs Ann; 1996:679–82.
[18] Ripaud E, Demeter D, Rousseau T, Boucard-Cétol E, Allain M, Po R, et al. Structure-properties relationships in conjugated molecules based on diketopyrrolopyrrole for organic photovoltaics. Dyes Pigment 2012;95(1):126–33.
[19] Potrawa T, Langhals H. Fluoreszenzfarbstoffe mit großen Stokes-Shifts – lösliche Dihydropyrrolopyrroldione. Chem Ber 1987;120:1075–8.
[20] Zambounis JS, Hao Z, Iqbal A. Latent pigments activated by heat. Nature 1997;388:131–2.
[21] Tamayo AB, Walker B, Nguyen TQ. A low band gap, solution processable oligothiophene with a diketopyrrolopyrrole core for use in organic solar cells. J Phys Chem C 2008;112(30):11545–51.
[22] Riggs RL, Morton CJH, Slawin AMZ, Smith DM, Westwood NJ, Austen WSD, et al. Synthetic studies related to diketopyrrolopyrrole (DPP) pigments. Part 3: syntheses of tri- and tetra-aryl DPPs. Tetrahedron 2005;61(47):11230–43.
[23] Zhang K, Tieke B. Highly luminescent polymers containing the 2,3,5,6-tetraarylated pyrrolo[3,4-c]pyrrole-1,4-dione (N-aryl DPP) chromophore in the main chain. Macromolecules 2008;41(20):7287–95.
[24] Luňák Jr S, Vyňuchal J, Hrdina R. Geometry and absorption of diketo-pyrrolo-pyrrole isomers and their π-isoelectronic furo-furanone analogues. J Mol Struct 2009;919(1–3):239–45.
[25] Luňák Jr S, Vala M, Vyňuchal J, Ouzzane I, Horáková P, Možíšková P, et al. Absorption and fluorescence of soluble polar diketo-pyrrolo-pyrroles. Dyes Pigment 2011;91(3):269–78.
[26] Luňák Jr S, Eliáš Z, Mikysek T, Vyňuchal J, Ludvík J. One electron vs. two electron electrochemical and chemical oxidation of electron-donor substituted diketo-pyrrolo-pyrroles. Electrochim Acta 2013;106:351–9.
[27] Frisch MJ, Trucks GW, Schlegel HB, Scuseria GE, Robb MA, Cheeseman JR, et al. Gaussian 09, Revision D.01. Wallingford CT: Gaussian, Inc.; 2009.
[28] Isse AA, Gennaro A. Absolute potential of the standard hydrogen electrode and the problem of interconversion of potentials in different solvents. J Phys Chem B 2010;114(23):7894–9.
[29] Evans DH. One-electron and two-electron transfers in electrochemistry and homogeneous solution reactions. Chem Rev 2008;108(7):2113–44.
[30] Adams CJ, da Costa RC, Edge R, Evans DH, Hood MF. On the causes of potential inversion in 1,2,4,5-tetrakis(amino)benzenes. J Org Chem 2010;75(4):1168–78.
[31] Brédas JL, Beljonne D, Coropceanu V, Cornil J. charge-transfer and energy-transfer processes in π-conjugated oligomers and polymers: a molecular picture. Chem Rev 2004;104(11):4971–5004.
[32] Vala M, Weiter M, Vyňuchal J, Toman P, Luňák Jr S. Comparative studies of diphenyl-diketo-pyrrolopyrrole derivatives for electroluminescence applications. J Fluoresc 2008;18(6):1181–6.
[33] Vala M, Vyňuchal J, Toman P, Weiter M, Luňák Jr S. Novel, soluble diphenyldiketo-pyrrolopyrroles: experimental and theoretical study. Dyes Pigment 2010;84(2):176–82.

Journal of Physics: Conference Series **356** (2012) 012040 doi:10.1088/1742-6596/356/1/012040

Characterization of electrophoretic suspension for thin polymer film deposition

D Mladenova[1,2,5], M Weiter[1], P Stepanek[3], I Ouzzane[1], M Vala[1], V Sinigersky[4] and I Zhivkov[1,2]

[1] Centre for Materials Research, Faculty of Chemistry, Brno University of Technology, 118 Purkynova, 612 00 Brno, The Czech Republic
[2] Institute of Optical Materials and Technologies, Bulgarian Academy of Sciences, Acad. G. Bonchev Str. Bl. 101, 1113 Sofia, Bulgaria
[3] Department of Supramolecular Polymer Systems, Institute of Macromolecular Chemistry, Academy of Sciences of The Czech Republic, 2 Heyrovskeho nam., 162 06 Praha 6, The Czech Republic
[4] Institute of Polymers, Bulgarian Academy of Sciences, Acad. G. Bonchev Str., Bl. 103A, 1113 Sofia, Bulgaria

E-mail: dnl@clf.bas.bg

Abstract. The optical absorption and fluorescence spectra of poly [2-methoxy-5-(3′,7′-dimethyloctyloxy)-1,4-phenylenevinylene] toluene solutions and 50:50% toluene/acetonitrile suspensions show clearly distinguishable differences (e.g., peak broadening and shifting), which could be used for characterization of suspensions with different acetonitrile content. The dynamic light scattering (DLS) measurement of the suspensions prepared showed a particle size of 90 nm. Thin films with thicknesses of about 400 nm were prepared by electrophoretic deposition (EPD) and spin coating. As the films are very soft, a contactless optical profilometry techique based on chromatic aberration was used to measure their thickness. AFM imaging of spin coated and EPD films revealed film roughness of 20÷40 nm and 40÷80 nm, respectively. The EPD film roughness seems to be less than the suspension particle size obtained by DLS, probably due to the partial film dissolving by the toluene present in the suspension.

1. Introduction

Among the variety of the methods for "wet" polymer thin film deposition [1] (e. g. spin and dip coating, spray and Langmuir-Blodgett deposition, and ink-jet printing), the electrophoretic deposition (EPD) [2] has the advantages of using a diluted suspension for deposition of relatively thick films, ability for covering a large area and the unique property of separating the solidification stage (precipitation of a solid phase in the suspension) from the film formation stage, which takes place on the electrode.

One of the main problems impeding the wide usage of EPD for thin polymer film preparation is the instability – the suspension particle size depends strongly on the precipitation conditions and tends to

[5] To whom any correspondence should be addressed.

grow with the time. This effect creates difficulties in controlling the EPD thin film structure and morphology.

This study aims to establish methods for characterization of critical stages of the EPD process of deposition of thin poly[2-methoxy-5-(3′,7′-dimethyloctyloxy)-1,4-phenylenevinylene] (MDMO-PPV) films.

2. Experimental details

The EPD suspension with MDMO-PPV (Sigma-Aldrich, catalogue number 546461) concentration of 0.0033 g l^{-1} and toluene/acetonitrile ratio of 50:50% (toluene 99.8%, acetonitrile 99.8%) was prepared and used immediately for measurement or deposition to prevent further particle coagulation.

Dynamic light scattering (DLS) measurements of the suspension prepared were performed on a Malvern Zetasizer Nano ZS instrument equipped with a helium-neon laser; the scattering angle was 173°. The data were processed taking into account the viscosity of the toluene/acetonitrile mixture with 50 % acetonitrile content [3].

The EPD thin film was deposited on the positive electrode at a current of about 50÷70 μA.

A solution with concentration of 8.95 g l^{-1} was prepared and spin coating at approx. 2500 rpm for 60 s was carried out on a KW-4A Chemat Technology Inc. spin coater.

The film thickness of the deposited MDMO-PPV films was determined by a MicroProf® FRT optical profilometer based on chromatic aberration. The method has the advantage of performing fast high-resolution contactless and non-destructive measurements, which is of paramount importance in our case of soft polymer films. The films were scratched by a sharpened tungsten wire then a thin (about 100 nm) Al film was deposited in vacuum to equalize the optical reflection from both scratched and unscratched areas.

Surface morphology images of MDMO-PPV films were taken by NTEGRA Prima AFM. The measurements were carried out in semicontacting mode (frequency of 170 kHz, amplitude 80÷100 nm and scanning rate of 0.5 Hz).

3. Results and discussion

3.1. Suspension characterization

3.1.1. Absorption spectra. Optical absorption spectra of a solution and a 50:50 % toluene/acetonitrile suspension with the same MDMO-PPV concentration of 0.0033 g l^{-1} are presented in figure 1. The solution spectrum (curve 1) consists of the characteristic MDMO-PPV absorption peak [4].

In the suspension (curve 2) spectrum, a "red" shoulder appears which leads to a broadening of the peak. This effect could be related to the appearance of a precipitated solid phase during the suspension formation caused by the precipitating polar acetonitrile.

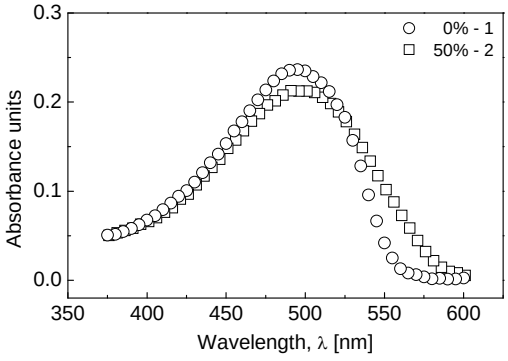

Figure 1. Absorption spectra of a MDMO-PPV solution (curve 1) and a suspension with 50% acetonitrile content (curve 2).

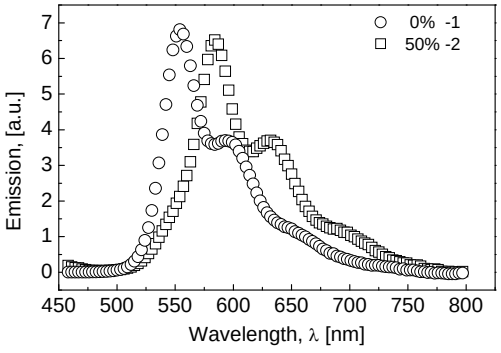

Figure 2. Fluorescence spectra of a MDMO-PPV solution (curve 1) and a suspension with 50% acetonitrile content (curve 2).

3.1.2. Fluorescence spectra. More detailed information about the material under study can be obtained from the fluorescence spectra, as they present information from two processes – absorption and subsequent emission. In figure 2, fluorescence spectra of a MDMO-PPV solution (curve 1) and a suspension with 50 % acetonitrile (curve 2) are plotted. The maximum of the spectrum in the suspension is "red" shifted by about 30 nm. The spectrum shift reflects more precisely the formation of the solid phase.

It could be concluded that effect of the peak broadening in the absorption spectra could be used for a qualitative estimation of the suspension properties, while the peak shifts in the fluorescence spectra yield more detailed information about the formation of a solid phase in the suspension.

3.1.3. Dynamic light scattering. The size of the particles forming the solid-state phase in the toluene/acetonitrile suspension with 50 % acetonitrile content was estimated by DLS. The typical correlation function obtained (figure 3) allows a straightforward determination of the particle size. The inset in the figure presents the particle size distribution by the intensity obtained using inverse Laplace transformation. The data obtained indicate an average particle diameter of 90 nm.

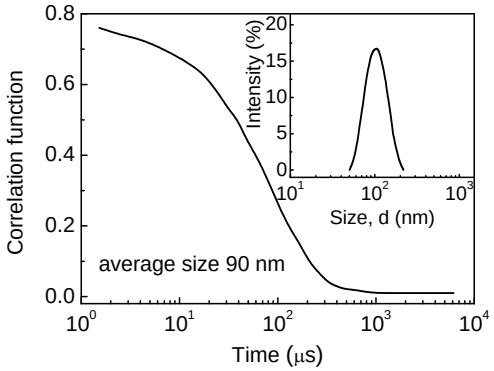

Figure 3. DLS measured curves.

3.2. Thin film characterization

3.2.1. Optical profilometer film thickness measurement. Figure 4, a) and b) present scanned optical aberration images of a scratched MDMOPPV. The scratched area is clearly distinguished, which allows a satisfactory film thickness determination. A film thickness of about 400 nm was determined by processing the data from a single profile line (figure 4, c). Optical-aberration 3D and 2D images can be used as a preliminary film-surface morphology estimation.

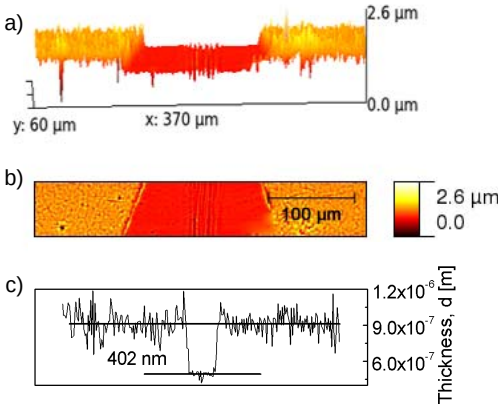

Figure 4. Optical aberration scanning of a scratched MDMO-PPV film: a) – 3D, b) – 2D and c) – 1D images.

A film thickness of about 400 nm was measured by the same procedure for the spin-coated films.

3.2.2. AFM imaging. 2D and 3D AFM images of EPD deposited films are shown in figure 5. The surface roughness observed is less than but comparable to the particle size as obtained by DLS. Despite the general assumption that the size of the particle in the suspension should be preserved after EPD of a film [5], partial dissolving of the particles deposited on the substrate by the solvent (50% toluene in the suspension) is possible, which decreases the film roughness. Thus, varying the toluene/acetonitrile ratio gives an opportunity to control the film roughness.

For comparison, the AFM image of a spin-coated film with similar thickness is presented in figure 6. The picture shows a predominant film surface roughness of 20÷40 nm, which is smoother than the surface of the EPD film. The peaks observed with height approx. 50÷70 nm could be connected with the presence of undissolved or aggregated MDMO-PPV particles due to the relatively high solution concentration.

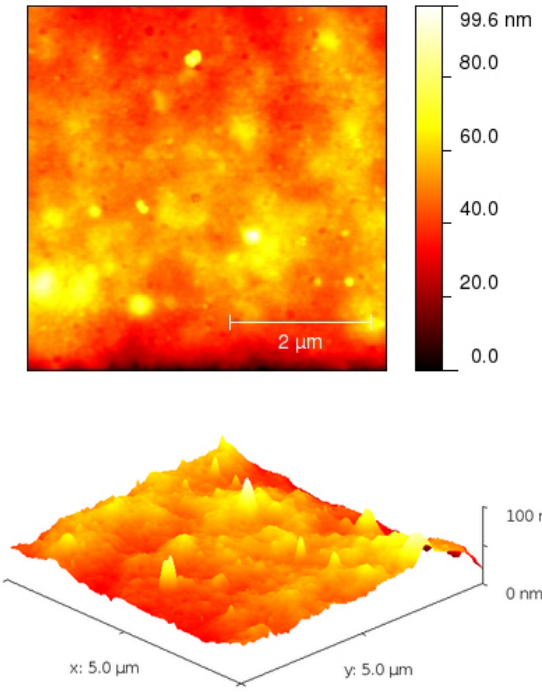

Figure 5. AFM 2D and 3D images of an EPD film measured on a 5×5 µm scanned area.

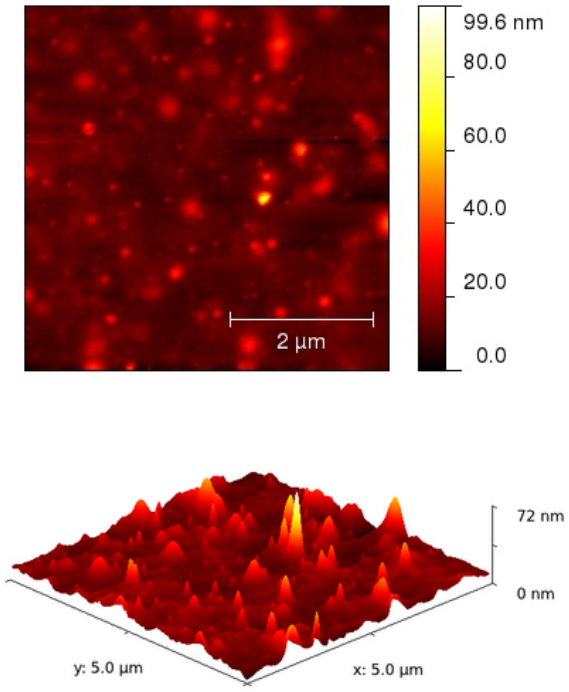

Figure 6. AFM 2D and 3D images of a spin coated film measured on 5×5 µm scanned area.

Conclusions

A combination of experimental methods was applied to the characterization of the different stages of the polymer electrophoretic deposition process. The methods could be used to control the suspension stability and the film structure and morphology, which are critical parameters during the EPD of thin polymer films for solar energy conversion purposes.

Acknowledgments

This work was supported by the South Moravian Region and the 7th Framework Program for Research and Development (Grant SIGA 885), and by the Bulgarian National Science Fund at the Ministry of Education, Youth and Science (Grant DO 02-254).

References

[1] Tada K and Onoda M 2009 *Molecular Crystals and Liquid Crystals* **505** 124-9
[2] Boccaccini A R and Zhitomirsky I 2002 *Current Opinion in Solid State and Materials Science* **6** 251-60
[3] Rltroulls G, Papadopoulos N and Jannakoudakls D 1986 *J. Chem. Eng. Data* **37** 146-8
[4] Quoc T V 2006 *Electrophoretic deposition of semiconducting polymer metal/oxide nanocomposites and characterization of the resulting films* (Dresden Technischen Universität Dresden Germany) p 109
[5] Landfester K, Montenegro R, Scherf U, Gqnter R, Asawapirom C, Patil S, Neher D and Kietzke T 2002 *Adv. Mater.* **14** 651

J Therm Anal Calorim (2012) 108:467–473
DOI 10.1007/s10973-011-1896-8

Stability and physical structure tests of piperidyl and morpholinyl derivatives of diphenyl-diketo-pyrrolopyrroles (DPP)

Jiří Kučerík · Jan David · Martin Weiter · Martin Vala · Jan Vyňuchal · Imad Ouzzane · Ota Salyk

3rd Joint Czech-Hungarian-Polish-Slovak Thermoanalytical Conference Special Chapter

Abstract Crystalline structure, thermo-oxidative and thermal stability of symmetrical and asymmetrical piperidyl and morpholinyl derivatives of both N-substituted and non-N-substituted butyl diphenyl-diketo-pyrrolopyrrole (DPP) pigments were studied using differential scanning calorimetry (DSC) and thermogravimetry (TG). Except for the asymmetrical morpholine DPP derivative, all the samples showed melting peaks which were relatively close to their degradation temperatures (from 260 to 430 °C). Using DSC, monotropic polymorphism was revealed in the symmetrical piperidyl-*N*-butyl-derivative which confirmed earlier observation about tendency of symmetrical *N*-alkyl DPP derivates to form several crystalline structures. TG carried out under nitrogen atmosphere served for distinguishing of evaporation/sublimation and degradation temperatures. Temperatures of evaporation/sublimation were typically 10–30 °C lower in comparison with temperatures of thermal degradation. The highest thermal (450 °C) and thermo-oxidative stability (around 360 °C) showed the DPP derivatives containing morpholine moieties with no alkyl substitution on NH-group of DPP core. The presence of the latter was found to be the most destabilizing factor. Piperidyl group showed more stabilizing effect due to its polar character and its influence on π–π intermolecular interactions of neighbouring phenyl groups. The highest stabilizing effect of morpholine moiety on DPP structure was explained based on the presence of polar oxygen atom in that group. The preparations of 3,6-di-(4-morpholinophenyl)-2,5-dihydro-pyrrolo-[3,4-*c*]pyrrole-1,4-dione and 3-(phenyl)-6-(4-morpholinophenyl)-2,5-dihydropyrrolo[3,4-*c*]pyrrole-1,4-dione are reported.

Keywords Derivatives · Diphenyl-diketo-pyrrolopyrrole (DPP) · Electroluminescent devices · Polymorphism · Thermal stability · Thermo-oxidative stability

Introduction

Currently, a strong effort to produce organic electroluminescent devices (OLED) usable as a new generation of lamps and full colour flat panel displays, can be recognized. The potential advantages of these devices are their high efficiency, low driving voltage, versatility in their application (e.g. flexibility and transparency), low mass and relatively low production costs [1]. In order to fulfil all the requested parameters, the interest is focused not only on their optical properties, but also on physical–chemical characteristics such as solubility, resistance against various influences such as oxygen or temperature fluctuation.

3,6-diphenyl-2,5-dihydro-pyrrolo[3,4-c]pyrrole-1,4-dione known as DPP and its whole family of derivates are nowadays of a great interest [1–10]. Similarly, as other organic pigments they consist of centrosymmetric molecule having zero dipole moment [7]. Despite being of a

J. Kučerík (✉)
Institute of Environmental Sciences, University of Koblenz-Landau, Fortstrasse 7, 768 29 Landau, Germany
e-mail: kucerik@uni-landau.de

J. Kučerík · J. David · M. Weiter · M. Vala · O. Salyk
Faculty of Chemistry, Brno University of Technology, Purkyňova 118, Brno 612 00, Czech Republic

J. David · M. Weiter · M. Vala · I. Ouzzane
Faculty of Chemistry, Centre for Materials Research CZ.1.05/2.1.00/01.0012, Brno University of Technology, Purkyňova 464/118, Brno 612 00, Czech Republic

J. Vyňuchal
Research Institute of Organic Syntheses, Rybitví 296, 533 54, Czech Republic

relatively low molecular weight, DPP is an insoluble, crystalline material, thermally stable up to approximately 400 °C [8]. Physical properties are related to the presence of strong intermolecular bonds, which stabilize the crystal structure [1].

The derivatization of DPP is essential since resulted materials have improved physical–chemical properties such as for example, solubility, keeping the same or even better application properties in comparison with the parental DPP. Recently, it has been demonstrated that the introduction of piperidino (donor) and cyano (acceptor) groups into the DPP molecule had a strong influence on its absorption maxima. While both types of substitution resulted in bathochromic and hyperchromic shifts with respect to the parental DPP, the influence of piperidino group appeared to have the strongest effect [7].

Another example is a symmetrical dipyridyl derivate (DPPP) which shows a high proton affinity and, therefore, represents a good candidate for H_2 gas sensors [9]. However, only one of two possible crystal phases of DPPP was shown to be sensitive for H_2 detection; the reason of inactivity of one form is the interaction between N atom of pyridyl rings and NH-group(s) of DPP skeleton [9].

Thermal analysis represents a powerful tool in analysis of inorganic and organic pigments. The most important techniques are thermogravimetric analysis (TGA) and differential scanning calorimetry (DSC), applied either separately, simultaneously or in combination with other techniques. Recently, those techniques were used in order to study the stability of DPP *N*-alkyl derivatives and polymorphism occurring upon fast and moderate cooling of the material [8].

More recently, the thermogravimetrical analysis of DPP derivatives of red-emitting diketopyrrolopyrrole-*alt*-phenylenevinylene [11] polymers and poly(arylene ethynylene)s derived from 1,4-diketo-3,6-diphenylpyrrolo[3,4-c] pyrrole [12] were reported. The thermal stability of the products were assessed in nitrogen atmosphere as ranging from 260 to 400 °C [11, 12].

The main aim of this study is the evaluation of the thermal and thermo-oxidative stability of DPP derivates with para-substituted phenyl groups and partially substituted NH-groups. Furthermore, DSC is employed in order to reveal possible phase transitions in heating run upon different cooling regimes. This should imitate the possible fluctuation of environmental conditions, which can hamper processing and possible applications of DPP derivatives. All parameters determined using thermo-analytical techniques are discussed with respect to the molecular structure of studied samples.

Experimental

Thermal analysis

TG studies were performed using TA Instruments TGA Q5000 (New Castle, DE, USA) device in 100-μL open platinum pans. The samples, typically around 5 mg, were heated by thermal ramp of 10 °C min^{-1} from 40 to 650 °C in a dynamic atmosphere of either nitrogen (thermal stability) or air (thermo-oxidative stability) of 25 mL min^{-1}.

Calorimetric analyses were carried out employing TA Instruments DSC Q200 calorimeter equipped with an external cooler RCS90 allowing experimental temperature range from −90 to 500 °C. Experiments were conducted in open TA Tzero™ open aluminium pans. Thermal history of all samples was set up to be the same using a heating ramp of 10 °C min^{-1} from 40 °C to the temperature of 5 °C lower than the degradation onset, which was previously determined using thermogravimetry. Next, the moderate cooling ramp (0.5 °C min^{-1}) was applied to reach −90 °C followed by 1 min of an isothermal stage. Next segment was performed using a heating ramp of 10 °C min^{-1} from −90 °C to the temperature of 5 °C lower than degradation onset. The last segment included a 10 °C min^{-1} heating run followed after the rapid equilibration of the sample down to −90 °C (quenching) and 1 min of isothermal stage. All DSC experiments were made under dynamic atmosphere of nitrogen, flow rate 50 mL min^{-1}. Before the analyses, the device was calibrated for temperature and enthalpy using deionized water (own production), indium and tin standards (Perkin Elmer, Waltham, MA, USA.).

Samples

Five DPP derivates were investigated in this study. The molecular structures of tested DPP derivatives are reported in Fig. 1. The preparation of DPP1, DPP4 and DPP5 is reported in Ref. [9]. Preparation of DPP2 and DPP3 is given in following paragraphs.

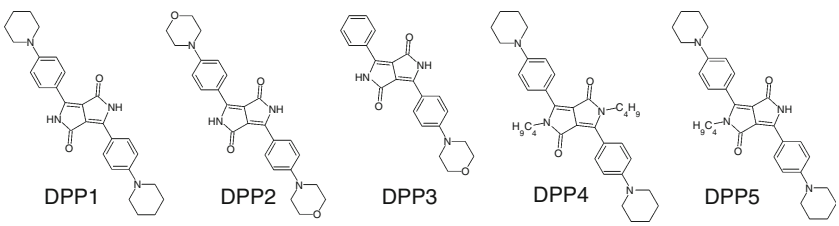

Fig. 1 Molecular structure of investigated DPP derivatives

Synthesis of 4-morpholine-1-yl-benzonitrile (starting nitrile)

Dry *N*,*N*-dimethylacetamide (p.a., 400 mL), *p*-fluorobenzonitrile (47.8 g; 0.4 mol) and morpholine (85 g; 0.98 mol) were charged into a 1-dm^3 Erlenmeyer flask equipped with a stirrer and condenser. The reaction was carried out at 100–110 °C for 8 h. The reaction gases from the reaction were let out to fume-chamber. Subsequently, the reaction mixture was poured onto 1 kg ice. The crude product was collected by filtration and recrystallized from 80% ethanol. Yield was 38 g (50%) of 4-morfoline-1-yl-benzonitrile (m.p. 53–55 °C).

Synthesis of DPP2 (3,6-di-(4-morpholinophenyl)-2,5–dihydro-pyrrolo[3,4-c]pyrrole-1,4-dione)

Tert-amyl alcohol (390 mL) and sodium metal (24.4 g, 1 mol, in three portions) were charged into an 1.5-L Keller flask equipped with a stirrer, reflux condenser, thermometer and nitrogen inlet. The sodium metal was dissolved under reflux in the presence of catalytic amount of $FeCl_3$ (which took approximately 2 h), and 4-morpholine-1-yl-benzonitrile (69 g, 0.37 mol) was added. After that, diisopropyl succinate (36.2 g, 0.18 mol) dissolved in *tert*-amyl alcohol (36.3 g) was added drop-wise within 3 h. Subsequently, this mixture was stirred under reflux for 1 h. The reaction mixture was cooled to 60 °C, and then 1000 mL of distilled water was added to protonate the salt. The protolysis was carried out at 80 °C for 2 h. The resulting hot suspension was filtered, and the filter cake was washed with hot water to neutral pH. The filter cake was dried and suspended in 800 mL acetone. The suspension was boiled and refluxed for 1 h. The hot suspension was filtered, washed with acetone and hot water. Yield of the DPP2 was 19.5 g (23.9%). Theoretical values of elemental analysis: C (68.11), H (5.72), N (12.22). Determined values of elemental analysis: C (67.89), H (5.75), N (12.05). ^{1}H chemical shifts: (500 MHz, DMSO) 10.99 (2H, s, NH); 8.40 (4H, m, Ar*H*); 7.11 (4H, m Ar*H*); 3.78 (8H, t, *H* morpholine); 3.39 (8H, t, *H* morpholine).

Synthesis of DPP3 (3-(Phenyl)-6-(4-morpholinophenyl)-2,5–dihydropyrrolo[3,4-c]pyrrole-1,4-dione)

Tert-amyl alcohol (80 mL) and sodium metal (2.8 g, 0.12 mol) were charged into a 250-cm^3 flask equipped with a stirrer, reflux condenser, thermometer and a nitrogen inlet. The sodium metal was dissolved under the reflux in the presence of catalytic amount of $FeCl_3$ (which approximately took 2 h), whereupon 4-morpholine-1-yl-benzonitrile (7.5 g, 0.04 mol) was added. After that, pyrrolinone ester (9.2 g, 0.04 mol, in small portions) was continuously added within 0.5 h. Finally, this mixture was stirred and refluxed for 2 h. The hot suspension of sodium salt of compound DPP3 was collected by suction. The filter cake was charged into 200 mL propan-2-ol/water mixture (3/2 by vol), and the suspension was heated to boiling and refluxed for 2 h. The product was collected by filtration, and the filter cake was charged into 100 mL methanol and refluxed for a short time. The hot suspension was filtered, the filter cake was washed with methanol, and finally with hot water. Yield: 5.3 g (36%) compound DPP3. Theoretical values of elemental analysis: C (70.76), H (5.13), N (11.25). Determined values of elemental analysis: C (70.06), H (5.10), N (10.98). ^{1}H chemical shifts: 500 MHz, DMSO) 11.19 (1H, s, NH); 11.16 (1H, s, NH); 8.46 (4H, m, Ar*H*); 7.57 (3H, m Ar*H*); 7.14 (2H, m Ar*H*); 3.78 (8H, t, *H* morpholine); 3.39 (8H, t, *H* morpholine).

Results and discussion

The derivative TG results, i.e. DTG of samples measured under nitrogen and air are reported in Figs. 2 and 3, respectively. As it can be seen, the DTG curves are reported in the reverse direction then calculated in order to simplify the data reading. Table 1 summarizes the data obtained from TG, DTG and DSC analysis of DPP derivates. DTG–air and DTG–nitrogen–evaporation onset results show the onsets determined from DTG records by the approach indicated in the small frame in Fig. 2. While DTG–air has the meaning of thermo-oxidative stability, the DTG–nitrogen–evaporation onset indicates the temperature of intensive mass loss onset, i.e. it indicates either evaporation or sublimation. The character of the process, if either evaporation or sublimation takes place, is discussed in following paragraphs with respect to the obtained DSC results. The DTG–nitrogen–degradation onset stands for

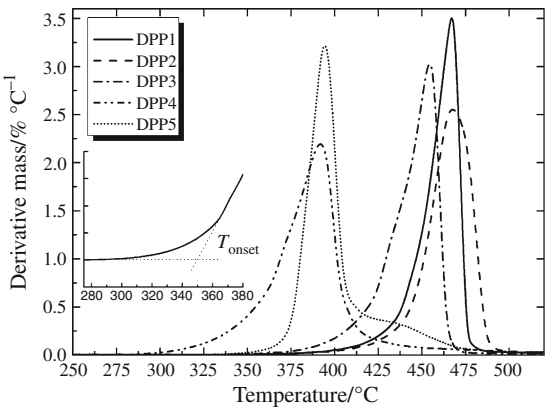

Fig. 2 Comparison of the first derivative of mass loss (DTG) of DPP derivatives in nitrogen, heating rate 10 °C min^{-1}

the thermal stability of a sample and it was determined from the second derivative as demonstrated in Fig. 4. This approach was developed and tested in Ref. [8]. Unlike for nitrogen experiments, the amount of char after air TG experiment is not reported since there was no rest after this kind of analysis. Regarding to the DSC results, Table 1 reports the enthalpies of melting and onset temperatures of respective events. For sample DPP2, the enthalpy of melting is not reported since the melting was immediately followed by the sample's evaporation and, therefore, peak area of melting was overlapped by the peak of evaporation. For the sample DPP3, no melting peak before the DTG onset was recorded, therefore, the nitrogen DTG onset indicates the temperature of sublimation.

By applying TG [8], it was showed the onset temperature of sublimation of parental non-substituted DPP under nitrogen (sublimation) as high as 383 °C (for a heating rate 10 °C min^{-1}). That process was followed by the thermal degradation at 408 °C and the thermo-oxidative stability was determined around 356 °C (under the same conditions as used in this study). Despite the fact that two crystallographic forms in parental DPP sample may occur, the DSC tests disclosed no significant phase transition such as melting or glass transition in the temperature interval from −90 to 383 °C. In contrast, the alkyl derivates (substitution of H in NH-group in parental DPP molecule) were less stable (a difference more than 100 °C) and their physical structure showed a strong dependence on the thermal pretreatment (thermal history). That was explained as a consequence of a molecular symmetry disturbance caused by the presence of alkyl chains in the structure of DPP derivatives. As stated previously, pure DPP is stabilized by means of 3D intermolecular hydrogen bonds based on –NH···O=C interaction, by π–π intermolecular interactions between adjacent phenolic groups, by electrostatic interactions of charged groups and partly also by van der Waals forces [10]. Substitution of one or both H atoms in the NH-groups by alkyl chains in DPP molecule caused the destabilization of crystalline structure of derivatives under study. In fact, significant differences were found in physical structures of derivates depending on the symmetry and/or asymmetry of derivatization. Symmetrical derivatives exhibited a strong dependency on the thermal history, i.e. differences were recorded in the DSC heating run of the sample which was previously cooled either quickly or slowly. Such approach revealed the polymorphism of symmetrical derivates with alkyl chains $–C_4H_9$ and $–C_7H_{15}$ but not for $–CH_3$. On the contrary, the asymmetrical

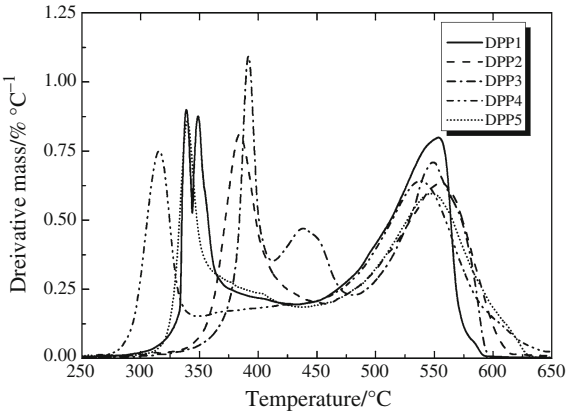

Fig. 3 Comparison of the first derivative of mass loss (DTG) of DPP derivatives in air, heating rate 10 °C min^{-1}

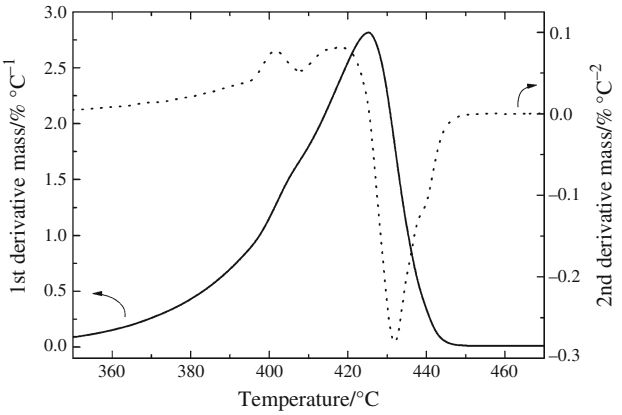

Fig. 4 The determination of degradation onset from the second derivative mass curve of sample DPP3

Table 1 Summary of TGA and DSC results, for detail explanation see the text

Sample	DPP1	DPP2	DPP3	DPP4	DPP5
DTG–air/°C	332	357	378	292	326
DTG–nitrogen–evaporation onset/°C	440	440	416	330	374
DTG–nitrogen–degradation onset/°C	446	459	441	373	383
Char in nitrogen/%	16.4	17.1	11.7	10.0	10.8
$T_{melting}$/°C	431	435	–	263	361
$\Delta H_{melting}$/J/g	213.7	n.d.	–	77.1[a]	91.8

[a] Only main melting peak is reported, minor ones are described in the text

derivates showed practically no response in physical structure when exposed to a different thermal history. It is noteworthy that glass transition was observed only in some samples regardless to the symmetry of the molecule.

Figure 2 reports the DTG of investigated samples in nitrogen. As already mentioned, the tests in nitrogen were carried out to obtain the temperatures of evaporation or sublimation; however, due to the intermolecular interactions stabilizing the DPP physical structure, processes of evaporation or sublimation are relatively slow and, therefore, the programmed continuous increase in the oven's temperature causes later the degradation of the rest of the sample which was not removed yet and remained on the pan. In practise, when the sample is evaporated to be deposited on a surface, this problem can be solved by pressure reduction and keeping constant temperature during the deposition [10]. However, it can be seen that except for sample DPP5, all samples gave only one intensive DTG peak which indicates the one-step process. For this reason, the second derivative of TG signal was calculated in order to reveal some possible overlapping processes. Indeed, two separated processes were disclosed and attributed to the evaporation followed by the degradation, similarly as proved and published recently [8]. A typical determination is reported in Fig. 4.

The highest onset in nitrogen TG experiments showed samples DPP1 and DPP2 followed by samples DPP3 and DPP5. The lowest onset was observed for sample DPP4. In contrast, experiments in oxidative atmosphere of air brought about a different order. The highest stability was observed for sample DPP3, further for DPP2. Under oxidative conditions, sample DPP1 showed a lower stability than DPP2 (difference 25 °C) and it was only slightly higher than the stability of sample DPP5. Again, the lowest stability was observed for sample DPP4.

Differences in stabilities under different conditions were accompanied also by differences in physical structures as revealed by DSC measurement. It can be identified in Table 1 that melting temperatures of samples DPP1, DPP2 and DPP5 are higher than DTG–air onset temperatures which suggest that samples underwent thermo-oxidative degradation before their melting. On the contrary, all the samples (except DPP3) were pre-melted before the onset determined by DTG under inert conditions.

In general, it can be stated that all DPP derivates investigated in this study showed higher stability than *N*-alkyl derivatives tested in Ref. [8]. In contrast, as follows from the above-statements, the parental DPP showed higher thermal stability than DPP5 and DPP4; the thermo-oxidative stability was higher than DPP5, DPP4, DPP1 and similar to DPP2.

Unlike the degradation in nitrogen, the degradation in oxidative atmosphere (Fig. 3) proceeded in several steps. The lowest stability showed samples with aliphatic chains in the structure. In fact, the mass loss extracted from TG curve in the temperature range corresponding to the first degradation step in sample DPP4 was about 20% which is equal to the molar fraction of alkyl part in that molecule. Analogous result can be obtained also for sample U5, i.e. detected mass loss was 11%. Therefore, it seems that the less stable part of the derivative molecule is the aliphatic chain attached to the N-molecular skeleton of DPP. The piperidine part of a molecule has less de-stabilizing effect, probably due to its polar character and its influence on π–π intermolecular interactions of phenyl groups. Employing the same approach as for aliphatic derivates for sample DPP1, the piperidyl group is decomposed in several steps. Figure 3 shows two identical peaks at 340 and 349 °C corresponding to 9 and 20% mass loss, respectively. At 37% of degradation (i.e. when both piperidyl groups are degraded) at 450 °C which corresponds to the minimum between two main degradation stages. Piperidyl group is more resistant against thermo-oxidative attack than simple aliphatic chain. This can be easily identified also when the most stable sample DPP1 (with no alkyl chain) is compared with DPP4 (symmetrical *N*-alkyl derivatization), which is less stable and with DPP5 (asymmetrical *N*-alkyl derivatization), which is only slightly less stable in air, however, significantly less stable in nitrogen. Such order also supports the observation which was done in the study with *N*-alkyl derivates that asymmetrical derivates of DPP have higher stability than the symmetrical ones.

Comparison of samples DPP1 and DPP2, i.e. samples with different para-substituents on phenyl groups of DPP showed only slight difference in thermo-oxidative stability while thermal stability was identical. The piperidyl groups showed lower stabilizing effect against oxidation than morpholine group which can be explained as a stabilizing effect of polar O atom in morpholine group. However, as indicated by DSC (Table 1) there is a similar influence of both substituents on melting temperature in both derivatives. Since parental DPP did not show any melting before the evaporation [8] it can be assumed that both substituents, donors of electrons, have an influence on the weakening or opening of the structure allowing the oxygen molecules to penetrate inside the structure and decompose the material. The degradation of morpholine groups in sample DPP2 above-mentioned approach, based on mass loss calculation, failed, which implies that the breaking down of that group proceeds in a more complicated way than aliphatic chains or piperidyl groups. Interestingly, such approach was successful in sample DPP3 where the mass loss of morpholine group corresponded to the minimum in DTG after the first degradation step.

Comparison of DSC records of DPP1 and DPP4 can shed an additional light on the influence of aliphatic chains

on the stability of DPP derivatives structure. As it can be seen, the alkyl chains destabilize significantly the structure and cause the lower stability of crystals in sample DPP4. Significantly higher melting enthalpy of sample DPP1 indicates the formation of completely different crystalline structure than in the case of *N*-alkyl derivates (their enthalpy of melting) was reported as significantly lower than those reported in Ref. [8].

Differences between samples DPP3 (asymmetrical substitution of DPP's phenyls) and DPP2 (symmetrical substitution) brought the insight into the influence of dipole moment on their thermal and thermo-oxidative stability. In contrast to DPP2, due to its asymmetry, the molecule DPP3 has non-zero dipole moment [13] stabilizing the structure against oxygen agitation. It is noteworthy that DPP3 is the only sample which had no melting before the DTG onset. Therefore, the present dipole moment destabilizes the structure and the sublimation (thermal stability) of sample DPP3 occurs at lower temperatures than for DPP 2.

As reported in Fig. 5, sample DPP4 showed a strong dependency on the thermal pre-treatment. When heated up without any pre-treatment, indicated as 'C' record in Fig. 4 (i.e. measured as received), there can be seen three melting events (in Table 1 only the last peak, the most intensive one is reported). Small peaks occurred at 153 and 166 °C with respective enthalpies of 0.7 and 11.7 J g^{-1}. On the other hand, when cooled quickly, indicated as 'A' record, a glass transition with midpoint at 58 °C accompanied by a slight enthalpic recovery appeared followed by two exotherms attributable to crystallization. Peaks occurred at 110 and 164 °C with enthalpies 39.8 and 5.1 J g^{-1}, respectively. Melting of present crystalline structure was observed at 263 °C. Finally, when cooled slowly, only the melting at 254 °C was observed with no pre-crystallization event ('B' record).

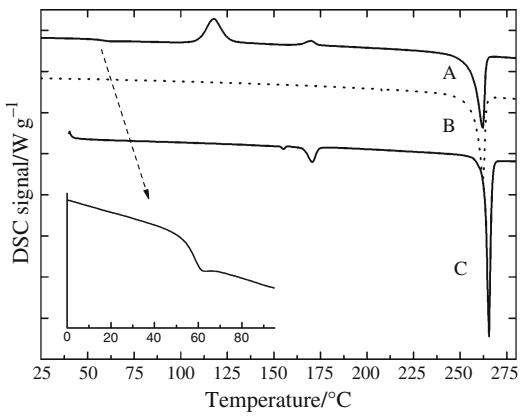

Fig. 5 Polymorphism of sample DPP4 as revealed by DSC measurement. *A* heating after rapid cooling, *B* heating after moderate cooling, *C* heating run without thermal pre-treatment

Such behaviour suggests the possible polymorphism of sample DPP4. As mentioned in previous paragraphs, similar, but not the same, temperature-dependent behaviour was observed for symmetrical *N*-alkyl DPP derivates, namely C_4H_9 and C_7H_{15} derivatives [8]. That was attributed to the melting of two different crystalline forms implying the monotropic polymorphism. The possible existence of several crystalline structures was observed only in the first 'C' record. The run 'A' which shows also the glass transition can be explained as a consequence of quick cooling; the movement of molecules otherwise forming crystals is decelerated and instead, they form amorphous structures. Heating up of the sample causes molecular segments relaxation (glass transition) followed by two steps of crystal perfection. Since aliphatic groups are involved in the crystalline structure, two phases may imply the progressive formation of both aliphatic and piperidyl moieties containing crystalline domains.

Conclusions

Thermal analysis has already showed its potential to study physical–chemical properties of pigments and dyes, e.g. refs. [8, 14, 15]. In this study, the physical–chemical properties of DPP derivates were investigated employing thermal analysis methods. The determined temperatures, especially the distinguishing between evaporation/sublimation and degradation temperatures is important for the designing of experimental conditions for deposition of such materials in the form of thin layers. The high thermal and thermo-oxidative stability of DPP materials which was determined using TG is a promising factor supporting their future application. Furthermore, the knowledge on the physical structure, as revealed by DSC showed the potential problem in manipulating with some DPP derivates since only an appropriate crystalline structure can be requested for the specific application.

Acknowledgements The financial support of the Ministry of Education of the Czech Republic - project MSM 0021630501, Academy of Sciences of the Czech Republic project KAN401770651 and Czech Science Foundation project GACR 203/08/1594 are acknowledged. This study was also supported by the project "Centre for Materials Research at FCH BUT" No. CZ.1.05/2.1.00/01.0012 from ERDF.

References

1. Vala M, Weiter M, Vyňuchal J, Toman P, Luňák S Jr. Comparative studies of diphenyl-diketo-pyrrolopyrrole derivatives for electroluminescence applications. J Fluoresc. 2008;18:1181–5.
2. Mizuguchi J. Correlation between crystal and electronic structures in diketopyrrolopyrrole pigments as viewed from exciton coupling effects. J Phys Chem A. 2000;104:1817–21.

3. Hoki T, Takahashi H, Suzuki S, Mizuguchi J. Hydrogen gas sensor based upon proton acceptors integrated in copper-tetra-2, 3-pyridinoporphyradine. IEEE Sensors J. 2007;7:808–13.
4. Beyerlein T, Tieke B, Forero-Lenger S, Brütting W. Red electroluminescence from a 1, 4-diketopyrrolo[3, 4-c]pyrrole (DPP)-based conjugated polymer. Synthetic Metals. 2002;130:115–9.
5. Potrawa T, Langhals H. Fluorescent dyes with large Stokes shifts - soluble dihydropyrrolopyrrolediones. Chemische Berichte. 1987;120:1075–8.
6. Fukuda M, Kodama K, Yamamoto H, Mito K. Evaluation of new organic pigments as laser-active media for a solid-state dye laser. Dyes Pigments. 2004;63:115–25.
7. Luňák S, Vyňuchal J, Vala M, Havel L, Hrdina R. The synthesis, absorption and fluorescence of polar diketo-pyrrolo-pyrroles. Dyes Pigments. 2009;82:102–8.
8. David J, Weiter M, Vala M, Vyňuchal J, Kučerík J. Stability and structural aspects of diketopyrrolopyrrole pigment and its *N*-alkyl derivatives. Dyes Pigments. 2011;89:137–43.
9. Vala M, Vyňuchal J, Toman P, Weiter M, Luňák S Jr. Novel, soluble diphenyl-diketo-pyrrolopyrroles: Experimental and theoretical study. Dyes Pigments. 2010;84:176–82.
10. Weiter M, Salyk O, Bednář P, Vala M, Navrátil J, Zmeškal O, Vyňuchal J, Luňák S Jr. Morphology and properties of thin films of diketopyrrolopyrrole derivatives. Mat Sci Eng B. 2009;165: 148–52.
11. Qiao Z, Xu Y, Lin S, Peng J, Cao D. Synthesis ands characterization of red-emitting diketopyrrolopyrrole-*alt*-phenylenevinylene polymers. Synthetic Metals. 2010;160:1544–50.
12. Palai AK, Mishra SP, Kumar A, Srivastava R, Kamalasana MP, Patri M. Synthesis and characterization of alternative donor-acceptor arranged poly(arylene enthylene)s derived from 1, 4-diketo-3, 6-diphenylpyrrolo[3, 4-c]pyrrole (DPP). Eur Polym J. 2010;46:1940–51.
13. Mizuguchi J, Imoda T, Takahashi H, Yamakami H. Polymorph of 1, 4-diketo-3, 6-bis-(4′-dipyridyl)-pyrrolo-[3, 4-c]pyrrole and their hydrogen bond network: A material for H2 gas sensor. Dyes Pigments. 2006;68:47–52.
14. Rotaru A, Moanta A, Popa G, Rotaru P, Segal. E. Thermal decomposition kinetics of some aromatic azomonoethers. full access. Part IV. Non-isothermal kinetics of 2-allyl-4-((4-(4-methylbenzyloxy)phenyl)diazenyl)phenol in air flow. J Therm Anal Calorim. 2009;97:485–91.
15. Rotaru A, Moanta A, Rotaru P, Segal E. Thermal decomposition kinetics of some aromatic azomonoethers Part III. Non-isothermal study of 4-[(4-chlorobenzyl)oxy]-4′-chloroazobenzene in dynamic air atmosphere. J Therm Anal Calorim. 2009;95:161–6.

Dyes and Pigments 91 (2011) 269–278

Contents lists available at ScienceDirect

Dyes and Pigments

journal homepage: www.elsevier.com/locate/dyepig

Absorption and fluorescence of soluble polar diketo-pyrrolo-pyrroles

Stanislav Luňák Jr. [a], Martin Vala [b,*], Jan Vyňuchal [a,c,d], Imad Ouzzane [b], Petra Horáková [a], Petra Možíšková [b], Zdeněk Eliáš [a], Martin Weiter [b]

[a] Faculty of Chemical Technology, University of Pardubice, Studentská 95, CZ-530 09 Pardubice, Czech Republic
[b] Faculty of Chemistry, Centre for Materials Research, Brno University of Technology, Purkyňova 464/118, CZ-612 00 Brno, Czech Republic
[c] Research Institute of Organic Syntheses, Rybitví 296, CZ-533 54 Rybitví, Czech Republic
[d] Synthesia a.s., Pardubice, Semtín 103, CZ-532 17 Pardubice, Czech Republic

ARTICLE INFO

Article history:
Received 26 October 2010
Received in revised form
29 April 2011
Accepted 4 May 2011
Available online 19 May 2011

Keywords:
Diketo-pyrrolo-pyrrole
Fluorescence
Solvatochromism
Solid-state fluorescence
Twisted intramolecular charge transfer
Organic electronics

ABSTRACT

Six soluble derivatives of 3,6-diphenyl-2,5-dihydro-pyrrolo[3,4-*c*]pyrrole-1,4-dione *N*-alkylated on pyrrolinone ring with polar substituents in *para* positions of pendant phenyl rings were synthesized; five of them are reported for the first time. Absorption and fluorescence spectra were studied in solvents of different polarity. The compounds show small solvatochromism of absorption and a moderate positive solvatochromism of fluorescence, especially when substituted by strong electron-donating piperidino substituent. A significant decrease of fluorescence quantum yields and its biexponential decay for dipolar derivatives in polar solvents was tentatively ascribed to the formation of twisted intramolecular charge transfer (TICT) excited state. All six compounds show fluorescence in polycrystalline solid-state with the maxima covering a range over 200 nm in visible and near infrared region.

1. Introduction

Although originally developed as high performance organic pigments [1,2,3], various structural modifications made diketo-pyrrolo-pyrroles (DPPs) interesting as advanced materials for modern optical and electronic technologies. The devices based on DPPs copolymerized with e.g. carbazoles [4] and especially with oligothiophenes [5,6] reached the promising efficiencies as organic field-effect transistors (OFET) [5] and bulk heterojunction (BHJ) photovoltaic solar cells (OPV) [4,6]. Aside from DPP copolymers, which form rather specific area with dramatically increasing number of references, DPP monomers have been recently found also to be perspective in photovoltaics, either in the BHJ OPV [7], or in dye-sensitized solar cells (DSSC) [8] type. The common structural features of DPP derivatives designed for these purposes are: The substituted (usually alkylated, in some cases acylated [9]) pyrrolinone nitrogens, changing the insoluble pigments to molecules enabling wet solution based processing, and the presence of electron-donating groups as a counterpart to diketo-pyrrolo-pyrrole core with an electron-accepting character.

We have recently published the syntheses and spectral properties of parent DPP chromophore 3,6-diphenyl-2,5-dihydro-pyrrolo[3,4-*c*]pyrrole-1,4-dione (**I**) and its electron-donor (piperidino) and electron-acceptor (cyano) symmetrically and unsymmetrically substituted derivatives (**II**–**VI**, Fig. 1) [10]. The derivatives have shown bathochromic and hyperchromic shift of absorption and bathofluoric shift of fluorescence with respect to parent compound **I** invoked above all by piperidino electron-donating substituent. Dimethyl sulfoxide (DMSO) was found to be the only common solvent able to dissolve all these pigments. In order to make these compounds better treatable we have decided to substitute them on pyrrolinone nitrogens and so eliminate the intermolecular hydrogen bonding [1]. On the contrary to more usual *N*-alkylation by alkylhalogen, used in our previous studies [11,12], we applied ethyl bromoacetate in this case (Fig. 1). Such substitution was reported only once resulting in compound **VII** with highly distorted structure in crystal according to X-ray diffraction [13] giving thus a good chance to be highly soluble because of the absence of π–π stacking, another insolubility implicating phenomenon aside from CO–NH hydrogen bonding [14]. Compounds **VIII**–**XII** were never reported, thus they are fully characterized in Experimental. This is the first case, to the best of our knowledge, when simple push-pull substituted well soluble DPP derivative (**XII**) is studied.

* Corresponding author. Tel.: +420 541 149 411; fax: +420 541 149 398.
E-mail address: vala@fch.vutbr.cz (M. Vala).

0143-7208/$ – see front matter © 2011 Elsevier Ltd. All rights reserved.
doi:10.1016/j.dyepig.2011.05.004

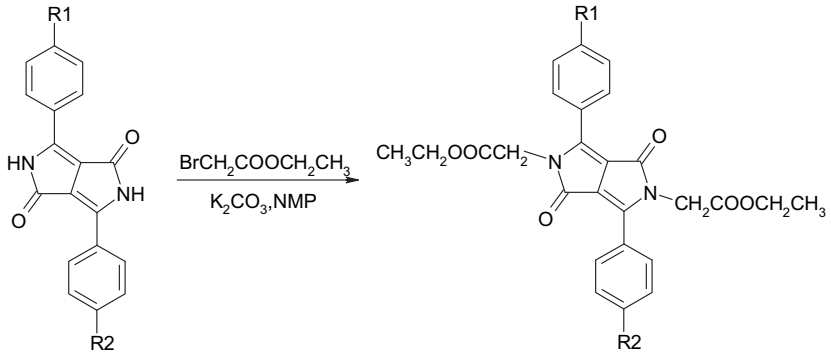

Symbol	R_1	R_2
I	H	H
II	CN	H
III	CN	CN
IV	H	
V		
VI	CN	

Symbol	R_1	R_2
VII	H	H
VIII	CN	H
IX	CN	CN
X	H	
XI		
XII	CN	

Fig. 1. General synthetic route and notation of the compounds under study.

DPP derivatives are known for a long time to be strongly fluorescent in solution [15]. The only reported exceptions to the best of our knowledge are the compounds, in which the pyrrolinone carbonyl group underwent a nucleophilic substitution by heteroarylacetonitrile [16] or bis(trimethylsilyl)carbodiimide [17] forming the products loosing the true DPP character. The aim of this study was thus first to investigate in detail the dependence of absorption and fluorescence spectra and fluorescence efficiencies in solution on the character of pendant phenyl substitution in **VIII**–**XII** with respect to on-phenyl unsubstituted **VII** and *N*-unsubstituted precursors **I**–**VI**. Contrary to hardly soluble pigments **I**–**VI**, it was possible also to measure a solvatochromism on **VII**–**XII**, which was never studied in detail before.

As we observed the luminescence of some of these *N,N′*-dialkylated DPPs in solid-state just by naked eye during the samples handling (opposite to totally non-luminescent precursors **I**–**VI**), we studied also this not particularly common behaviour but being of growing interest [18,19,20]. Since the pioneering work of Langhals [21], the solid-state fluorescence of several DPP derivatives was mentioned in literature [9,22,23], but the full understanding of this phenomenon requires more systematic studies on the representative series of derivatives.

2. Experimental

2.1. Syntheses and analyses

The synthesis of the starting derivatives **I**–**VI** was described in Ref. [10]. Compound **VII** was synthesized from compound **I** in a similar way as described earlier and confirmed by melting point 210–212 °C (lit. [13]. 207–208 °C). *N*-methyl-2-pyrrolidone (NMP), ethyl bromoacetate and potassium carbonate were purchased from Sigma-Aldrich, so as the three solvents used in the spectral studies.

2.1.1. Preparation of diethyl-3-(phenyl)-6-(4-cyanophenyl)-2,5-dihydropyrrolo[3,4-c]pyrrole-1,4-dione-diacetate (**VIII**)

Compound **II** (8 g, 0.0256 mol), potassium carbonate (35.4 g, 0.256 mol) and NMP (480 ml) were charged to a three-necked flask. Reaction mixture was heated to 120 °C. Ethyl bromoacetate (42.8 g, 0.256 mol) in NMP (185 ml) was added to the reactor dropwise during 40 min. Then the reaction was stirred and heated to 120 °C for 2 h. After cooling, the reaction was slowly poured onto ice-cold water (1400 ml). The obtained precipitate was filtered off and washed with water until neutral washings. The crude product was recrystallized from a mixture of methanol and water (2:1). Yield: 2.02 g (16.29%) of compound **VIII**. m.p. 139–141 °C.

Calculated: C (66.90), H (4.78), N (8.66), Found: C (66.84), H (4.73), N (8.46)

MW = 485 Da; Positive-ion APCI-MS: *m/z* 486 $[M + H]^+$, (100%)

^{1}H chemical shifts: 8.12 (2H, m, Ar*H*); 7.99 (2H, m, Ar*H*); 7.84 (2H, m, Ar*H*); 7.66 (3H, m, Ar*H*); 4.64 (2H, s, −N*CH*$_2$,); 4.63 (2H, s, −N*CH*$_2$,); 4.115 (2H, q, J = 7.1 Hz, −O*CH*$_2$); 4.110 (2H, q, J = 7.1 Hz, −O*CH*$_2$); 1.142 (3H, t, J = 7.1 Hz, −CH$_2$*CH*$_3$); 1.140 (3H, t, J = 7.1 Hz, −CH$_2$*CH*$_3$)

^{13}C chemical shifts: 168.37 (1C, >*C*=O); 168.29 (1C, >*C*=O); 161.30 (1C, >*C*=O); 161.03 (1C, >*C*=O); 149.52 (1C, Ar*C*); 145.37 (1C, Ar*C*); 133.02 (2C, Ar*C*); 132.09 (1C, Ar*C*); 131.33 (1C, Ar*C*); 129.26 (2C, Ar*C*); 129.21 (2C, Ar*C*); 128.68 (2C, Ar*C*); 126.88 (1C, Ar*C*); 118.26 (1C, −*C*≡N); 113.52 (1C, Ar*C*); 109.90 (1C, Ar*C*); 108.47

(1C, ArC); 61.41 (1C, N–CH_2); 61.38 (1C, N–CH_2); 43.38 (1C, –OCH_2); 43.26 (1C, –OCH_2); 13.92 (2C, –CH_2CH_3)

*2.1.2. Preparation of diethyl-3,6-di-(4-cyanophenyl)-2,5-dihydropyrrolo[3,4-c]pyrrole-1,4-dione-diacetate (**IX**)*

Compound **III** (5 g, 0.0148 mol), potassium carbonate (20.42 g, 0.148 mol) and NMP (272 ml) were charged into a three-necked flask. Reaction mixture was heated to 120 °C and ethyl bromoacetate (24.7 g, 0.148 mol) in NMP (116 ml) was added dropwise to the reactor during 40 min. Then the reaction was stirred and heated to 120 °C for 2 h. After cooling, the reaction was slowly poured onto ice-cold water (760 ml). The obtained precipitate was filtered off and washed with water until neutral washings. The crude product was recrystallized from methanol. Yield: 0.81 g (10.7%) of orange compound **IX**, m.p. 177–179 °C.

Calculated: C (68.49), H (6.12), N (7.73), Found: C (68.49), H (6.04), N (7.63)

^{1}H chemical shifts: 8.14 (4H, m, Ar*H*); 8.01 (4H, m, Ar*H*); 4.64 (4H, s, –NCH_2); 4.10 (4H, q, J = 7.1 Hz, –OCH_2); 1.13 (6H, t, J = 7.1 Hz, –CH_2CH_3)

^{13}C chemical shifts: 168.23 (2C, >*C*=O); 160.97 (2C, >*C*=O); 146.92 (2C, Ar*C*); 133.05 (4C, Ar*C*); 131.06 (2C, Ar*C*); 129.33 (4C, Ar*C*); 118.36 (2C, –*C*≡N); 113.82 (2C, Ar*C*); 109.82 (2C, Ar*C*); 61.45 (2C, N–CH_2); 43.40 (2C, –OCH_2); 13.90 (2C, –CH_2CH_3)

*2.1.3. Preparation of diethyl-3-(phenyl)-6-(4-piperidinophenyl)-2,5-dihydropyrrolo[3,4-c]pyrrole-1,4-dione-diacetate (**X**)*

Dry and pure NMP (150 ml), compound **IV** (3.7 g, 0.01 mol) and potassium carbonate (15.2 g, 0.11 mol) were charged to a three-necked flask. Reaction mixture was heated to 120 °C. Ethyl bromoacetate (18.4 g, 0.11 mol) in NMP (80 ml) was added dropwise to the reactor during 40 min. Then the reaction mixture was stirred and heated to 120 °C for 2 h. After cooling, the reaction was slowly poured onto ice-cold water (500 ml). The obtained precipitate was filtered off and washed with water until neutral washings. The crude product was recrystallized from methanol. Yield: 3.2 g (59%) of compound **X**, m.p. 207–214 °C.

Calculated: C (65.88), H (4.34), N (10.97), Found: C (65.47), H (4.44), N (10.82)

MW = 510 Da; Positive-ion APCI-MS: m/z 511 $[M + H]^+$ (100%)

^{1}H chemical shifts: 7.83 (2H, m, Ar*H*); 7.78 (2H, m, Ar*H*); 7.61 (3H, m, Ar*H*); 7.1 (2H, m, Ar*H*); 4.66 (2H, s, –NCH_2); 4.61 (2H, s, –NCH_2); 4.17 (2H, q, J = 7.1 Hz, –OCH_2); 4.12 (2H, q, J = 7.1 Hz, –OCH_2); 3.48 (4H, m, –$CH_2CH_2CH_2$N); 1.64 (6H, m, –$CH_2CH_2CH_2$N and –$CH_2CH_2CH_2$N); 1.19 (6H, t, J = 7.1 Hz, –CH_2CH_3); 1.15 (6H, t, J = 7.1 Hz, –CH_2CH_3)

^{13}C chemical shifts: 168.65 (1C, >*C*=O); 168.61 (1C, >*C*=O); 161.99 (1C, >*C*=O); 161.06 (1C, >*C*=O); 152.74 (1C, Ar*C*); 149.20 (1C, Ar*C*); 144.33 (1C, Ar*C*); 131.05 (1C, Ar*C*); 130.70 (2C, Ar*C*); 129.03 (2C, Ar*C*); 128.45 (2C, Ar*C*); 127.59 (1C, Ar*C*); 114.51 (1C, Ar*C*); 113.47 (2C, Ar*C*); 108.75 (1C, Ar*C*); 105.91 (1C, Ar*C*); 61.29 (1C, N–CH_2); 61.21 (1C, N–CH_2); 47.69 (2C, –$CH_2CH_2CH_2$N); 43.88 (1C, –OCH_2); 43.34 (1C, –OCH_2); 25.00 (2C, –$CH_2CH_2CH_2$N); 24.07 (1C, –$CH_2CH_2CH_2$N); 14.02 (1C, –CH_2CH_3); 13.97 (1C, –CH_2CH_3)

*2.1.4. Preparation of diethyl-3,6-di-(4-piperidinophenyl)-2,5-dihydropyrrolo[3,4-c]pyrrole-1,4-dione-diacetate (**XI**)*

Compound **V** (5 g, 0.011 mol), potassium carbonate (15.2 g, 0.11 mol) and NMP (205 ml) were charged into three-necked flask. Reaction mixture was heated to 120 °C and ethyl bromoacetate (18.38 g, 0.11 mol) in NMP (80 ml) was added dropwise to the reactor during 40 min. Then the reaction was stirred and heated to 120 °C for 2 h. After cooling, the reaction was slowly poured onto ice-cold water (600 ml). The obtained precipitate was filtered off and washed with water until neutral washings. The crude product was recrystallized from methanol. Yield: 3.57 g (54.3%) compound **XI**, m.p. 213–217 °C.

Calculated: C (68.99), H (6.75), N (8.94), Found: C (68.80), H (6.85), N (8.78)

MW = 626 Da; Positive-ion APCI-MS: m/z 627 $[M + H]^+$ (100%)

^{1}H chemical shifts: 7.75 (4H, m, Ar*H*); 7.01 (4H, m, Ar*H*); 4.64 (4H, s, –NCH_2); 4.16 (4H, q, J = 7.2 Hz, –OCH_2); 3.41 (8H, m, –$CH_2CH_2CH_2$N); 1.64 (12H, m, –$CH_2CH_2CH_2$N and –$CH_2CH_2CH_2$N); 1.18 (6H, t, J = 7.2 Hz, –CH_2CH_3)

^{13}C chemical shifts: 130.27 (4C, Ar*C*); 113.67 (4C, Ar*C*); 61.19 (2C, N–CH_2); 47.83 (4C, –$CH_2CH_2CH_2$N); 43.80 (2C, –OCH_2); 24.97 (4C, –$CH_2CH_2CH_2$N); 14.04 (2C, –CH_2CH_3); Remaining signals were not detected due to low solubility of the sample.

*2.1.5. Preparation of diethyl-3-(4-cyanophenyl)-6-(4-piperidinophenyl)-2,5-dihydropyrrolo[3,4-c]pyrrole-1,4-dione-diacetate (**XII**)*

Compound **VI** (3 g, 0.0076 mol), potassium carbonate (10.5 g, 0.076 mol) and NMP (140 ml) were charged into three-necked flask (500 ml). Reaction mixture was heated to 120 °C and ethyl bromoacetate (14 g, 0.082 mol) in NMP (60 ml) was added dropwise to the reactor during 40 min. Then the reaction was stirred and heated to 120 °C for 2 h. After cooling, the reaction was slowly poured onto ice-cold water (400 ml). The obtained precipitate was filtered off and washed with water until neutral washings. The crude product was recrystallized from the mixture of n-hexan and methanol (7:3). Yield: 2.26 g (70.4%) of compound **XII**, m.p. 192–195 °C.

Calculated: C (67.59), H (5.67), N (9.85), Found: C (67.40), H (5.72), N (9.65)

MW = 568 Da; Positive-ion APCI-MS: m/z 569 $[M + H]^+$ (100%)

^{1}H chemical shifts: 8.08 (2H, m, Ar*H*); 8.01 (2H, m, Ar*H*); 7.87 (2H, m, Ar*H*); 7.10 (2H, m, Ar*H*); 4.69 (2H, s, –NCH_2); 4.65 (2H, s, –NCH_2); 4.17 (2H, q, J = 7.0 Hz, –OCH_2); 4.11 (2H, q, J = 7.1 Hz, –OCH_2); 3.50 (4H, s, –$CH_2CH_2CH_2$N); 1.65 (6H, s, –$CH_2CH_2CH_2$N and –$CH_2CH_2CH_2$N); 1.19 (3H, t, J = 7.1 Hz, –CH_2CH_3); 1.15 (3H, t, J = 7.0 Hz, –CH_2CH_3)

^{13}C chemical shifts: 168.62 (1C, >*C*=O); 168.57 (1C, >*C*=O); 162.07 (1C, >*C*=O); 160.80 (1C, >*C*=O); 152.95 (1C, Ar*C*); 150.68 (1C, Ar*C*); 141.33 (1C, Ar*C*); 132.92 (2C, Ar*C*); 131.85 (1C, Ar*C*); 131.07 (2C, Ar*C*); 129.04 (2C, Ar*C*); 118.44 (1C, –*C*≡N); 114.04 (1C, Ar*C*); 113.36 (2C, Ar*C*); 112.73 (1C, Ar*C*); 110.35 (1C, Ar*C*); 105.81 (1C, Ar*C*); 61.39 (1C, N–CH_2); 61.32 (1C, N–CH_2); 47.63 (2C, –$CH_2CH_2CH_2$N); 44.05 (1C, –OCH_2); 43.37 (1C, –OCH_2); 25.05 (2C, –$CH_2CH_2CH_2$N); 24.10 (1C, –$CH_2CH_2CH_2$N); 14.04 (1C, –CH_2CH_3); 13.97 (1C, –CH_2CH_3)

2.2. Structure and purity characterization

2.2.1. Mass spectrometry

The ion trap mass spectrometer MSD TRAP XCT Plus system (Agilent Technologies, USA) equipped with APCI probe was used. Positive-ion and negative-ion APCI mass spectra were measured in the mass range of 50–1000 Da in all the experiments. The ion trap analyzer was tuned to obtain the optimum response in the range of the expected m/z values (the target mass was set from m/z 289 to m/z 454). The other APCI ion source parameters: drying gas flow rate 7 dm^3 min^{-1}, nebulizer gas pressure 60 psi, drying gas temperature 350 °C, nebulizer gas temperature 350 °C. The samples were dissolved in a mixture of DMSO/acetonitrile and methanol in various ratios. All the samples were analyzed by means of direct infusion into LC/MS.

2.2.2. Elemental analysis

Perkin-Elmer PE 2400 SERIES II CHNS/O and EA 1108 FISONS instruments were used for elemental analyses.

2.2.3. Nuclear magnetic resonance

Bruker AVANCE 500 NMR spectrometer operating at 500.13 MHz for ^{1}H was used for measurements of the ^{1}H NMR spectra. The compounds were dissolved in hexadeuteriodimethyl sulfoxide used as deutered standard. The ^{1}H chemical shifts were referred to the central signal of the solvent ($\delta = 2.55$).

2.3. Optical characterization

2.3.1. UV–VIS absorption and fluorescence spectroscopy

The referred UV–VIS absorption spectra in solution were recorded using Varian Carry 50 UV–VIS spectrometer. The fluorescence spectra in solution were measured in 90° configuration at Aminco Bowmann S2 fluorimeter. The solid-state luminescence spectra were recorded on Perkin-Elmer LS 55 equipped with an accessory for solid-state measurements from the same producer. Polycrystalline samples were placed under quartz plate and the emission spectra were recorded using front face geometry.

2.3.2. Fluorescence quantum yields

The fluorescence quantum yields (φ_F) in solution were calculated according to the comparative method [24], where for each test sample gradient of integrated fluorescence intensity versus absorbance $F = f(A)$ is used to calculate the φ_F using two known standards. The standards were previously cross-calibrated to verify the method. This calibration revealed accuracy about 5%. As the reference we used Rhodamine B and Rhodamine 6G with φ_{Fl} 0.49 [25] and 0.950 ± 0.005 [26], respectively. The excitation wavelength was chosen to be the same as for the laser excited experiments i.e. 532 nm. Since the **VII** has very low absorption coefficient at this exciting wavelength, we used Fluorescein (0.91 ± 0.02) [20] and Coumarin 6 (0.78) [27] because of the better spectral overlap. The excitation wavelength in this case was 460 nm.

2.3.3. Fluorescence lifetimes

The fluorescence lifetime τ_F was measured using Andor Shamrock SR-303i spectrograph and Andor iStar ICCD camera. The samples were excited by third harmonic of EKSPLA PG400 Nd:YAG laser (355 nm) with light pulse time duration of ~30 ps. The temporal resolution of the system is approximately 25 ps. In order to avoid chromatic aberrations, the emitted light from the sample was collected by two off-axis mirrors.

2.4. Computational procedures

All theoretical calculations for compounds **VII**–**XII** were carried out on exactly same level as for previously reported precursors **I**–**VI** [10], in order to be directly comparable. The ground state (S_0) geometry was optimized using quantum chemical calculations based on DFT. Hybrid three-parameter B3LYP functional in combination with 6-311G(d,p) basis was used. No constraints were preliminary employed, but, as the nonconstrainted computations converged to symmetrical structures for compounds **VII**, **IX** and **XI**, the final computations were carried out with C_i symmetry constraint. No imaginary frequencies were found by vibrational analysis, confirming that the computed geometries were real minima on the ground state hypersurfaces.

TD DFT computations of the vertical excitation energies were carried out on the computed S_0 geometries. The same exchange-correlation functional (B3LYP) was used in TD DFT calculations with rather broader basis set (6-311+G(2d,p)). Solvent effect of DMSO was involved by non-equilibrium PCM.

All methods were taken from Gaussian09W program suite [28], and the default values of computational parameters were used. The results were analyzed using GaussViewW from Gaussian Inc, too.

3. Results and discussion

3.1. Syntheses

Although looking quite simple (Fig. 1), *N*,*N*-dialkylation of DPPs is a two-step process complicated by extremely low solubility of starting pigments, which sometimes leads to the presence of mono-alkylated intermediate in reaction mixture, even if an excess of both alkylating agent and HBr neutralizing potassium carbonate is used [11]. In-depth study of this reaction was recently carried out [29]. The reports on the syntheses targeted directly on *N*-mono-alkylated DPPs are relatively rare, but there was recently shown, that these compounds can be highly sensitive and selective fluorescent sensors for fluoride anions [30]. All six DPP derivatives **VII**–**XII** in the presented study were prepared with moderate to high yields and the special purification procedures like chromatography or fractional crystallization were not necessary in order to obtain the product of the desired quality. We ascribe this fact to higher reactivity of bromine on ethyl bromoacetate as compared to e.g. *n*-butyl bromide. The compounds show good solubility over a wide range of solvents, so we have carried out the spectral measurements in highly polar DMSO, in order to have direct comparison with our previous results obtained for *N*-non-alkylated pigment precursors **I**–**VI** [10] or *N*-butylated analogues of **VII** and **XI** [11,12], in acetonitrile, as a representative of less polar solvents, and in almost non-polar but easily polarizable toluene.

3.2. DFT computed structure

As expected, DFT optimized geometries of **VII**–**XII** predict non-zero dihedral angles, describing phenyl-pyrrolinone rotation (Table 1), on the contrary to strictly planar precursors **I**–**VI** [10]. The computed values of dihedral angles are the result of a compromise between sterical effect of methylene and *ortho* phenyl hydrogens (more or less the same for all six derivatives), invoking nonplanarity, and conjugation effect (dependent primarily on *para* phenyl substituent of each derivative), maximal for planar arrangement. The effect of the substituent on opposite pendant phenyl is marginal (less than 1°). Average values are thus 26°, 36° and 38° for piperidino, cyano and unsubstituted phenyls, respectively.

As these dihedral angles are crucial for the interpretation of absorption spectra, they should be verified by comparison with the experiment. The only known X-ray diffraction structure of compound **VII** [13] is a bit problematic from this point of view. The molecule is highly unsymmetrical in crystal with $\alpha = 36.5°$, i.e. quite close to the computed value 38.2°, and $\beta = 68.8°$, i.e. totally out of a reasonable agreement. These results show a dramatic role of packing forces in DPP crystal. As discussed earlier [31], there are always some perturbation of planarity even for theoretically planar DPP pigments, bearing evidence of relatively flat minima of ground state geometry with respect to phenyl-pyrrolinone rotation. One can expect, that the equilibrium between sterical and conjugation

Table 1
DFT computed phenyl–pyrrolinone dihedral angles and PCM (DMSO) TD DFT computed excitation energies converted to wavelengths.

Compound	α [°]	β [°]	λ_{00} [nm]	f_{osc}
VII	38.2	38.2	465	0.512
VIII	34.7	38.2	495	0.563
IX	36.3	36.3	509	0.615
X	38.0	26.1	518	0.835
XI	26.6	26.6	546	1.138
XII	35.2	25.5	561	0.923

α [°] = R_1-phenyl-pyrrolinone dihedral angle; β [°] = R_2-phenyl-pyrrolinone dihedral angle; λ_{00} [nm] = theoretical excitation energy; f_{osc} = oscillator strength.

effects may be even more fragile for *N*-alkylated derivatives and thus the effect of packing forces may be more dramatic. That is probably the case of the X-ray structure of **VII**. Unfortunately, such distorted molecular structure can give only limited evidence on the accuracy of the computed structures. We have tested the relevance of DFT method to predict the dihedral angles of *N,N*-disubstituted compound **I** on another two known X-ray structures, in which C_i molecular symmetry in crystal is retained. The results were quite encouraging. The computed value for *N,N*-dimethyl **I** (30.3°) matches well the experimental one (30.4° [32]), and an agreement for *N,N*-diallyl **I** (theor. 31.2°, exp. 35.8° [13]) is also acceptable. There are no X-ray data for *N,N*-di-*n*-butyl **I** available, but a lot of them exist, for its derivatives (see bellow), so we computed also the dihedral angle for this compound. Its value (26.4°) is considerably lower, than for compound **VII** (38.2°).

We searched the Cambridge structural database (CSD) using *ConQuest* procedure [33] in order to find the structures similar to the derivatives **VII**–**XII**. There were found four files with X-ray structures of DPP derivatives with both pyrrolinone nitrogen substituted by *n*-butyl and at least one pendant phenyl either unsubstituted, or substituted with amino or cyano groups in *para* position: KAKMAL (R_1 = CN, R_2 = H, α = 45.2°, β = 32.6°) [34], XATKIN ($R_1 = R_2$ = CN, $\alpha = \beta$ = 43.1°), NAWREJ (R_1 = H, R_2 = diphenylamino, α = 32.8°, β = 30.5°) and XATKEJ (R_1 = H, R_2 = 4-MeO-phenyl, α = 41.0°, β = 42.3°) [35]. Another relevant data come from recently published *N,N*-dibenzylated DPPs. Such group recall probably similar steric hindrance with respect to phenyl, as dihedral angles of chlorinated derivative ($R_1 = R_2$ = Cl, α = 41.6°, β = 43.9°) [23] are very similar to *N,N*-dibutylated dibromo derivative found in CSD in XATJAE file ($R_1 = R_2$ = Br, $\alpha = \beta$ = 45.0°) [35]. So the results for *N,N*-dibenzylated dimorfolino derivative ($R_1 = R_2$ = morfolino, $\alpha = \beta$ = 28.1°) [23] are close to those obtained for diphenylamino substituent (file NAWREJ) in accordance with an interpretation based of a mixing of two resonance structures for dimorfolino (and generally diamino) DPP derivatives [23].

Finally, DFT predicted decrease of the phenyl-pyrrolinone dihedral angle accompanying *p*-piperidino substitution is in accordance with the relevant experimental data, at least qualitatively. On the other hand, small lowering of this dihedral angle connected with *p*-cyano substituent is inconsistent not only with the data coming from both above mentioned *p*-cyano substituted derivatives, but even with a general trend represented by other electron-accepting substituents, i.e. halogens.

In order to test the sensitivity of dihedral angles of CN substituted derivatives on a quantum chemical method, we carried out the calculations on Hartree–Fock (HF) level with the same 6-311G(d,p) basis set. We obtained the dihedral angles considerably higher (α = 52.4°, β = 52.1° for **VIII**, $\alpha = \beta$ = 52.4° for **IX** and, α = 52.5°, β = 47.9° for **XII**) compared to those ones coming from DFT calculations (Table 1). But these computations also do not considerably distinguish 4–CN–phenyl-pyrrolinone and phenyl-pyrrolinone dihedral angles.

3.3. Absorption and fluorescence spectra in DMSO

The absorption maxima of **VII**–**XII** in DMSO show hypsochromic and hypochromic shifts (Table 2a, Fig. 2) with respect to corresponding precursors **I**–**VI** [10]. Hypsochromic shift is in fact a net effect of three contributions: 1) An increase of excitation energy due the less efficient conjugation because of the loss of molecular planartity, 2) the redistribution of the intensities of vibronic sub-bands from 0–0 maximum of **I**–**VI** in favour of 0–1 in **VII**–**XII**, as shown by a successive *N*-alkylation of **I** and **V** [11,12] and 3) the opposite effect – the decrease of excitation energy due to the increase of electron-donating strength of a pyrrolinone nitrogens in central DPP core composed of two coupled merocyanines (H-chromophore). We consider that the second and third contributions are almost constant over the whole series and the differences in hypsochromic shifts caused by *N*-alkylation go almost exclusively on account of the first one, i.e. the substituent dependent changes in the ground state planarity.

The highest hypsochromic shift with respect to non-alkylated precursor was found for di-cyano substituted **IX** (59 nm), mono-cyano substituted **VIII** (53 nm) and rather lower for unsubstituted **VII** (45 nm). On the other hand the lowest hypsochromic shift was observed for di- and mono-piperidino substituted **XI** (20 nm) and **X** (24 nm), while the shift of unsymmetrical compound **XII** (35 nm) with both types of substituents lies between the symmetrically

Table 2
The spectroscopic properties of **VII**–**XII** in a) DMSO, b) acetonitrile and c) toluene.

Compound	λ_A (nm)	ε (λ_A) (l mol^{-1} cm^{-1})	λ_F(nm)	φ_F	$\Delta\lambda_{Stokes}$ (cm^{-1})	τ_F (ns)
a) DMSO						
VII	460	15,800	519	0.56	2470	7.34 ± 0.08
VIII	471	16,000	547	0.51	2950	7.07 ± 0.03
IX	480	13,300	557	0.72	2880	6.50 ± 0.04
X	516	32,200	601	0.12	2740	1.17 ± 0.02
						6.7 ± 1.2
XI	540	45,100	603	0.45	1940	3.45 ± 0.02
XII	541	42,300	654	<0.01	3190	0.217 ± 0.002
						3.72 ± 0.10
b) Acetonitrile						
VII	454	19,200	512	0.31	2490	6.70 ± 0.04
VIII	464	16,900	538	0.75	2960	5.78 ± 0.03
IX	473	19,400	549	0.32	2930	6.67 ± 0.04
X	500	35,400	587	0.01	2960	1.12 ± 0.01
						2.70 ± 0.20
XI	523	50,500	590	0.20	2170	3.70 ± 0.03
XII	524	34,800	638	<0.01	3410	<0.10
						3.57 ± 0.02
c) Toluene						
VII	462	18,500	520	0.36	2410	5.93 ± 0.04
VIII	472	22,570	544	0.43	2800	4.24 ± 0.02
IX	482	17,700	558	0.29	2830	6.48 ± 0.04
X	499	35,000	563	0.34	2280	4.00 ± 0.02
XI	520	44,400	575	0.38	1840	3.20 ± 0.02
XII	527	36,500	603	0.16	2390	4.41 ± 0.05

λ_A – the position of the absorption maximum; ε – molar absorption coefficient at the λ_A; λ_F – the position of the fluorescence maximum; φ_F – the fluorescence quantum yield; $\Delta\lambda_{Stokes}$ – the Stokes shift (λ_F–λ_A); τ_F – the observed fluorescence lifetime.

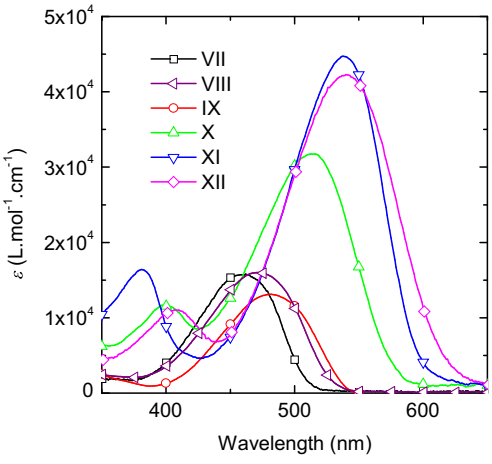

Fig. 2. Molar absorption coefficients of the studied DPP derivatives in DMSO.

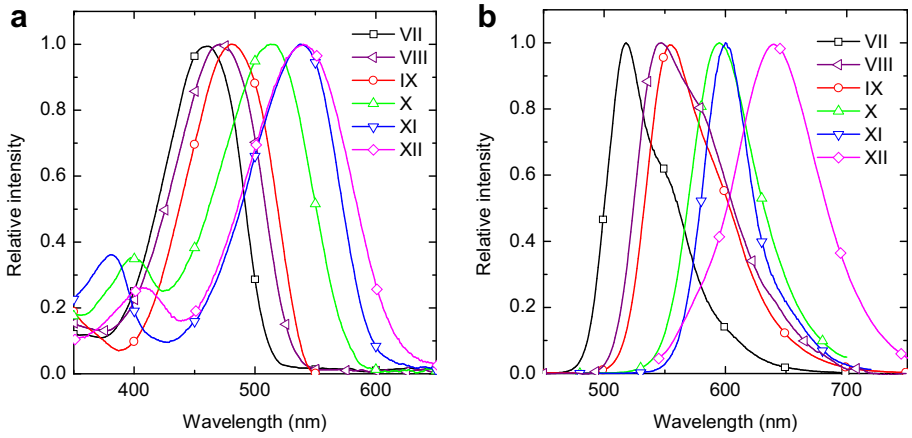

Fig. 3. Normalized absorption (a) and fluorescence (b) spectra of **VII**–**XII** in DMSO.

substituted **IX** and **XI**. Although solute–solvent interaction may play some role, we relate this behaviour mainly to the dependence of the dihedral angle describing the phenyl-pyrrolinone rotation on a nature of *para* substituent of this pendant phenyl. The conclusion is thus clear: piperidino substitution dramatically decreases the phenyl-pyrrolinone dihedral angles in accordance with DFT predictions, while cyano substitution increases these angles considerably, contrary to theory.

PCM TD DFT computed data relate to the experimental maxima only qualitatively. More precisely, the series can be divided into two groups of derivatives. The first one (**VII**, **X** and **XI**) show the deviation between computed λ_{00} (Table 1) and experimental λ_A (Table 2a) 2–6 nm, while the difference for cyano substituted derivatives is significantly bigger (20–22 nm for mono-cyano substituted **VIII** and **XII** and even 29 nm for di-cyano **IX**). As there were no such discrepancies between theory and experiment for planar derivatives **I**–**VI** [10], we ascribe this inconsistency also to underestimated dihedral angles in DFT calculated geometries.

Finally, the suspicion revealed in part 3.2. filled up and the absorption spectra clearly show, that the dihedral angle between *p*-cyano-phenyl and pyrrolinone rings should be relatively higher than for unsubsubstituted phenyl-pyrrolinone case, contrary for the DFT prediction. PCM (DMSO) TD DFT 6-311 + G(2d,p) calculations carried out on the above mentioned more distorted HF geometry resulted in a considerable blue shift (λ_{00} = 426.nm for **VIII**, 435 nm for **IX** and 477 nm for **XII**), compared the values obtained on DFT geometry (Table 1), i.e. the values of λ_{00} are in this case much lower compared to the experimental λ_A (Table 2a) showing an evidence on nonrealistic distortion coming from HF geometries.

The hypsochromic shift of **VII** with respect to *N,N*-dibutylated **I** (7 nm) [12] and opposite bathochromic shift of **XI** with respect to *N,N*-dibutylated **V** (−4 nm) [12] do not support, that $-CH_2COOCH_2CH_3$ grouping is sterically significantly more efficient than $-CH_2CH_2CH_2CH_3$ as it would relate to the computed difference of phenyl rotation in **VII** (38.2°) and *N,N*-dibutylated **I** (26.4°). The absorption spectra do not corfirm that unsymmetrical highly distorted X-ray structure of **VII** [13] is retained in solution.

The relation between fluorescence maxima of corresponding members of *N*-alkylated and non-alkylated sets is different from absorption and much less clear on the first view (Table 2a, Fig. 3). The maxima of unsubstituted **I** with respect to **VII** are almost the same (+2 nm on behalf of **VII**), while **IX** shows hypsofluoric shift with respect to **III** (−8 nm). The fluorescence maximum of compound **VIII** shows also a hypsofluoric shift with respect to **II** (−3 nm, i.e. *exactly* between +2 nm and −8 nm for symmetrical pairs **I**/**VII** and **III**/**IX**). *N,N*-dialkylated electron-donor substituted derivatives **X** (+14 nm) and **XI** (+15 nm) show moderate bathofluoric shifts as compared to **IV** and **V**, respectively. Push-pull derivative **XII** shows almost identical maximum as **VI** (the difference is +1 nm), i.e. its value lies between **III**/**IX** and **V**/**XI** pairs as in absorption. As a consequence the Stokes shift of compound **XII** is absolutely the highest one (3190 cm^{-1}), i.e. significantly higher than for non-alkylated compound **VI** (2060 cm^{-1}). An increment of a Stokes shift increase connected with *N,N*-disubstitution is relatively similar (1090–1270 cm^{-1}) for all three pairs of piperidino substituted compounds and rather higher (1930–2070 cm^{-1}) for unsubstituted or only cyano substituted pairs.

The main reason for the general increase of the Stokes shift due to *N*-alkylation is caused by the fact, that it is considered as a difference between absorption and fluorescence maxima. The maxima correspond to 0–0 vibronic transition in fluorescence spectra for all twelve compounds, to 0–0 vibronic transition in absorption for **I**–**VI** [10] and to 0–1 transition for **VII**–**XII** (Fig. 3). An increase of Stokes shift caused by a redistribution of vibronic bands intensities in absorption may not be strictly constant, but probably quite similar for all six pairs. The rest of the changes in Stokes shift goes on account of the differences in internal (geometrical) and external (solvent) relaxation, when going from vertical Franck-Condon (FC) state to relaxed excited state. Internal relaxation is probably mainly connected with the changes of above discussed dihedral angles. In order to have a better view on external contribution, it was necessary to carry out the spectral measurements in other solvents with different (lower) polarity.

3.4. Solvatochromism

It was impossible to measure the absorption and fluorescence solvatochromism of **I**–**VI** because of their insolubility in other than highly polar solvents able to form H-complexes with solute. The spectral data for *N*-alkylated derivatives in toluene and acetonitrile are summarized in Table 2b, c and the spectra are shown on Figs. 4 and 5. The shape of the absorption spectra is the same in all three solvents, i.e. the vibronic structure is completely unresolved even in toluene, while the vibronic structure of fluorescence spectra is best resolved for all compounds in toluene, in which clearly 0–0 vibronic transition is the absolute maximum, and its resolution decreases in acetonitrile and is almost lost in DMSO.

Compound **VII** shows small negative solvatochromism, when going from toluene to acetonitrile (−8 nm) and almost the same positive shift from acetonitrile to DMSO (+6 nm). The shifts of its fluorescence maxima are almost identical, thus Stokes shift is the

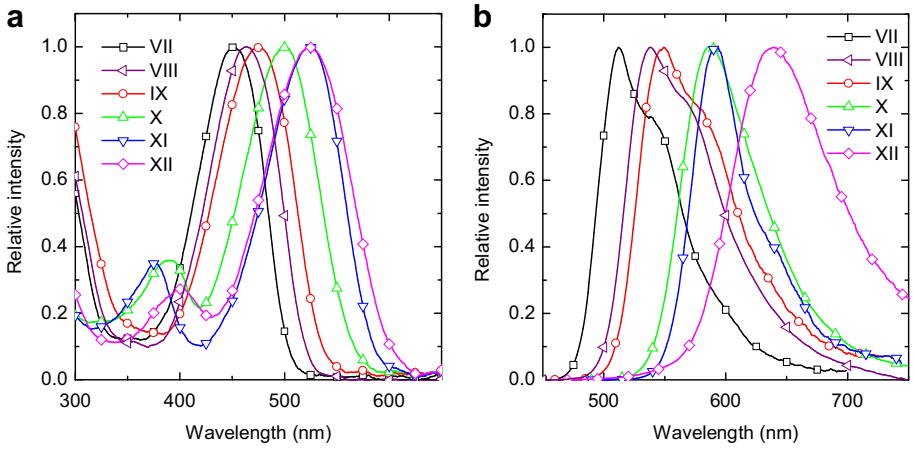

Fig. 4. Normalized absorption (a) and fluorescence (b) spectra in acetonitrile.

same in all three solvents. The solvent induced shifts of **IX** are nearly the same within 1 nm. The spectral shifts when going from toluene to acetonitrile markedly evoke the situation found for BODIPY dyes [36] and the interpretation is the same. While the absorption maximum of their hybrid **VIII** lies exactly between **VII** and **IX** in all solvents, the fluorescence maximum is generally closer to **IX** and a small growth of Stokes shift with solvent polarity from toluene (2800 cm^{-1}) to acetonitrile (2960 cm^{-1}) is observed. Thus **VIII** is only a bit more polar in relaxed than in FC excited state.

The introduction of piperidino group brings two general trends with respect to excited state relaxation in compounds **X**–**XII**: The contribution of internal relaxation is decreased, which well relates with lower rotation of *p*-piperidino-phenyl in FC state, while the external contribution is increased, as the electron-donating substitution changes the intramolecular charge distribution. The former statement can be documented by lower Stokes shift of **XI** (1840 cm^{-1}) with respect to **VII** (2410 cm^{-1}) in non-polar toluene. The latter sentence is generally proved by a dependence of Stokes shift on a solvent polarity, i.e. its increase is less than 160 cm^{-1} for **VII**–**IX** and notably higher for **XI** (330 cm^{-1}), **X** (680 cm^{-1}) and especially **XII** (1020 cm^{-1}) when going from toluene to acetonitrile. Thus, the largest observed Stokes shift of **XII** (3190 cm^{-1} in DMSO) is in fact mainly done by donor-acceptor substitution (2060 cm^{-1} in DMSO for **VI** [10]) and the additional effect of *N*-alkylation goes mainly on account of a redistribution of vibronic intensities in absorption spectrum of **XII**.

The solvent induced shifts in absorption of **X**–**XII** are less than 4 nm when going from toluene to acetonitrile, reflecting very similar polarity of the ground and excited FC states. Positive solvatochromism of fluorescence is moderate: 15 nm for symmetrical **XI**, and 24 and 35 nm for asymmetrical **IX** and **XII**, respectively, that can be ascribed to relaxed excited state solvent stabilization. The positive solvatochromism in absorption of **X**–**XII** when going from acetonitrile to DMSO is almost constant (16–17 nm), very similar to the corresponding shift in fluorescence (13–16 nm) and a bit higher than for **VII**–**IX** (6–7 nm in absorption and 7–9 nm in fluorescence). It means, that further increase of solvent polarity does not lead to additional excited state relaxation and the energy of the excited FC and relaxed states is lower only because the excited state charge distribution interacts more favourably than the ground state itself with the reaction field of more polar solvent (induced by ground state distribution) [37].

The highest solvent induced rise of Stokes shift, i.e. for compound **XII** between toluene and acetonitrile (+1020 cm^{-1}), is significantly lower than for 4-(dimethylamino)-4′-cyano-1,4-diphenylbutadiene (**DCB**, +4640 cm^{-1} between n-hexane and acetonitrile [38]), in which only central 1,4-diphenyl-butadiene backbone of **XII** is push-pull substituted. This difference goes exclusively on account of much lower value of positive fluorescence solvatochromism of compound **XII** (+35 nm) with respect to **DCB** (+129 nm), while the solvatochromism of absorption is almost the same (−3 nm for **XII** and +2 nm for **DCB**), i.e. negligible between above mentioned

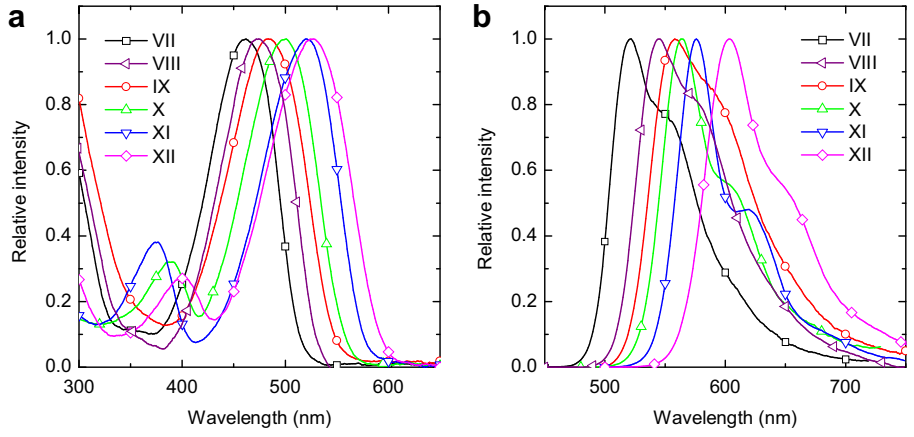

Fig. 5. Normalized absorption (a) and fluorescence (b) spectra in toluene.

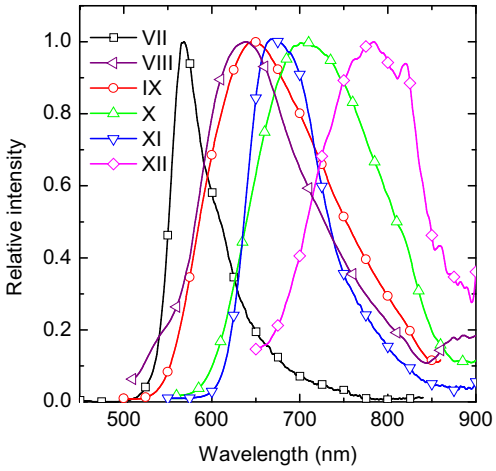

Fig. 6. Solid-state fluorescence spectra of DPP derivatives.

non-polar and polar solvents. Thus, although compounds **X** and **XII** behave qualitatively like push-pull like chromophores, quantitatively their fluorescence solvatochromism is quite limited.

Compound **XI** is formally a quadrupolar molecule with D-π-A-π-D character. Such compounds may or may not undergo an excited state symmetry-breaking in highly polar solvents [39]. The shifts of absorption (3 nm) and fluorescence (15 nm) maxima of **XI**, when going from toluene to acetonitrile, is relatively small (although not as small as for e.g. squaraines [39]), indicating very small (if any) excited state perturbation. Compound **XI** is thus an intermediate quadrupolar chromophor with expected high two-photon absorption cross-section. Their relatively high values estimated for *N*-octylated *p*-diphenylamino substituted DPPs confirm this idea [40].

3.5. Photophysical behaviour

Fluorescence quantum yields (φ_F) and lifetimes (τ_F) for **VII**–**XII** in all three solvents are summarized in Table 2. Corresponding photophysical data for non-alkylated precursors **I** (φ_F = 0.74, τ_F = 6.21 ns) and **V** (φ_F = 0.58, τ_F = 3.66 ns) in DMSO were reported previously [12] and we now supply them by φ_F and τ_F for further two piperidino substituted precursors **IV** (φ_F = 0.48, τ_F = 3.49 ns) and **VI** (φ_F = 0.14, τ_F = 3.90 ns) also in DMSO and not published in Ref. [10]. Both these compounds show monoexponential fluorescence decay.

All six compounds **VII**–**XII** also show a relatively high φ_F in toluene and the fluorescence decay is strictly monoexponential with lifetimes similar to corresponding non-alkylated precursors in DMSO. However, there is a dramatic change for compounds **X** and **XII** when going to polar solvents. The quantum yields of fluorescence are significantly decreased, especially for **XII** (Table 2b, c), and the decay is biexponential. It implies, that some specific process connected with the excited state intramolecular charge transfer (ICT) must be present. Such behaviour may be connected with a conformational change in excited state known as twisted intramolecular charge transfer (TICT). 4-piperidinobenzonitrile is known to undergo such process even more willingly than 4-dimethylamino-benzonitrile, a prototype molecule with respect to TICT [41]. Nevertheless, it is generally very difficult to prove this idea, if not supported by two emission bands in steady-state fluorescence. According to our opinion, the observable fluorescence of **XII** in polar solvents comes from the minor portion of excited molecules, for which the charge separating twist did not pass. Nevertheless this explanation is only speculative and the final solution of this problem would require further sophisticated photophysical experiments that are out of the scope of this article.

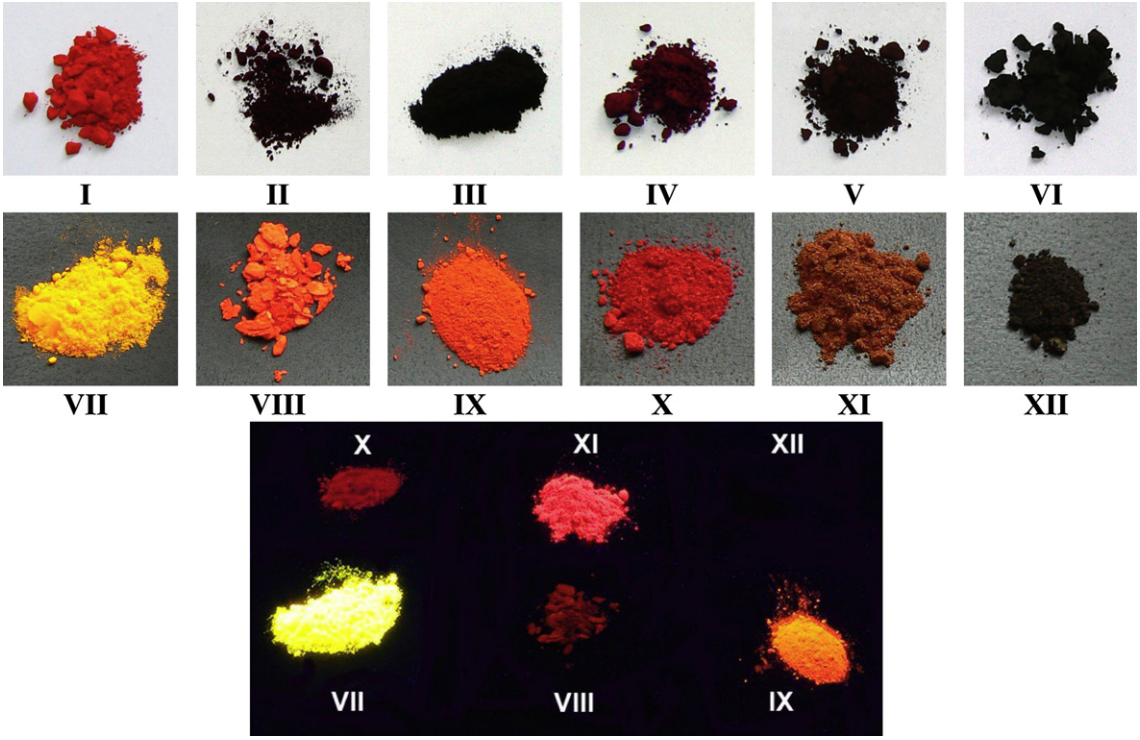

Fig. 7. Polycrystalline samples of **I**–**XII** under daylight (top) and fluorescence of the samples of **VII**–**XII** under UV irradiation (365 nm) with the same settings of Panasonic DMC-FZ7 camera (bottom).

3.6. Solid-state fluorescence

All six studied DPP derivatives show pronounced solid-state fluorescence, on the contrary to any of their non-alkylated precursors **I**–**VI**. The spectra are shown on Fig. 6. The fluorescence of symmetrical **VII**, **IX** and **XI** is strong, easily observable by naked eye under UV irradiation (Fig. 7). The fluorescence of unsymmetrical **VIII** and **X** is less intense, but observable. Solid-state fluorescence of push-pull derivative **XII** is almost not observable (and totally undetectable by a camera – Fig. 7) partly because of its significantly lower intensity and also as it falls almost fully into the infrared region. The values of emission maxima in polycrystalline phase are 568 nm (**VII**), 639 nm (**VIII**), 648 nm (**IX**), 708 nm (**X**), 670 nm (**XI**) and 784 nm (**XII**), and hence, their sequence corresponds to that one in polar solvent (Table 2a) except the changeover of **X** and **XI** pair. The corresponding changeover of dipolar **VIII** and formally quadrupolar **IX** did nor occur, but the fluorescence maximum of hybrid **VIII** in solid state is significantly closer to parent **IX** than to **VII**. The spectral maxima are shifted bathochromically with respect to even the most polar solvent (DMSO). The smallest shift was found for compound **VII** (49 nm) without any polar substituent, the moderate one for centrosymmetric compounds **XI** (67 nm) and **IX** (91 nm), and the highest one for polar **VIII** (92 nm) and **X** (107 nm) and, especially, for push-pull substituted **XII** (130 nm).

Although the intermolecular interactions in highly organized crystal phase cannot be in principle described by simple solute–solvent terminology, the red shifts probably predicate about the polarity inside the crystal environment, i.e. 1) it is effectively more polar than DMSO in all cases and 2) the highest effect is of course in crystals composed from the molecules with non-zero dipole moment. The changeover of solid-state fluorescence maxima of **X** and **XI** is thus a logical continuation of the trend observed in solvents with increasing polarity (Table 2a–c). Although the crystal of **XII** has evidently more polar environment than in DMSO solution, the fluorescence of **XII** does not definitely diminishes in it. We consider this phenomenon as further support of TICT role in the deactivation cascade of **XII** in DMSO, while the excited state twisting is disabled in rigid crystal environment. Almost identical behaviour and interpretation was reported for push-pull substituted 1,6-diphenyl-1,3,5-hexatriene [42].

Generally, the solid-state fluorescence of organic pigments is considered as a property of individual molecule conserved in crystal phase [43]. In other words, the quenching process connected with electron-phonon coupling in crystals of **I**–**VI**, eliminated by *N,N*-dialkylation in their derivatives **VII**–**XII**, relate very probably to impossibility of π–π stacking in crystal [21]. Such disabled stacking may come either from intramolecular sterical hindrance, i.e. molecular nonplanarity, or the intermolecular one, e.g. disabled proximity of molecular planes due to large volume side chains. We consider the former contribution as crucial in this case.

4. Conclusions

Six *N*-alkylated soluble DPP derivatives with polar substituents in *para* positions of pendant phenyls were synthesized, in order to make original non-alkylated pigment precursors better treatable. The compounds are non-planar with phenyl rings rotated out of diketo-pyrrolo-pyrrole plane. The degree of this rotation is decreased by the electron-donating substituents, while increased by the electron-withdrawing substituents, contrary to the DFT predictions. The compounds show small solvatochromism of absorption and a moderate positive solvatochromism of fluorescence, if substituted by strong electron-donating substituent. The significant decrease of fluorescence quantum yields and its biexponential decay for dipolar derivatives in polar solvents was tentatively ascribed to the formation of non-fluorescent TICT excited state. All compounds show fluorescence in polycrystalline solid-state with the maxima covering a range over 200 nm in visible and near infrared region, where the solid-state fluorescence is quite rare [18].

Acknowledgement

The research was supported by the Academy of Sciences of the Czech Republic via project KAN401770651, by the Ministry of Industry and Trade of the Czech Republic via 2A-1TP1/041 project, by the Czech Science Foundation via P205/10/2280 project and by the project "Centre for Materials Research at FCH BUT" No. CZ.1.05/2.1.00/01.0012 from ERDF.

References

[1] Iqbal A, Jost M, Kirchmayer R, Pfenninger J, Rochat AC, Wallquist O. Synthesis and properties of 1,4-diketopyrrolo[3,4-c]pyrroles. Bulletin des Societes Chimiques Belges 1988;97(8–9):615–43.
[2] Wallquist O. Diketopyrrolopyrrole (DPP) pigments. In: Smith HM, editor. High performance pigments. Weinheim: Wiley-VCH; 2002. p. 159–84.
[3] Herbst M, Hunger K. Industrial organic pigments. Weinheim: Wiley-VCH; 2004. pp. 487–494.
[4] Aïch RB, Zou Y, Leclerc M, Tao Y. Solvent effect and device optimization of diketopyrrolopyrrole and carbazole copolymer based solar cells. Org Electron 2010;11(6):1053–8.
[5] Bürgi L, Turbiez M, Pfeiffer R, Bienewald F, Kirner HJ, Winnewisser C. High-mobility ambipolar near-infrared light-emitting polymer field-effect transistors. Adv Mater 2008;20(11):2217–24.
[6] Bijleveld JC, Zoombelt AP, Mathijssen SGJ, Wienk MM, Turbiez M, De Leeuw DM, et al. Poly(diketopyrrolopyrroleterthiophene) for ambipolar logic and photovoltaics. J Am Chem Soc 2009;131(46):16616–7.
[7] Walker B, Tamayo AB, Dang XD, Zalar P, Seo JH, Garcia A, et al. Nanoscale phase separation and high photovoltaic efficiency in solution-processed, small-molecule bulk heterojunction solar cells. Adv Funct Mater 2009; 19(19):3063–9.
[8] Qu S, Wu W, Hua J, Kong C, Long Y, Tian H. New diketopyrrolopyrrole (DPP) dyes for efficient dye-sensitized solar cells. J Phys Chem C 2010;114(2): 1343–9.
[9] Tamayo AB, Walker B, Nguyen TQ. A low band gap, solution processable oligothiophene with a diketopyrrolopyrrole core for use in organic solar cells. J Phys Chem C 2008;112(30):11545–51.
[10] Luňák Jr S, Vyňuchal J, Vala M, Havel L, Hrdina R. The synthesis, absorption and fluorescence of polar diketo-pyrrolo-pyroles. Dyes Pigm 2009;82(2): 102–8.
[11] Vala M, Weiter M, Vyňuchal J, Toman P, Luňák Jr S. Comparative studies of diphenyl-diketo-pyrrolopyrrole derivatives for electroluminescence applications. J Fluoresc 2008;18(6):1181–6.
[12] Vala M, Vyňuchal J, Toman P, Weiter M, Luňák Jr S. Novel, soluble diphenyl-diketo-pyrrolopyrroles: experimental and theoretical study. Dyes Pigm 2010;84(2):176–82.
[13] Colonna G, Pilati T, Rusconi F, Zecchi G. Synthesis and properties of some new N, N′-disubstituted 2,5-dihydro-1,4-dioxo-3,6-diphenylpyrrolo[3,4-c]pyrroles. Dyes Pigm 2007;75(1):125–9.
[14] Thetford D, Cherryman J, Chorlton AP, Docherty R. Theoretical molecular modelling calculations on the solid state structure of some organic pigments. Dyes Pigm 2004;63(3):259–76.
[15] Potrawa T, Langhals H. Fluorescent dyes with large stokes shifts-soluble dihydropyrrolopyrrolediones. Chem Ber 1987;120(7):1075–8.
[16] Fischer GM, Ehlers AP, Zumbusch A, Daltrozzo E. Near-infrared dyes and fluorophores based on diketopyrrolopyrroles. Angew Chem Int Ed 2007; 46(4):3750–3.
[17] Imoda T, Mizuguchi J. Strikingly different luminescent properties arising from single crystals grown from solution or from the vapor phase in a diketo-pyrrolo-pyrrole analog. J Appl Phys 2007;102(7):073529(1)–073529(7).
[18] Park SY, Kubota Y, Funabiki K, Shiro M, Matsui M. Near-infrared solid-state fluorescent naphtooxazine dyes attached with bulky dibutylamino and perfluoroalkenyloxy groups at 6- and 9-positions. Tetrahedron Lett 2009;50(10): 1131–5.
[19] Matsui M, Ikeda R, Kubota Y, Funabiki K. Red solid-state fluorescent aminoperfluorophenazines. Tetrahedron Lett 2009;50(35):5047–9.
[20] Park SY, Ebihara M, Kubota Y, Funabiki K, Matsui M. The relationship between solid-state fluorescence intensity and molecular packing of coumarin dyes. Dyes Pigm 2009;82(3):258–67.
[21] Langhals H, Potrawa T, Nöth H, Linti G. The influence of packing effects on the solid-state fluorescence of diketopyrrolopyrroles. Angew Chem Int Ed 1989; 28(4):478–80.

[22] Tamayo AB, Tantiwiwat M, Walker B, Nguyen TQ. Design, syntheses, and self-assembly of oligothiophene derivatives with a diketopyrrolopyrrole core. J Phys Chem C 2008;112(39):15543–52.
[23] Kuwabara J, Yamagata T, Kanbara T. Solid-state structure and optical properties of highly fluorescent diketopyrrolopyrrole derivatives synthesized by cross-coupling reaction. Tetrahedron 2010;66(21):3736–41.
[24] Williams ATR, Winfield SA, Miller JN. Relative fluorescence quantum yields using a computer-controlled luminescence spectrometer. Analyst (Cambridge, United Kingdom) 1983;108(1290):1067–71.
[25] Casey KG, Quitevis EL. Effect of solvent polarity on nonradiative processes in xanthene dyes: rhodamine B in normal alcohols. J Phys Chem 1988;92(23): 6590–4.
[26] Magde D, Wong R, Seybold PG. Fluorescence quantum yields and their relation to lifetimes of rhodamine 6G and fluorescein in nine solvents: improved absolute standards for quantum yields. Photochem Photobiol 2002;75(4): 327–34.
[27] Reynolds GA, Drexhage KH. New coumarin dyes with rigidized structure for flashlamp-pumped dye lasers. Opt Commun 1975;13:222–5.
[28] Gaussian 09, Revision A.1, Frisch MJ, Trucks GW, Schlegel HB, Scuseria GE, Robb MA, Cheeseman JR, et al., 2009.
[29] Stas S, Sergeyev S, Geerts Y. Synthesis of diketopyrrolopyrrole (DPP) derivatives compridsing bithiophene moieties. Tetrahedron 2010;66(10):1837–45.
[30] Qu Y, Hua J, Tian H. Colorimetric and ratiometric red fluorescent chemosensor for fluoride ion based on diketopyrrolopyrrole. Org Lett 2010;12(15):3320–3.
[31] Luňák Jr S, Vyňuchal J, Hrdina R. Geometry and absorption of diketo-pyrrolopyrrole isomers and their π-isoelectronic furo-furanone analogues. J Mol Struct 2009;919(1–3):239–45.
[32] Mizuguchi J, Grubenmann A, Wooden G, Rihs G. Structures of 3,6-diphenylpyrrolo[3,4-c]pyrrole-1,4-dione and 2,5-dimethyl-3,6-diphenylpyrrolo [3,4-c]pyrrole-1,4-dione. Acta Crystallogr B 1992;48(5):696–700 (The value in the text was taken from file KUHKUT in CSD).
[33] Bruno IJ, Cole JC, Edgington PR, Kessler M, Macrae CF, McCabe P, et al. New software for searching the Cambridge Structural Database and visualizing crystal structures. Acta Crystallogr B 2002;58(3–1):389–97.
[34] File KAKMAL cited in CSD as: Poppe M, Gompper R, Polborn K. 2005, Private Communication.
[35] Files XATKIN, NAWREJ, XATKEJ and XATJAE cited in CSD as: Ostermann D, Gompper R, Polborn K. 2005, Private Communication.
[36] Qin W, Rohand T, Baruah M, Stefan A, Van der Auweraer M, Dehaen W, et al. Solvent-dependent photophysical properties of borondipyrromethene dyes in solution. Chem Phys Lett 2006;420(4–6):562–8.
[37] Zoon PD, Brouwer AM. A push-pull aromatic chromophore with a touch of merocyanine. Photochem Photobiol Sci 2009;8(3):345–53.
[38] El-Gezawy H, Rettig W, Lapouyade R. Solvatochromic behaviour of donor-acceptor-polyenes: dimethylamino-cyano-diphenylbutadiene. J Phys Chem A 2006;110(1):67–75.
[39] Terenziani F, Painelli A, Katan C, Charlot M, Blanchard-Desce M. Charge instability in quadrupolar chromophores: symmetry breaking and solvatochromism. J Am Chem Soc 2006;128(49):15742–55.
[40] Guo EQ, Ren PH, Zhang YL, Zhang HC, Yang WJ. Diphenylamine end-capped 1,4-diketo-3,6-diphenylpyrrolo[3,4-c]pyrrole (DPP) derivatives with large two-photon absorption cross-sections and strong two-photon excitation red fluorescence. Chem Commun 2009;39:5859–61.
[41] Grabowski ZR, Rotkiewicz K, Rettig W. Structural changes accompanying intramolecular electron transfer: focus on twisted intramolecular charge-transfer states and structures. Chem. Rev. 2003;103(10):3899–4031.
[42] Sonoda Y, Goto M, Tsuzuki S, Tamaoki N. Fluorescence spectroscopic properties and crystal structure of a series of donor–acceptor diphenylpolyenes. J Phys Chem A 2006;110(50):13379–87.
[43] Plötner J, Dreuw A. Solid state fluorescence of pigment yellow 101 and derivatives: a conserved property of the individual molecules. Phys Chem Chem Phys 2006;8(10):1197–204.

J Biochem Tech (2010) 2(5):S44-S45
ISSN: 0974-2328

Tayloring of molecular materials for organic electronics

Martin Vala*, Martin Weter, Patricie Heinrichova, Martin Sedina, Imad Ouzzane, Petra Moziskova

Received: 25 October 2010 / Received in revised form: 13 August 2011, Accepted: 25 August 2011, Published: 25 October 2011

Abstract

An example of targeted modification of chemical structure in order to extent utilisation of diketo–pyrrolo–pyrroles in organic electronics is presented. The introduction of solubilising groups opens solution–based techniques for device preparation and therefore reduces the manufacturing cost. The influence of the substitution on the optical activity is discussed.

Keywords: Organic electronics, diketo–pyrrolo–pyrroles

Introduction

Diketo-pyrrolo-pyrroles (DPPs) comprise one of the promissing classes of materials suitable for organic electronics. Nowadays, the DPPs are mainly used as high performance industrially important pigments. This requires excelent photostability, high absorption coeficients but also low solubility. However, the ability to solubilize these materials would open the possibility to use solution–based techniques (spin–coating, drop–casting, inject printing, etc.) to prepare devices from DPPs. One of the reason for the insolubility is the existence of hydrogen bonds between the –NH group and oxygen. Since the basic DPP core is perfectly planar, a π-π electrons overlap occurs in solid state and also contributes to their insolubility. These interactions can be so strong, that cause colour change between solid and dissolved form and influence also other properties, e.g. fluorescence and Stokes shift (Song et al. 2007). It is therefore clear, that to modify the solubility one has to introduce the *N*–substituion and/or break the molecule planarity (Potrawa and Langhals 1987). In this contribution, we will discuss the influence of such substitution on the optical properties of the DPPs with respect to the utilization in organic electronics and possibly in bielectronics in future.

Martin Vala*, Martin Weiter, Patricie Heinrichova, Martin Sedina, Imad Ouzzane, Petra Moziskova

Brno University of Technology, Faculty of Chemistry, Purkyňova 464/118, Brno 61200, Czech Republic

*Tel: +420 541 149 411, Fax: +420 541 211 697
E-mail: vala@fch.vutbr.cz

Materials and Methods

All of the studied derivatives (Fig 1) were synthesised by Research institute of organic synthesis (RIOS, a.s.). The samples were dissolved in dimethylsulfoxide (Aldrich).

Results and Discussion

Substitution of an alkyl group on the nitrogen on the DPP core decreases molar absorption coefficient (hypochromic shift) and simultaneously the longer wavelength maximum is shifted towards higher energy region (hypsochromic shift). Furhermore, the vibration structure is less pronounced. As was pointed out in our previous paper reporting different structures (Vala et al. 2008), this is caused by torsion between pyrrolinone central part and phenyl adjacent to the alkyl group and consequently, is caused by loss of molecule planarity which is in turn responsible for loss of effective conjugation. Since the addition of second alkyl rotates also the second phenyl group, this effect is even more pronounced. The loss of vibration structure can be attributed to the increased dipole moment interacting with polar DMSO solvent. The dipole–dipole interaction of bi–substituted derivatives with the completely non–planar structure is the most pronounced. No dependency on the length of the alkyl used was found.

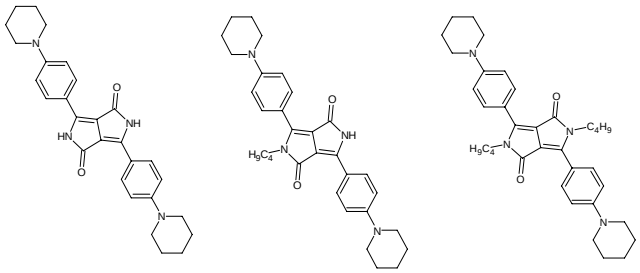

Figure 1: The studied derivaties of diphenyl–diketopyrrolo– pyrrole

Conclusions

It was found, that the *N*–alkylation only does not significantly influence the fluorescence quantum yield. On the other hand the Stokes shift is gradually increased going from the monoalkylated to dialkylated derivatives. The observed spectra are characteristic by graduate loss of mirror symmetry of absorption–fluorescence and vibronic structure. The phenyl torsion due to the *N*–alkylation is the main mechanism for this behaviour in polar DMSO.

Acknowledgement

The work was supported by Grant Agency of the Czech Republic via project No. P205/10/2280.

References

Potrawa T, Langhals H (1987) Fluorescent dyes with large stokes shifts - soluble dihydropyrrolopyrrolediones. Chemische Berichte-Recueil 120(7):1075-1078

Song B, Wei H, Wang ZQ, Zhang X, Smet M, et al. (2007) Supramolecular nanoribers by self-organization of bola-amphiphiles through a combination of hydrogen bonding and pi-pi stacking interactions. Advanced Materials 19(3):416

Vala M, Weiter M, Vynuchal J, Toman P, Lunak S (2008) Comparative Studies of Diphenyl-Diketo-Pyrrolopyrrole Derivatives for Electroluminescence Applications. Journal of Fluorescence 18(6):1181-1186

9 Annex

9.1 Quantum chemical calculation of DPP used for ASE

Time-dependent density functional method is an effective and rather accurate tool for single point calculation, but they're not suitable for the excited state conformation optimization for luminescence spectra simulation. Such methods rather well reproduce the experimental peak positions, but does not consider vibrational structure of the first transition.

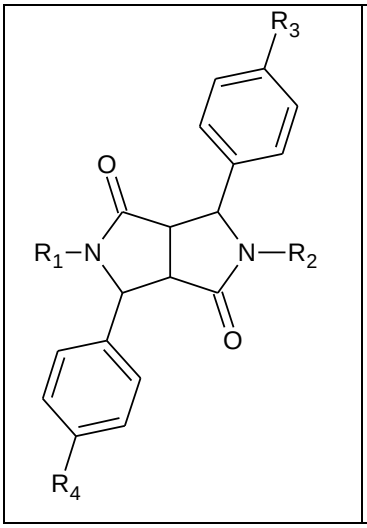

	R_1	R_2	R_3	R_4
DPP VI	C_7H_{15}	C_7H_{15}	-	-
DPP VII	C_4H_9	C_4H_9		
DPP VIII	$CH_2COOC_2H_5$	$CH_2COOC_2H_5$		
DPP IX	$CH_2COOC_2H_5$	$CH_2COOC_2H_5$		-
DPP X	$CH_2COOC_2H_5$	$CH_2COOC_2H_5$	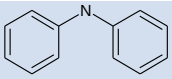	-

***Figure A1**: DPP derivatives investigated for the amplified spontaneous emission study*

***Table 9.1**: Quantum chemical calculation of DPP derivatives (ASE).*

	α[°]	β[°]	$E_{S_0 \rightarrow S_1}$ [eV]	E_{lum}[eV]	$\Delta E_{Stockes}$[eV]	E_{def}[eV]
DPP VI	30.1	30.1	2.62 (0.42)	2.28	0.34	0.16
DPP VII	29.9	29.9	2.50 (0.94)	2.19	0.29	0.13
DPP VIII	27.6	27.6	2.49 (1.02)	2.25	0.24	0.24
DPP IX	25.3	36.5	2.58 (0.73)	2.25	0.33	0.31
DPP X	32.5	36.8	2.50 (0.77)	1.81	0.69	0.29

9.2 Electron distribution of DPP used for ASE

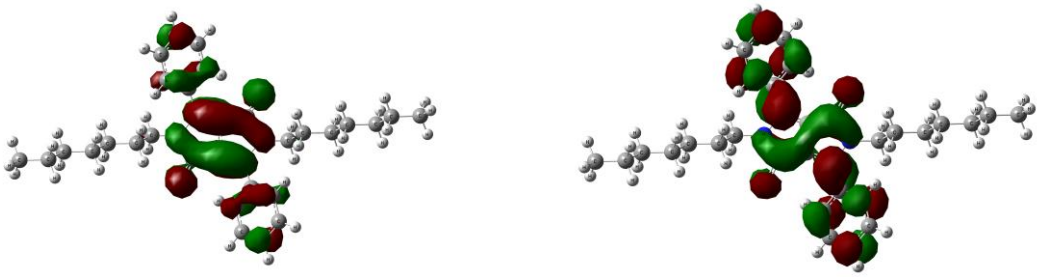

HOMO LUMO

(a)

HOMO LUMO

(b)

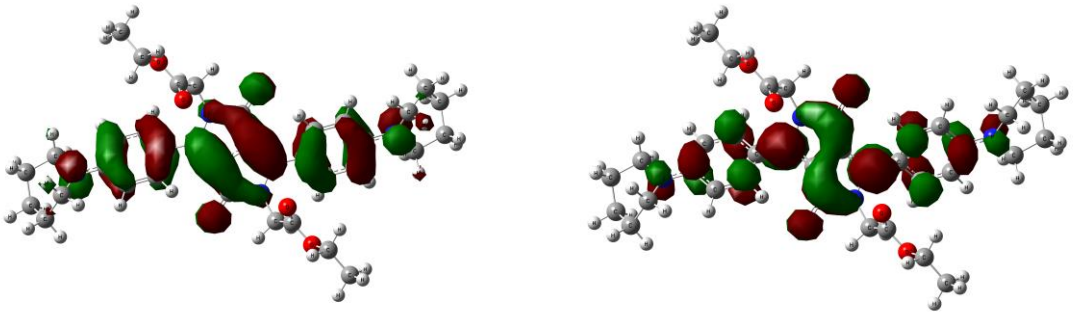

HOMO LUMO

(c)

***Figure A2**: Representation of the electronic density of HOMO and LUMO level of DPP **VI** (a), **IX** (b) and **VIII** (c).*

9.3 Theoretical absorption DFT for ASE

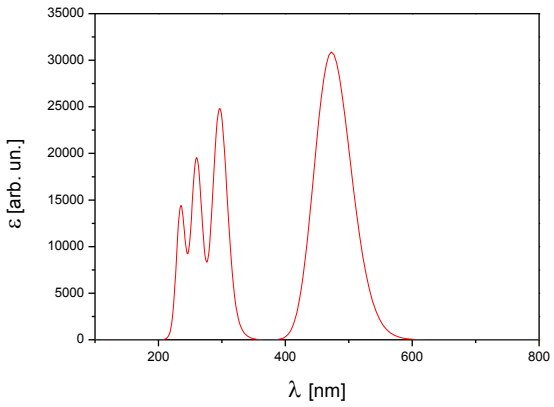

VI

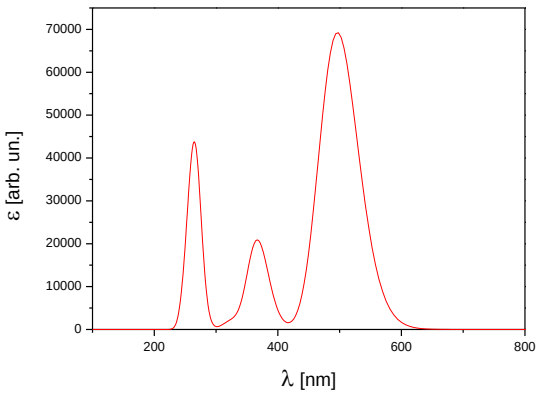

VII

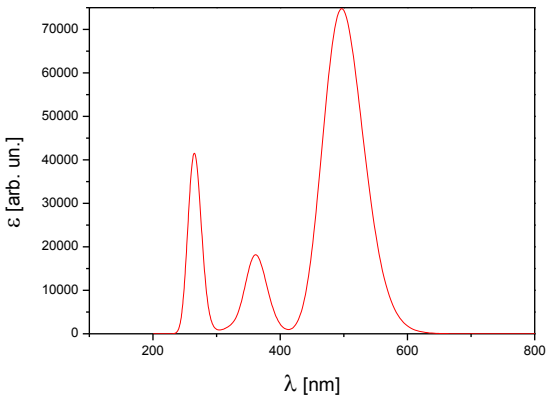

VIII

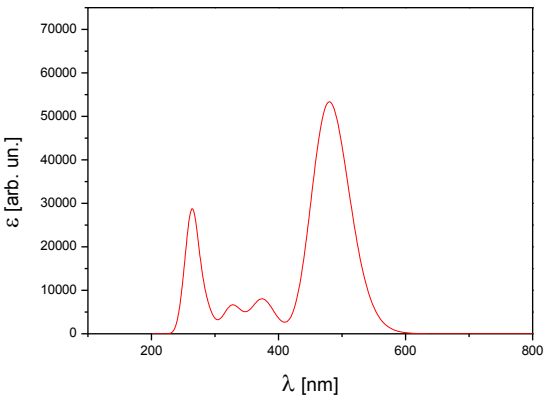

IX

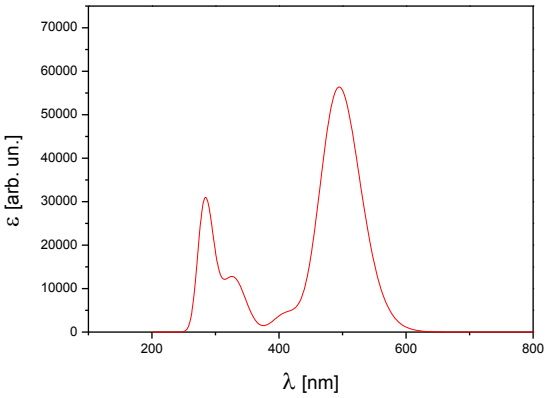

X

Figure A3*: Theoretical absorption of DPP derivatives (**VI-X**) used for the amplified spontaneous emission.*

9.4 DPP derivatives in acetonitrile and toluene for the OPA and TPA study

***Table 9.4.1**: Optical properties of DPP derivatives solubilized in acetonitrile (* dm^{-3} mol^{-1} cm^{-1}).*

DPPs	λ_A (nm)	$\varepsilon(\lambda_A)$	λ_F (nm)	ϕ_F	$\Delta\lambda_{Stokes}$ (nm)	τ_F (ns)
I	454	19200	512	0.31	58	6.70±0.04
II	473	19400	549	0.32	76	6.67±0.04
III	500	35400	587	0.01	87	1.115±0.010 2.70±0.20
IV	523	50500	590	0.20	67	3.70±0.03
X	524	34800	638	<0.01	114	< 0.10 3.57±0.02

***Table 9.4.2**: Optical properties of DPP derivatives solubilized in toluene (* dm^{-3} mol^{-1} cm^{-1}).*

DPPs	λ_A (nm)	$\varepsilon(\lambda_A)$ *	λ_F (nm)	ϕ_F	$\Delta\lambda_{Stokes}$ (nm)	τ_F (ns)
I	462	18500	520	0.36	58	5.93±0.04
II	482	17700	558	0.29	76	6.48±0.04
III	499	35000	563	0.34	64	4.00±0.02
IV	520	44378	575	0.38	55	3.20±0.02
X	527	36500	603	0.16	76	4.41±0.05

9.5 Preliminary results of new DPP derivatives as potential candidates for the TPA

***Table 9.5.1**: Newly synthetized DPP derivatives containing diphenylamino groups.*

DPP	R_1	R_2	R_3	R_4
U69	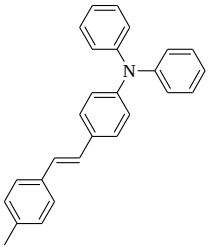	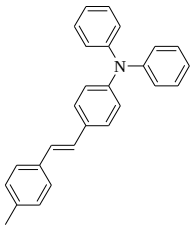	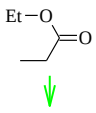	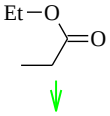
U70	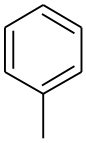	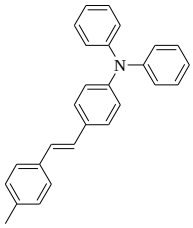	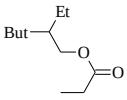	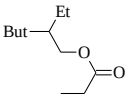
U97	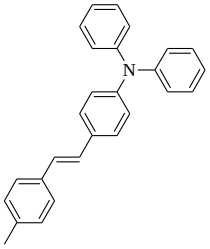	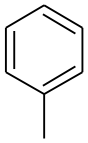	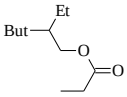	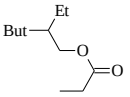
U99	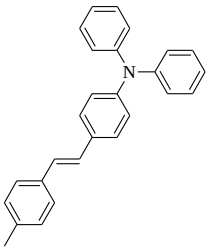	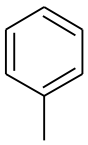	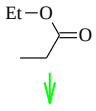	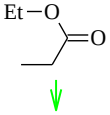

***Table 9.5.2**: Absorption, fluorescence emission, quantum yields, molar coefficient and lifetime results of new DPP derivatives in DMSO (* l mol^{-1} cm^{-1}).*

DPP in DMSO	λ_A (nm)	*Ex* (nm)	λ_F (nm)	ϕ_F (%)	$\varepsilon(\lambda_A)$	τ_F (ns)
DPP69	531	530	565 weak	-	4,20E+04	-
DPP70	500	500	750 weak	-	1,88E+04	-
DPP97	533	532	467 X 500-800 weak	-	2,94E+04	-
DPP99	500	485	815	-	3,14E+04	-

***Table 9.5.3**: Absorption, fluorescence emission, quantum yields, molar coefficient and lifetime results of new DPP derivatives in Toluene.*

DPP in Toluen	λ_A (nm)	*Ex* (nm)	λ_F (nm)	ϕ_F (%)	$\varepsilon(\lambda_A)$ (l mol^{-1} cm^{-1})	τ_F (ns)
DPP69	523	523	605/ 660	<10 0	7,46E+04	2
DPP70	500	485	580	40	2,84E+04	2.1
DPP97	528	526	606/ 660	<50	8,71E+04	-
DPP99	495	485	588/ 627	<80	4,65E+04	2.1

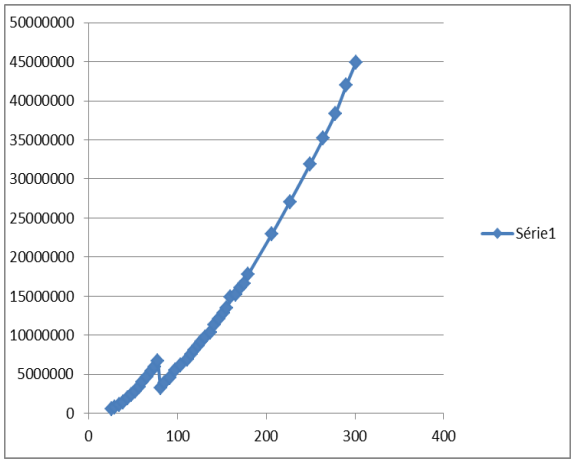

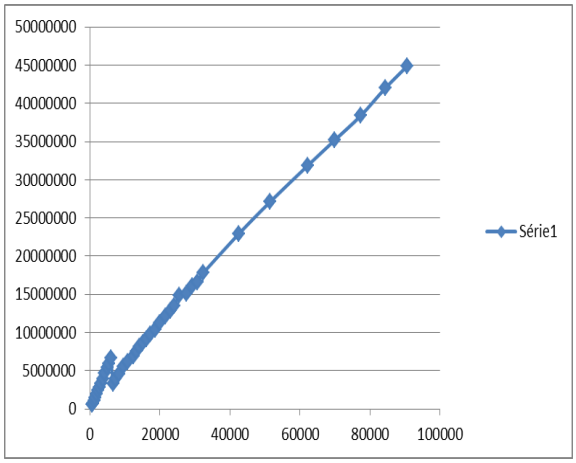

DPP69

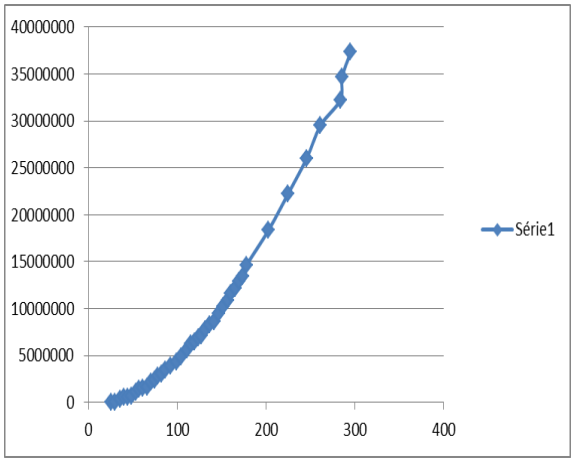

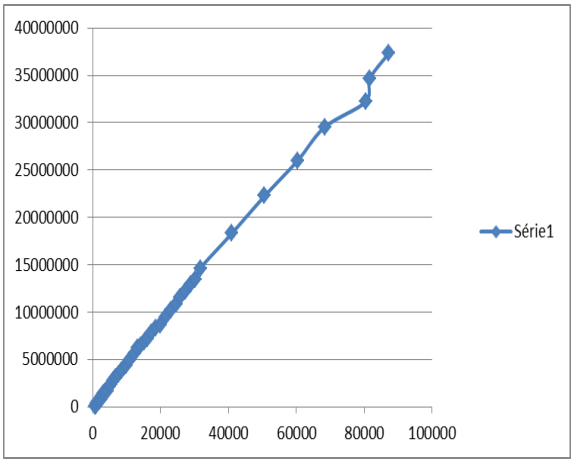

DPP70

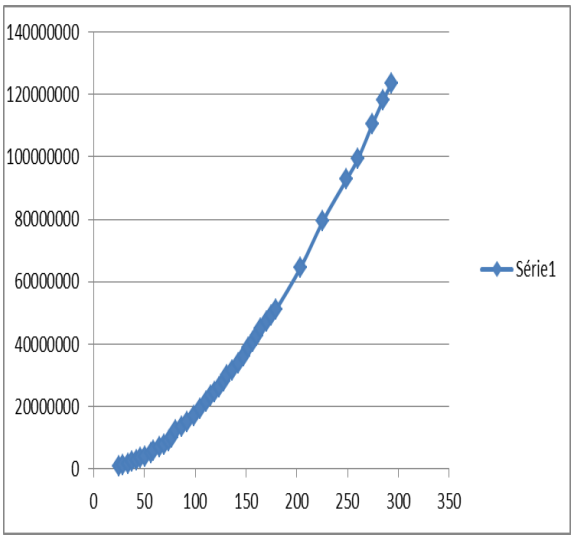

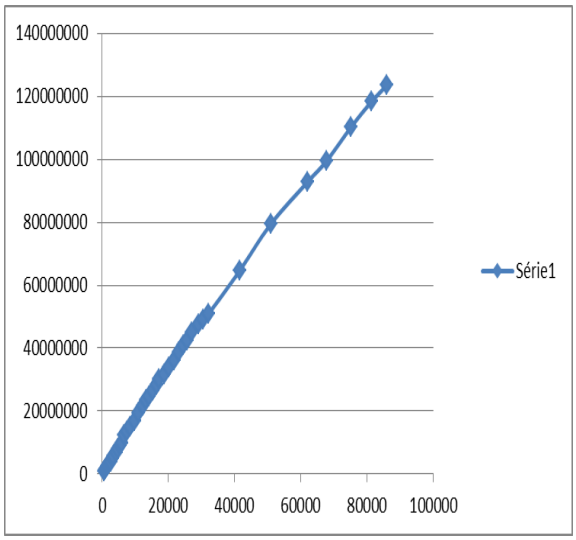

DPP97

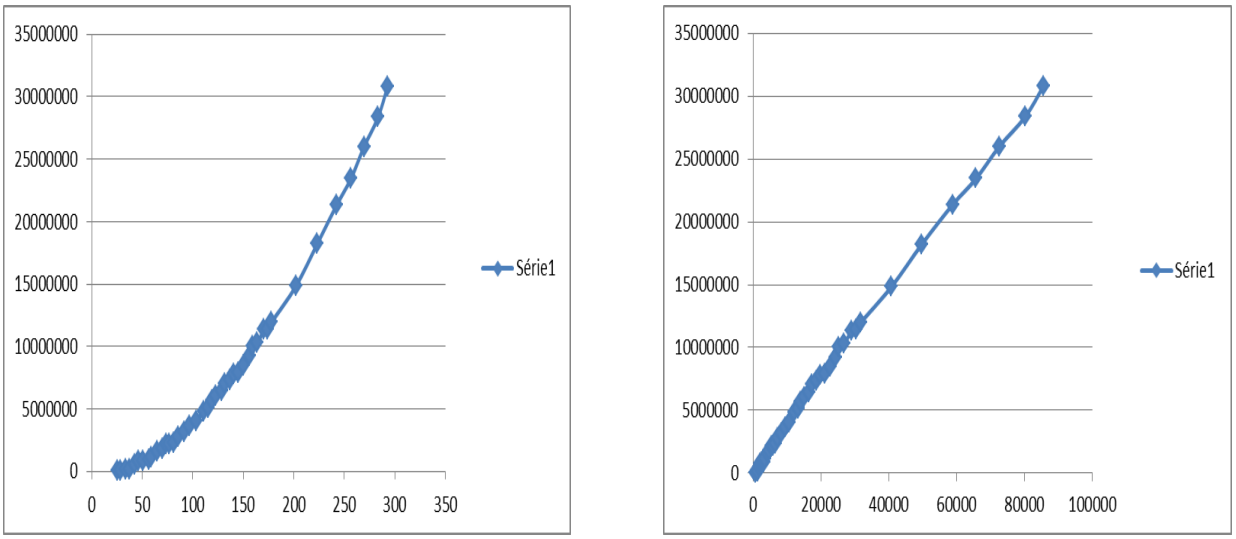

DPP99

***Figure A4**: Integrated fluorescence (F) intensity on the incident incoming light power (P) (left graphic) and linear fit of F versus P^2 (right graphic) of newly synthetized DPP derivatives.*

Special acknowledgment

This work was written on a free linux operating system with free open source software:

Thanks to Apache Open Office (openoffice), Libre office, PDF Creator (pdfforge), PDF Split And Merge (pdfsam), EYE, ACD/ChemSketch, GNU Image Manipulation Program (gimp).